ABSTRACT

Title of Dissertation: SOLDER INTERCONNECT LIFE PREDICTION UNDER COMPLEX TEMPERATURE CYCLING WITH VARYING MEAN AND AMPLITUDE

Fei Chai, Ph.D, 2013

Directed By: George E. Dieter Professor, Michael Pecht, Mechanical Engineering

Electronic devices are under concurrent loading of the power cycling of the devices and the temperature cycling from the surrounding environment. Temperature histories resultant from these concurrent loading would be a complex temperature cycling with varying cyclic temperature mean and amplitude, as well as spatial thermal gradient.

This study developed modeling approaches and quantified accuracies for predicting solder interconnect life under complex temperature cycling. Three modeling approaches were presented in this study: 1) modeling the strain energy under the

resultant complex temperature cycling and employing the energy based fatigue life models; 2) segmenting the resultant complex temperature cycle into multiple simple temperature cycles with a single temperature range for each first, then assessing the life expectancy of the solder interconnect under the segmented simple temperature cycles and at last applying Miner's rule to superpose the damage; 3) estimating solder damage under the resultant complex temperature cycling by a standard temperature cycling with a single temperature range.

Two case studies were included in this thesis: 1) chamber controlled complex temperature cycling with mini cycles occurring at the upper excursion on ceramic leadless chip carriers assembled by Sn36Pb62Ag2 and SnAg3.0Cu0.5 solder (without spatial thermal gradient); 2) combined temperature and power cycling on plastic ball grid array assembled by Sn63Pb37 and SnAg3.0Cu0.5 solder (with spatial thermal gradient). Physical tests were also conducted to quantify the developed modeling approaches.

SOLDER INTERCONNECT LIFE PREDICTION UNDER COMPLEX TEMPERATURE CYCLING WITH VARING MEAN AND AMPLITUDE.

By

Fei Chai

Dissertation submitted to the Faculty of the Graduate School of the
University of Maryland, College Park, in partial fulfillment
of the requirements for the degree of
Doctor of Philosophy
2013

Advisory Committee:
Professor Michael Pecht, Chair
Dr. Michael Osterman
Professor David Barbe
Professor Bongtae Han
Professor Patrick McCluskey
Professor Peter Sandborn

Dedication

To my mother, Aihua Yang, who not only gave my life, but also granted me with the courage and tenacity to conquer all the difficulties in life. Even though she left me five days before my graduation, but she will escort me forever in my heart.

Acknowledgements

I would like to thank Professor Pecht, my dissertation advisor, for his guidance and support on my dissertation. His training of critical thinking would be the most precious value to my future.

I would like to express gratitude to Dr. Osterman, my research supervisor. His innumerous time and attention on all the details helped the success of this work.

I would also like to thank Prof. Han, Prof. McCluskey, Prof. Sandborn and Prof. Barbe for serving on my dissertation committee and providing valuable suggestions from time to time.

Last but not least, I gratefully acknowledge the CALCE consortium members to provide the financial and technical support on this work.

Table of Contents

Chapter 1 Introduction

1.1 Problem statement and objectives

It is a common practice in the industry to use temperature cycling tests to assess the thermo-mechanical fatigue reliability of solder interconnects. Often, electronic products under these tests are not powered and the temperature ranges are exerted by environmental chamber. These temperature cycling tests apply two temperature extremes, constant ramp rates, and constant hold times at the temperature extremes of the cycle, such as those specified in IPC standards [IPC-SM-785, IPC-9701]. However, in the field, electronic devices often work under user-controlled on and off cycles, experience non-constant workloads, and temperature changes in the surrounding environment. Thus, temperature cycling tests fail to capture the multiple temperature ranges (ΔT) in the cyclic excursion and the spatial thermal gradient which occur in actual use.

This paper added to the body of knowledge by developing simulation approaches for predicting solder interconnect life under complex temperature cycling with varying mean and amplitude, as well as spatial thermal gradient, and quantifying the predicting accuracies by physical tests.

1.2 Literature review

This section reviewed the past knowledge on four solder-interconnect-related topics: fatigue life models, modeling approaches for complex temperature cycling, the effect of spatial thermal gradient on complex temperature cycling, and the linear damage superposition.

1.2.1 Life prediction approaches for solder interconnects

Fatigue life models are used to predict solder interconnect life not only under temperature cycling specified in standards [IPC-SM-785, IPC-9701], but also under the field conditions. Solder interconnect experienced low cycle fatigue under temperature cycling loading. Fatigue life models targeting for predicting solder life under this type of loading can be divided into two categories, strain range based and cyclic strain energy density based models, in which the strain and energy are damage metrics (or inputs) of the fatigue life models.

1.2.1.1 Strain range ($\Delta\gamma$) based approaches

The Coffin Mansion model [Coffin, 1954; Manson, 1965] in Eqn. 1.1 relates the completely reversed plastic strain range ($\Delta\gamma_p$) to the cycles-to-failure (N_f) in power law form with the help of two temperature-dependent material constants, fatigue ductility coefficient (ε_f) and fatigue ductility exponent (c) that are determined empirically.

$$N_f = \frac{1}{2}\left(\frac{\Delta\gamma_p}{2\varepsilon_f}\right)^{\frac{1}{c}} \qquad \textbf{Eqn. 1.1}$$

Engelmaier [Engelmaier 1983] further developed the Coffin-Manson model by including the effect of mean temperature and dwell time into the fatigue ductility exponent (c), and define:

$$c = c_0 + c_1 T_{sj} + c_2 \ln\left(1 + \frac{360}{t_{dwell}}\right) \qquad \textbf{Eqn. 1.2}$$

where T_{sj} is the cyclic mean temperature of the solder and t_{dwell} is the average dwell time at the two extremes. Constants c_0, c_1, and c_2 are model constants dependent on the solder material. Typically, the strain range ($\Delta\gamma_p$) are analytically calculated by:

$$\Delta\gamma_p = \mathrm{F}\left(\frac{\mathrm{L_d}(\alpha_s - \alpha_c)\Delta\mathrm{T}}{\mathrm{h}}\right) \quad \textbf{Eqn. 1.3}$$

where L_d is longest distance to the neutral point of expansion; α_c and α_s are the coefficients of thermal expansion of the component and PCB, respectively; ΔT is the temperature range applied on the solder, h is the effective solder joint height and F is the empirical "non-ideal" factor accounting for second-order effects.

For analytical models such as the Engelmaier model, the model inputs are only one ΔT as specified in Eqn. 1.3. Thus, Engelmaier model cannot be employed directly to predict solder interconnect life under complex temperature cycling with multiple ΔT.

1.2.1.2 Cyclic strain energy density based approaches

Morrow's model [Morrow, 1965] was defined by the exponential correlation between strain energy density accumulated per cycle (ΔW) and the mean cycles to failure (N)

$$N = C(\Delta W)^n \quad \textbf{Eqn. 1.4}$$

where C is the fatigue coefficient, and n is the fatigue exponent.

Morrow's model constants (C and n) from past work are listed in Table 1.1. None of those constants were generated from the test results of leadless chip carriers, and the model constants for SAC305 were not available in the literature. Thus, the applicability of Morrow's model constants for predicting the solder interconnect life of LLCs, especially for those assembled by SAC305, remains unknown.

Energy partitioning model future partitions the total strain energy density ΔW under the stress/strain hysteresis curve into elastic energy (U_e), plastic energy (U_p), and creep energy (U_{cr}). The life expectancies (N_{fe}, N_{fp}, and N_{cr}) corresponding to these three portions of energy are generated based on Eqn. 1.5 and the life prediction under the total energy are calculated by Eqn. 1.6:

$$\Delta W_{total} = \Delta W_{el} + \Delta W_{pl} + \Delta W_{cr} = U_{eo} N_{fe}^{b'} + U_{po} N_{fp}^{c'} + U_{co} N_{fc}^{d'} \quad \textbf{Eqn. 1.5}$$

$$\frac{1}{N} = \frac{1}{N_{fe}} + \frac{1}{N_{fp}} + \frac{1}{N_{fc}} \quad \textbf{Eqn. 1.6}$$

Darveaux's model [Darveaux, 1992, 1995, 2000] relates laboratory measurements of fatigue crack initiation and crack growth rates to the inelastic work of the solder.

$$N_0 = K_1 (\Delta W)^{K_2} \quad \textbf{Eqn. 1.7}$$

$$\frac{da}{dN} = K_3 (\Delta W)^{K_4} \quad \textbf{Eqn. 1.8}$$

$$\alpha = N_0 + \frac{a}{\frac{da}{dN}} \quad \textbf{Eqn. 1.9}$$

where N_0 is the mean cycles to crack initiation, a is the entire solder joint equivalent length (e.g. diameter), da/dN is crack propagation rate, K_1-K_4 are crack growth correlation constants, ΔW is the strain energy density per cycle, and α is the characteristic solder joint fatigue life.

Table 1.1: Constants of Morrow's model in the literature

Author	Solder	C	n	Package Type	Test Condition
[Zhang, 2002]	Sn37Pb	16794	-0.8533	Bottom leaded Plastic	Temperature Cycling
[Spraul 2004]	Sn37Pb	537.15	-1.0722	Ball Grid Array (BGA)	Thermal Shock
[Schubert 2003]	Sn59Pb40Ag1	210	-1.2	BGA	Temperature Cycling
[Ghorbani 2007]	SnAgCu	3578.9	-2.2652	CR2512 Resistor	Temperature Cycling /Thermal Shock
	Sn37Pb	5348	-0.7349		
[Perkins 2007]	Sn37Pb	15.79	-1.438	BGA	Temperature Cycling
	Pb90Sn10	25.25	-1.28		
[Andersson 2005]	SnPb37	7.14E-11	-2.7	Shear specimen	Isothermal Mechanical Fatigue Testing
	SAC405	5.80E-09	-2.33		
Dudek [2004]	SAC387	345	-1.02	Shear specimen	Temperature Cycling /Thermal Shock
[Lai 2004]	Sn37Pb	4287	-1.275	BGA	Cyclic Bending
[Hannach 2009]	Sn37Pb	610.86	-1.977	BGA	Temperature Cycling

Energy-based fatigue life models can capture the solder stress/strain hysteresis without simplification of the complex thermal loading, since the strain energy expended during a complex temperature excursion with multiple peaks and valleys can be determined. The finite element method (FEA) is often employed to provide the strain energy, as the input for energy-based fatigue life models. Field thermal conditions with multiple ΔT and spatial thermal gradients add more complexity to the finite element modeling process compared with modeling non-powered temperature cycling tests with single ΔT and uniform temperature across the assembly, such as those specified the standard [IPC-SM-785, IPC-9701]. Existing fatigue life model constants were

derived from the data of temperature cycling tests with a single ΔT and the applicability of using the same modeling approach to predict the complex field thermal conditions has not been quantified.

1.2.2 Modeling approaches on complex temperature cycling

Very limited research has been conducted to analyze the solder interconnect durability under complex temperature cycling with varying temperature mean and amplitude. Pei et al. [Pei 2006] numerically analyzed solder strain energy under a complex temperature cycle with mini-cycles occurring at the upper excursion, and employed Darveaux's fatigue life model to provide a life prediction. Lai et al. [Lai, 2008] numerically analyzed solder interconnect behavior under combined temperature and power cycling condition by solving for the temperature history and mechanical response in sequence. However, either [Pei] or [Lai] provided life prediction accuracies under complex temperature cycling with multiple ΔT and spatial thermal gradient.

1.2.3 Effects of spatial thermal gradients on solder interconnect reliability

Spatial thermal gradients occur during power cycling since heat is generated in die and dissipated to the printed circuit board (PCB) and surrounding environment. Engelmaier provided an analytical method to calculate the strain range under power cycling considering the temperature difference between component and PCB [Engelmaier 1983]. When the coefficient of thermal expansion (CTE) of device is smaller than the PCB board, spatial thermal gradients can decrease the expansion mismatch between the device and board because the temperature at device has a higher temperature than that of board [Sham 2008, Hegde 2008]. If the thermal gradient between

device and the board is even higher than what is required to balance the expansion mismatch, the assembly could change from concave bending under non-powered temperature cycling to convex under power cycling which will aggregate the curvature of as-reflowed assembly [Hall 1983]. However, all these works limited to the power cycling with only one temperature range (single ΔT), and no research has shown the effect of spatial temperature gradient on solder reliability under complex temperature cycling with varying temperature mean and amplitude (multiple ΔT).

1.2.4 Linear damage superposition

Palmgren [Palmgren, 1924] first proposed the linear damage model and Miner [Miner, 1945] further developed it. It is commonly referred as Miner's rule. The hypothesis of Miner's rule is that damage can be superposed linearly and that failure occurs when the cumulative damage fraction (defined as the fraction of life used up by an event or a series of events) equals unity.

$$\sum_{i=1}^{k} \frac{n_i}{N_i} = 1 \qquad \text{Eqn. 1.10}$$

Where n_i and N_i is the cycles conducted and the total cycles to failure for each loading, k is the number of loading source.

Miner's rule has been used to superpose damage from different loading source occurred concurrently (such as thermal cycling and vibration cycling [Upadhyayula 1997, Qi 2006]), and same type of loadings at different stress levels (such as sequential temperature cycling [George 2011], and random vibration [Che 2009]). However, no literature has reported to use Miner's rule to model the complex temperature cycling. In past, complex temperature cycling occurred with

multiple ΔT occurred in the field was simplified into standard temperature cycling with only one ΔT, since method to segment the complex temperature cycling as a prerequisite of employ damage superposition was unknown.

The limitation of Miner's rule is it does not consider load sequence effects. The hypothesis assumes the damage caused by a stress cycle is independent of where it occurs in the load history. Also, it does not capture the influence of stress level on the rate of damage accumulation. However, Miner's rule is still the most popular approach for simplicity of use and acceptable accuracies in the past studies.

1.3 Overview of the dissertation

This study developed modeling approaches and quantified accuracies for predicting solder interconnect life under complex temperature cycling. The modeling approaches includes: 1) modeling the strain energy under the resultant complex temperature cycling and employing the energy based fatigue life models; 2) segmenting the resultant complex temperature cycle into multiple simple temperature cycles with a single temperature range for each first, then assessing segmented simple temperature cycles and at last applying Miner's rule to superpose the damage; 3) approximating solder damage under the resultant complex temperature cycling by a standard temperature cycling with a single temperature range.

In chapter 2 the modeling approach for complex temperature cycling without spatial thermal gradient will be presented by a case study of chamber controlled complex temperature cycling with

mini cycles occurring at the upper excursion. The test samples are ceramic leadless chip carriers assembled by Sn36Pb62Ag2 and SnAg3.0Cu0.5 solder. In chapter 3, the modeling approach for combined temperature and power cycling (with spatial thermal gradient) will be presented. The test samples are plastic ball grid array packages assembled by Sn63Pb37 and SnAg3.0Cu0.5 solder. Physical tests were also provided to quantify the developed modeling approaches. Contributions of the dissertation and suggestions for future work are presented in Chapter 4.

Chapter 2 Chamber Controlled Complex Temperature Cycling with Mini-cycles Occurring at the upper excursion

In this study, strategies for assessing solder fatigue interconnect reliability under a chamber controlled complex temperature cycle with mini cycles occurring at the upper excursion are investigated. Modeling the solder interconnect life expectancy under this complex condition follows a three-step process. First, the complex temperature cycle is segmented into multiple standard temperature cycles with single temperature range (ΔT) in each. Second, the life expectancy of the solder interconnect under each segmented temperature cycle is predicted using the Engelmaier model and Morrow's Model. Third, Miner's rule (linear damage accumulation) is applied to superpose the damage of the segmented cycles and predict solder interconnect fatigue life under the complex temperature cycle. Several modeling strategies based on different segmenting schemes are presented, and the one that compares best with the physical test results is identified. At the meantime, a standard temperature cycling profile (with single ΔT) ignoring the fluctuation at the upper excursion is also identified to approximate the complex temperature cycling without damage superposition.

2.1 Chamber controlled complex temperature cycling tests

To evaluate the strategies for modeling solder interconnect fatigue life under complex temperature cycles, test specimens were created, and a complex temperature cycle test was conducted. The test specimens consisted of ceramic leadless chip carriers (CLCCs) surface-mounted on printed circuit

boards (PCBs) with Sn62Pb36Ag2, SAC305, or SN100C solder. Each test board had two 84 I/O CLCCs and two 68 I/O CLCCs, as shown in Figure 2.1. The dimensions of the 68 I/O and 84 I/O CLCCs were 24mm × 24mm and 30mm × 30mm, respectively. The FR4 laminate test boards were each 2.3 mm thick, and the exposed copper surfaces were coated with organic solderability preservative (OSP) finish. Each assembly combination had four samples. Once mounted on the test board, each CLCC part created an electrical resistance network that could be monitored for failure during an applied temperature cycling condition. For these assembled parts, only the 8 corner solder interconnects were included in a resistance daisy chain, based on the assumption that corner solder interconnects were under the most severe thermal expansion mismatch. The complex temperature cycling profile is depicted in Figure 2.2. The lower dwell was at -25 ^{o}C for 15 minutes. At the upper end, there were six temperature cycles between 55 ^{o}C and 75 ^{o}C with dwells for 5 minutes at each extreme. The overall cycle duration was about 110 minutes, and the rate of temperature change was approximately 10 ^{o}C/min. Interconnect failure was defined as a 20% increase in nominal resistance in 5 consecutive reading scans, based on IPC-9701A [IPC-9701A 2002]. The test was terminated when all components met the failure criteria.

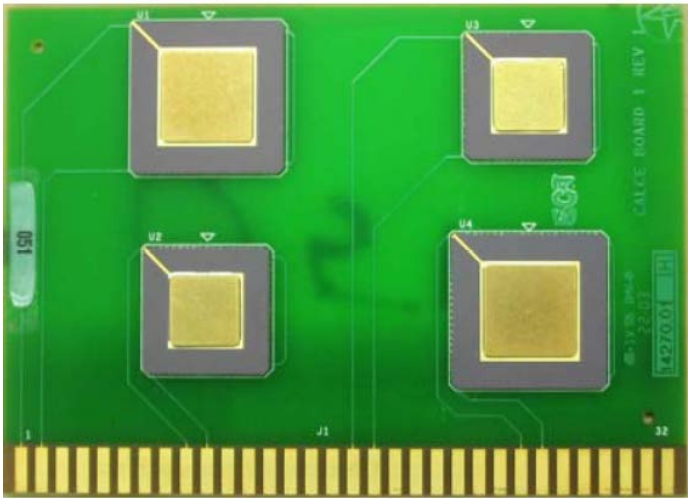

Figure 2.1: Test vehicle.

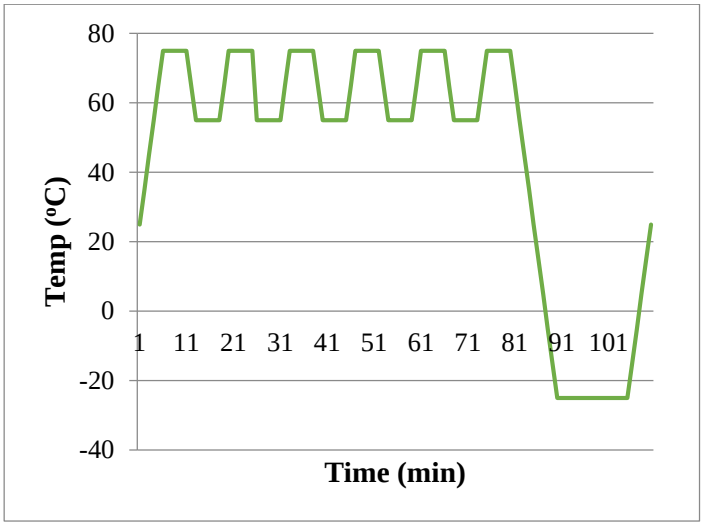

Figure 2.2: Complex temperature cycling profile.

2.2 Failure analysis of CLCC solder interconnects

The corner solder interconnects of the first and last to fail CLCC components were compared in Figure 2.3. It was found from the side view optical inspection that the last to fail parts had bigger

fillet area than the first to fail parts. From the cross-sectional analysis in Figure 2.4, the crack propagated along the bulk $Au(Sn)_4$ intermetallic compound, and also along beneath the CLCC component. The gold was from the surface finish of the part terminals.

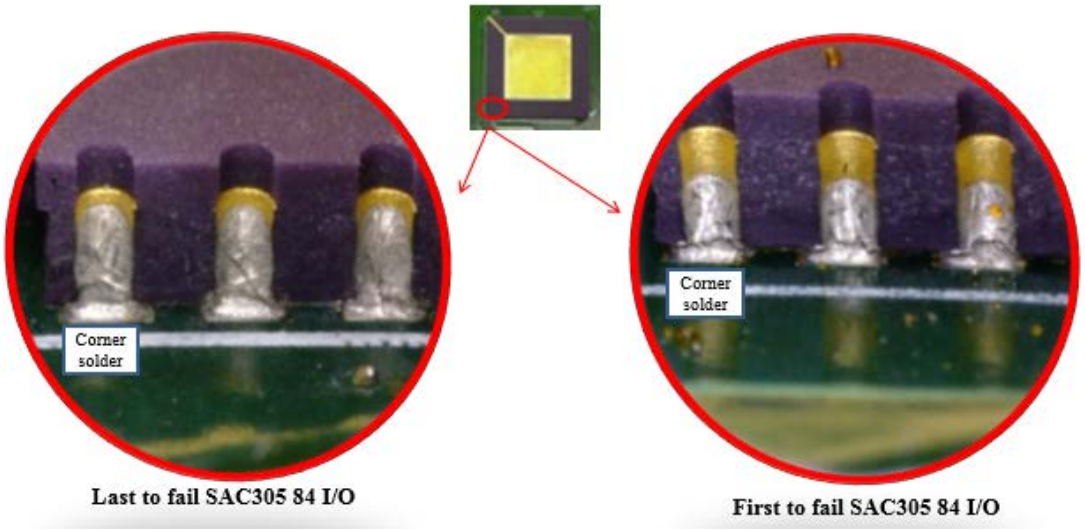

Figure 2.3: Comparison (side view) between the first and last to fail solder interconnects

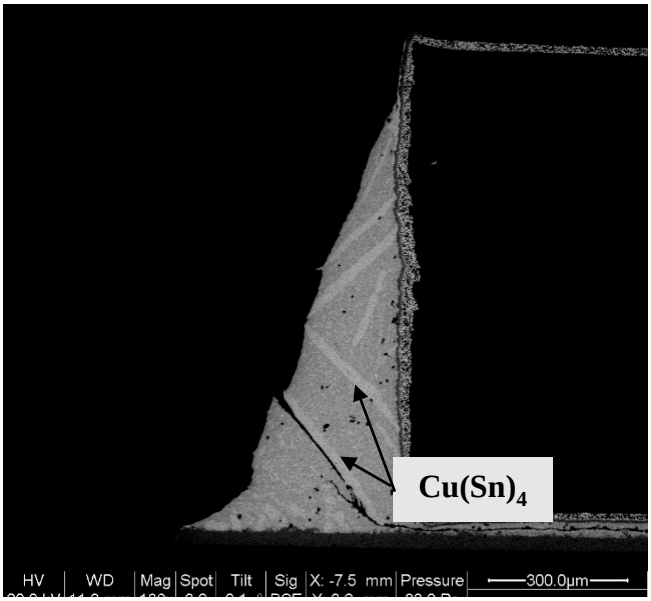

Figure 2.4: Cross-sectional view of crack propagation

2.3 CLCC Solder Interconnect Life Prediction

Parameters of the Engelmaier model and Morrow's model for standard temperature cycling (with single ΔT) were generated by non-linear regression processes based on past temperature cycling test results obtained from the literature [Osterman 2009, 2011]. Then, the complex temperature cycling profile as in Figure 2.2 was segmented into a set of standard cycles (with single ΔT), with each of the segmented cycles assessed by the Engelmaier model and Morrow's model. Finally, Miner's rule was applied to superimpose the damage of the segmented cycles. The superimposed cycles to failure were compared with the complex thermal cycling test results in order to provide a more accurate cycle segmentation method than the other possibilities mentioned in this study.

Modeling the standard temperature cycle as accurately as possible was a prerequisite for modeling the complex temperature cycling. There were 9 sets of simple temperature cycling tests in [Osterman 2009, 2011], and those test profiles are presented in Table 2.1. These simple temperature cycling tests were conducted on the same batch of assemblies as those used in the complex test in the present study, with the same test vehicles and solder materials. In order to make the model parameter robust, the Engelmaier model and Morrow's model constants for predicting the solder interconnect life under standard temperature cycling (with single ΔT) were generated in this section, prior to applying the models on the segmented cycles.

Table 2.1: Standard Temperature Cycling Profiles in Literature

Test No.	Max Temp (°C)	Min Temp (°C)	Upper Dwell Time (min)	Lower Dwell Time (min)
1	125	25	15	15
2	75	-25	15	15
3	75	-25	75	15
4	75	-25	120	15
5	125	25	75	15
6	50	-50	15	15
7	100	0	15	15
8	75	-25	15	75
9	75	25	15	15

2.3.1 **Regression for the constants of Engelmaier model**

The Engelmaier Model [Engelmaier 1983] is a strain range-based model which defines mean cycles to failure as:

$$N_{50} = \frac{1}{2}\left(\frac{\Delta\gamma}{2\varepsilon_f}\right)^{\frac{1}{c}} \qquad \textbf{Eqn. 2.1}$$

where $\Delta\gamma$ is the cyclic strain range, ε_f is the fatigue ductility constant for the solder, and c is the fatigue ductility exponent, defined as:

$$c = c_0 + c_1 T_{sj} + c_2 \ln\left(1 + \frac{360}{t_{dwell}}\right) \qquad \textbf{Eqn. 2.2}$$

where T_{sj} is the cyclic mean temperature of the solder and t_{dwell} is the average dwell time at the two extremes. Constants c_0, c_1, and c_2 are model constants based on the solder material. For leadless packages, the strain range can be approximated as:

$$\Delta\gamma = \left(\frac{L_d(\alpha_s - \alpha_c)\Delta T}{h}\right) \qquad \textbf{Eqn. 2.3}$$

where L_d is the diagonal length from the center to the corner of the CLCC component, since it is the maximum distance to the neutral point over which thermal expansion will occur; αc and αs are the coefficients of thermal expansion of the CLCC component and PCB, respectively; ΔT is the temperature range applied on the solder; and h is the effective solder joint height.

The effective solder joint height (h) is defined as the distance between the chip carrier and the PCB substrate if the solder pads on the printed circuit board do not extend beneath the border of the chip carrier or beyond the sides of the chip carrier, as depicted in Figure 2.5(a). If the copper pad extends beyond the package border, solder will take total areas of the metalized connection area and form a castellated solder shape, as depicted in Figure 2.5(b). In Kojima et al.'s [Kojima 1989] study, the distance between the chip carrier and the PCB (h1 in Figure 2.5(b)) was adopted as the solder height, regardless of the solder shape. In contrast, Engelmaier only specified that "h is the solder height," without clearly indicating the location [Engelmaier 1983]. However, castellated and column-like solders with the same distance between the chip carrier and the PCB (h in Figure 2.5(a) and h1 in Figure 2.5(b)) lead to different solder attachment reliabilities when exposed to temperature cycling, so it is not appropriate to define h1 as the solder height of the castellated solder. Osterman et al. [Osterman 2006] used h2, an intersected line 45˚ up from the projection of the bottom corner of the chip carrier on the pad, in order to compensate for the support from the side solder, as depicted in Figure 2.5(b). In this study, h2 was adopted as the effective solder height. The effective solder height is measured to be 0.365 mm, as shown in Figure 2.6.

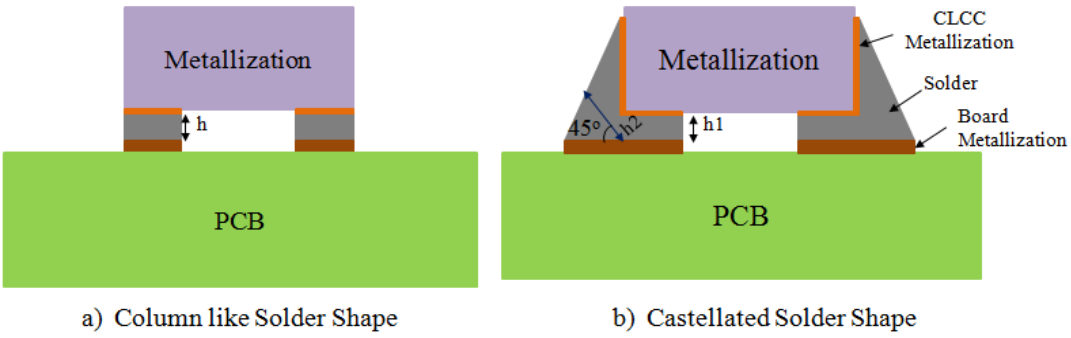

Figure 2.5: Solder heights for different shapes of solder

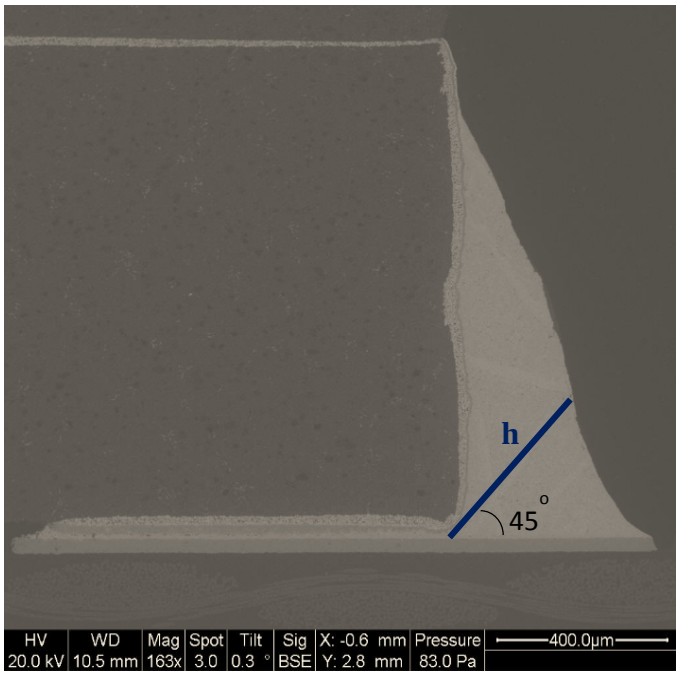

Figure 2.6: Effective solder height by sectioned view of CLCC solder joint.

A commercially available non-linear regression solver was used to determine the material-dependent model constants ε_f, c_0, c_1, and c_2. The fitted model parameters from this non-linear regression are presented in Table 2.2, and evaluation of the fitted parameters is presented in Table 2.3.

In these tables, prob(f) represents the probability that all the parameters are 0, with a smaller prob(f) indicating a greater confidence that the sets of parameters have some correlation to the model. The P values represent the percentage of the distribution that is farther from the mean than the precision of the regression coefficient (standard error divided by the mean), with a smaller P value indicating more confidence that each parameter has some correlation to the model. The P value and prob(f) represent the confidence level that the parameters have some correlation to the model, rather than the size of the effect that the parameters have on the model. R^2 is the fraction of the variation of the model output explained by the regression model, with a larger R^2 value (from 0 to 1) indicating better precision of the model using the fitted model parameters, and 1 indicating a perfect fit. The root mean squares of the prediction errors through all 9 simple temperature cycle conditions are about 21%, 22%, and 26% for the Sn62Pb36Ag2, Sn96.5Ag3Cu0.5, and SN100C solder interconnects, respectively, using the Engelmaier model and the fitted constants from this study.

Table 2.2: Fitted Engelmaier Model Parameters

Parameters	SnPbAg	SAC305	SN100C
c_0	-0.496	-0.367	-0.370
c_1	-1.38E-03	-9.69E-04	-9.83E-04
c_2	2.40E-02	2.21E-02	2.28E-02
ε_f	0.513	0.286	0.255

Table 2.3: Evaluation of Fitted Parameters

Correlation	Parameters	SnPbAg	SAC305	SN100C
P Value	c_0	0	0	0
	c_1	0	0	0
	c_2	0.00901	0.00611	0.00409
	ε_f	0.00142	0.00003	0.00001
prob(f)		0	0	0
R^2		0.978	0.985	0.987

2.3.2 **Regression of the Constants of Morrow's model**

Morrow's model [Morrow 1965] uses the exponential correlation between strain energy density accumulated per cycle (ΔW) and the mean cycles to failure (N), as described in Eqn. 2.4:

$$N = C(\Delta W)^n \qquad \textbf{Eqn. 2.4}$$

where C is the fatigue coefficient, and n is the fatigue exponent.

2.3.2.1 **Finite element analysis**

A finite element analysis was conducted to simulate the strain energy density under each temperature loading condition, and the global-local modeling strategy was applied. The global model was solved first for each of the thermal loading conditions, and the displacement of the global model was then applied as the boundary condition for the local model. A quarter of the CLCC assembly was modeled in the global model, as shown in Figure 2.7. A symmetric boundary condition was imposed on the cut areas, and the node at the bottom center of the PCB board was fixed. This study focused on the second-level solder interconnects that connect the chip carrier and

the PCB board, so the dummy die in the chip carrier was not modeled. This global model included chip carrier, solder interconnects, copper pads on the PCB, and the PCB board. The local model consisted of the solder joint at the corner of the CLCC package and its attachment, with finer mesh than that in the global model, as shown in Figure 2.8. For the local model, the solder between the part and the board was modeled with four layers of elements, while only 1 layer was used in the global model. Since the elastic-plastic constitutive properties of SAC305 have not been established in the literature, in this study, the elastic and plastic properties of SnAg3.8Cu0.7 solder was substituted for SAC305. For the same reason, the material properties of Sn37Pb solder were substituted for the Sn62Pb36Ag2 solder.

In both the global and the local models, only solder was modeled with temperature-dependent elastic and inelastic properties. Other materials were modeled with a linear elasticity, as presented in Table 2.4. Elastic-plastic deformation of solder was modeled by Ramberg-Osgood strain hardening rule:

$$\sigma = C_{pl}\varepsilon_{pl}{}^{n} \qquad \textbf{Eqn. 2.5}$$

where C_{pl} and n are temperature-dependent constants, which are summarized in Table 2.5.

The creep of solder was modeled by the generalized Garofalo equation (3). The model constants for solder are summarized in Table 2.6:

$$\frac{\partial \varepsilon}{\partial t} = C_1[\sinh(C_2\sigma)]^{C_3}\exp(\frac{-C_4}{T}) \qquad \textbf{Eqn. 2.6}$$

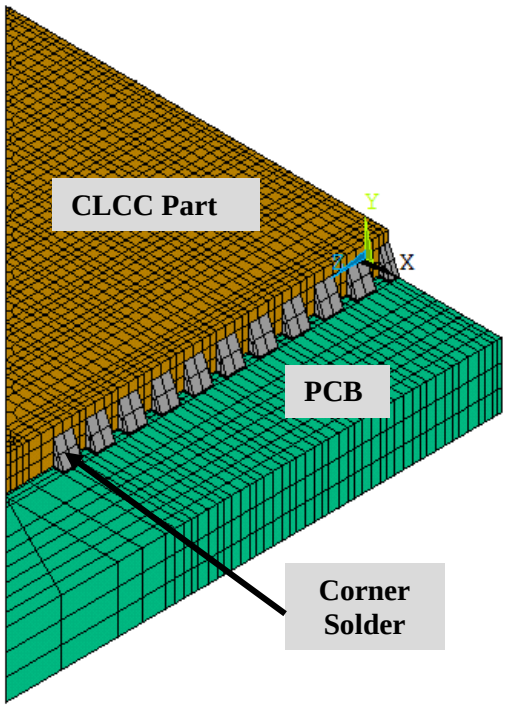

Figure 2.7: Global model.

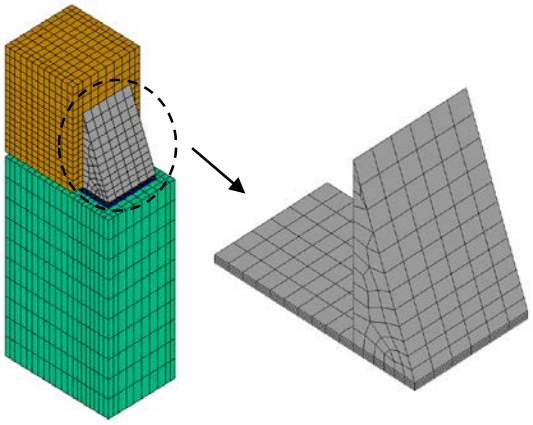

Figure 2.8: Local model.

Table 2.4: Elastic material properties [Dan 2001]

Material	E(MPa)	CTE (ppm/°C)	Poisson's Ratio
Ceramic	351645	5.8	0.17
Copper Pad	76000	17	0.34
PWB	17200	X/Y: 16.4	0.28
		Z: 64	
Sn37Pb [Zhang 2004] (Sn62Pb36Ag2)	2.92E4-44.2T(K)	23.9	0.4
SnAg3.8Cu0.7 [Zhang 2004] (SAC305)	4.37E4-22.3T(K)	20.9	0.4

Table 2.5: Plastic model constants for Sn37Pb and SAC305 [Zhang 2004]

Solder Alloy	C_{pl} (MPa)	n
Sn37Pb (Sn62Pb36Ag2)	152.5-0.6*T(oC)	0.25-0.00028*T(oC)
SAC387 (SAC305)	121.6-0.4*T(oC)	0.29-0.00046*T(oC)

Table 2.6: Solder creep model constants

Solder Alloy	C1 (1/s)	C2 (1/Pa)	C3	C4 (K)
Sn37Pb [Zhang 2004] (Sb62Pb36Ag2)	6640	1.15E-07	2.2	7130
SAC305 [Cuddalorepatta 2010]	6.07	1.8E-07	2.3	6714

The analysis get stabilized within three temperature cycles, and the strain energy density accumulated in the third cycle was used as the input for Morrow's model. A typical von-Mises stress at the end of the third upper dwell from the local model is presented in Figure 2.9. The von-Mises stress is much higher at the location beneath the chip carrier than the triangular fillet side area, and there is stress concentration at the component/solder interface near the component bottom

corner. Since the intermetallic compound was not included in the FEA model, the energy density averaged across only the central two layers of the bottom solder (as shown in Figure 2.10) was taken for ΔW.

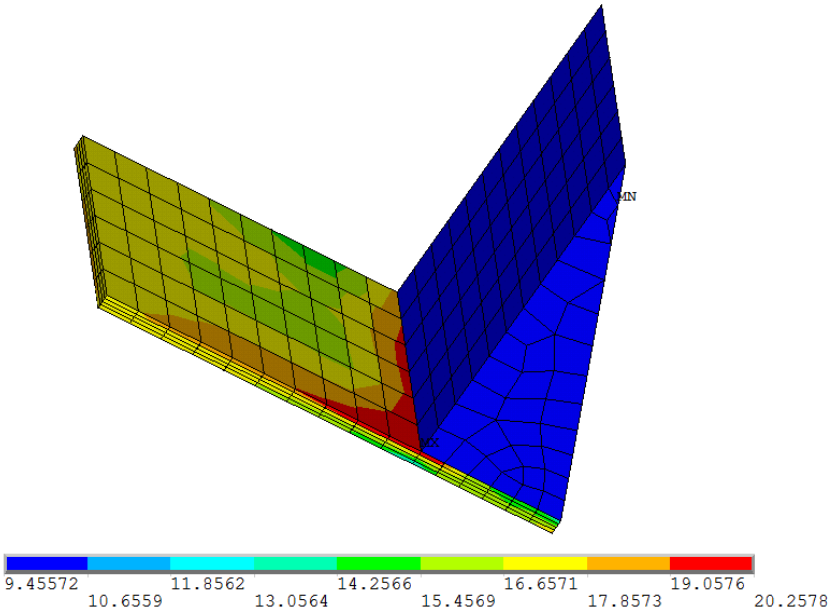

Figure 2.9: Strain energy density (MPa) of solder joint in local model.

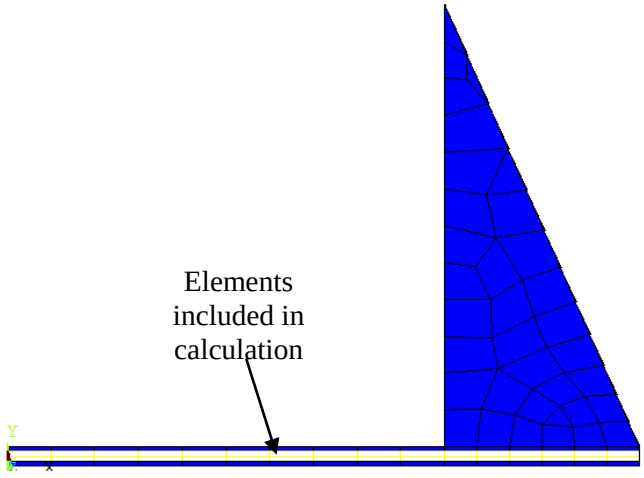

Figure 2.10: Central two layers included in calculation.

2.3.2.2 **Parameter Regression for Morrow's Model**

The cyclic strain energy density (ΔW) versus mean cycles to failure (N_{50}) from the nine reported temperature cycling tests is plotted in Figure 2.11 in a log-log scale. As a comparison, the correlation between cyclic total strain-range (Δɣ) versus mean cycles to failure (N_{50}) is plotted in Figure 2.12. For both the charts, a cross point between SnPbAg and SAC solder was observed. The fitted constants for an energy-based model (Morrow's model) and strain-based mode (Coffin-Mansion model) are presented in Table 2.7, and evaluation of the fitted constants is presented in Table 2.8. From Table 2.8, it could be found that the energy-based model has a better correlation to test data than the strain-range-based models.

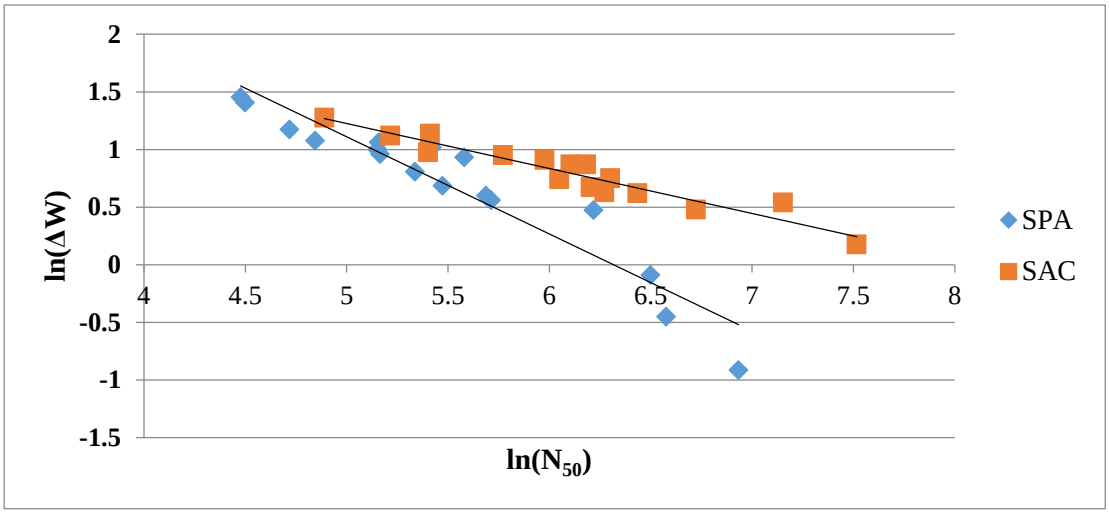

Figure 2.11: Energy-based correlation between ΔW and N50.

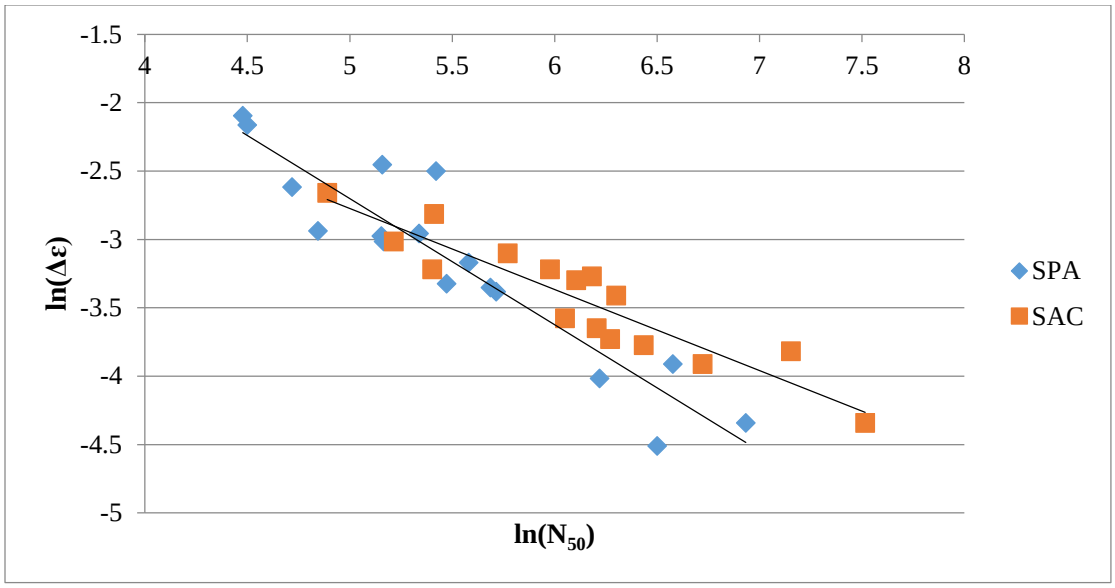

Figure 2.12: Strain-range-based correlation between ΔɣW and N50.

Table 2.7: Fitted constants for total energy and total strain-range based models

		n	C
Sn62Pb36Ag2	**ΔW**	-1.171	538.5
	ΔɣW	-1.085	7.9
SAC305	**ΔW**	-2.571	3533
	ΔɣW	-1.695	1.4

Table 2.8: Evaluation of fitted constants

Damage Matrix	Correlation		Sn62Pb36Ag2	SAC305
ΔW	P value	C	0	0
		n	0	0
	prob(f)		0	0
	R^2		0.959	0.918
Δɣ	P value	C	0.002	0.02
		n	0	0
	prob(f)		0	0
	R^2		0.867	0.858

The damage metric, namely the ΔW and Δε, were obtained from finite element analysis in this study. Therefore, the author recommended the future user of the constants in Table 2.7 employing the same sets of constitutive material properties as well as element selection scheme for volumetric averaging as in this study, in order to achieve the best prediction accuracy. It has to be noted that the constitutive properties of Sn62Pb36Ag2 and Sn63Pb37 were deemed to be the same, so did the elastic-plastic properties of SnAg3.8Cu0.7 and SnAg3.0Cu0.5.

2.3.3 **Complex Cycle Segmentation**

In this study, four approaches to cycle segmentation were used. In methods 1 through 3, the complex cycle was segmented into a primary cycle to represent the general ΔT of the complex profile and 6 consecutive mini-cycles to represent the minor temperature fluctuations at the upper dwell of the complex profile, as depicted in Figure 2.13 through Figure 2.16. The upper dwells of the primary cycles were at the minima, mean, and maxima of the upper excursions of the complex profile for methods 1, 2, and 3, respectively, and the lower dwells of the primary cycles were the

same as that of the complex profile for all three methods. In method 4, the complex cycle was segmented according to the sequence of occurrence, with 5 mini-cycles (in contrast to the 6 mini-cycles in methods 1 through 3) starting at the end of the primary cycle.

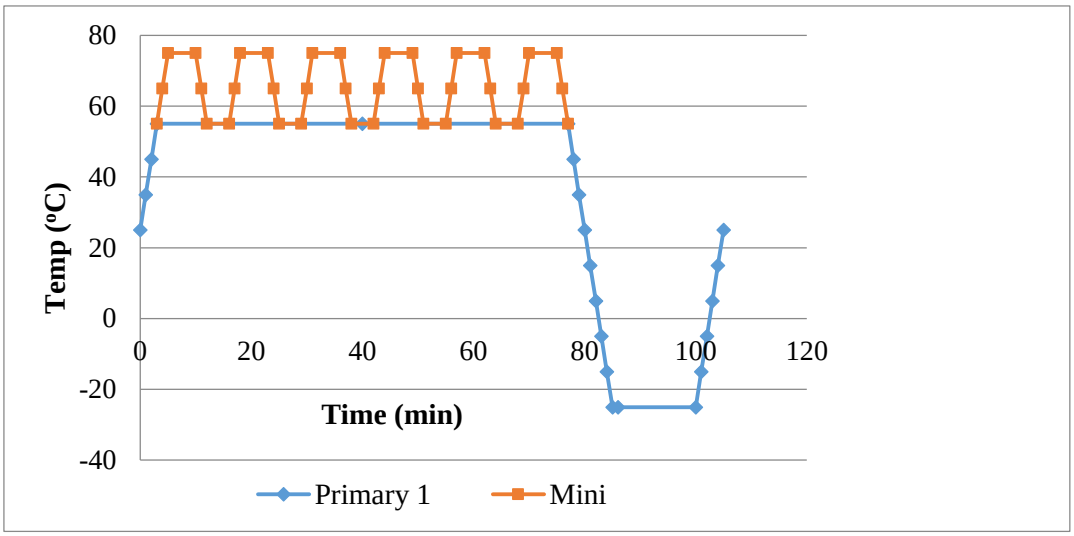

Figure 2.13: Segmenting method 1.

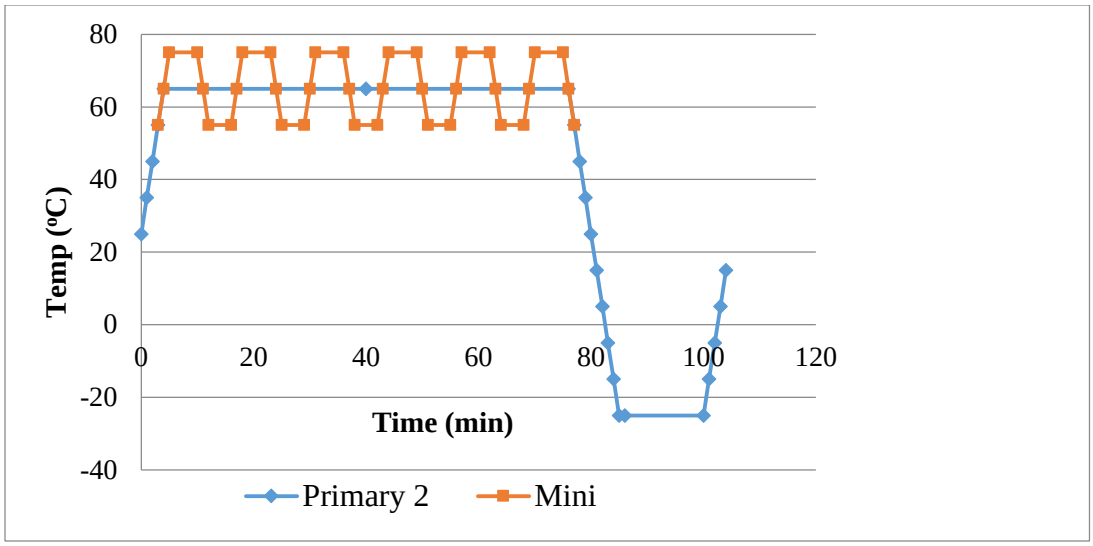

Figure 2.14: Segmenting method 2.

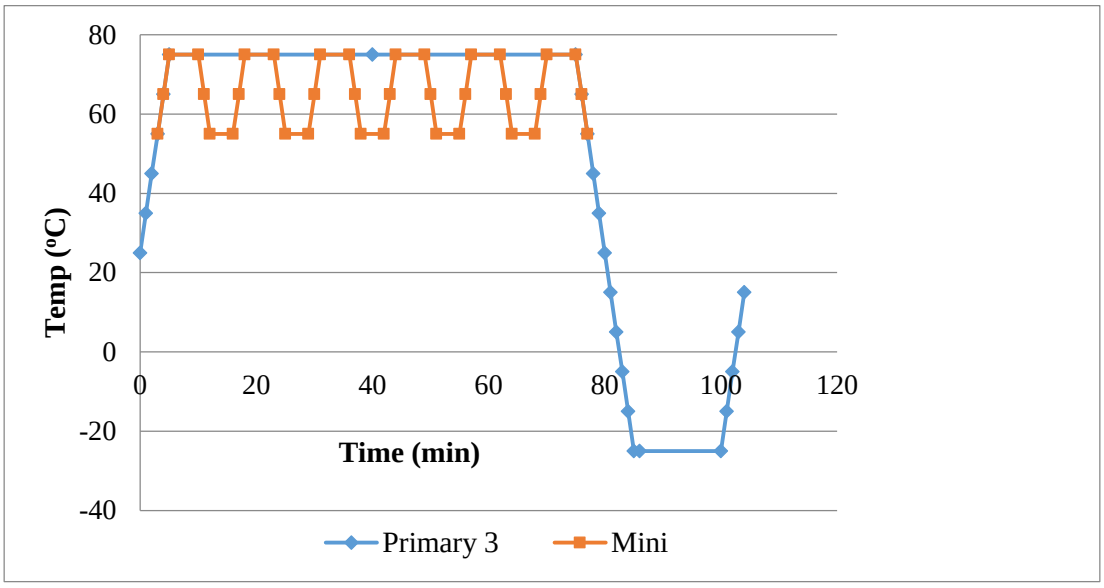

Figure 2.15: Segmenting method 3.

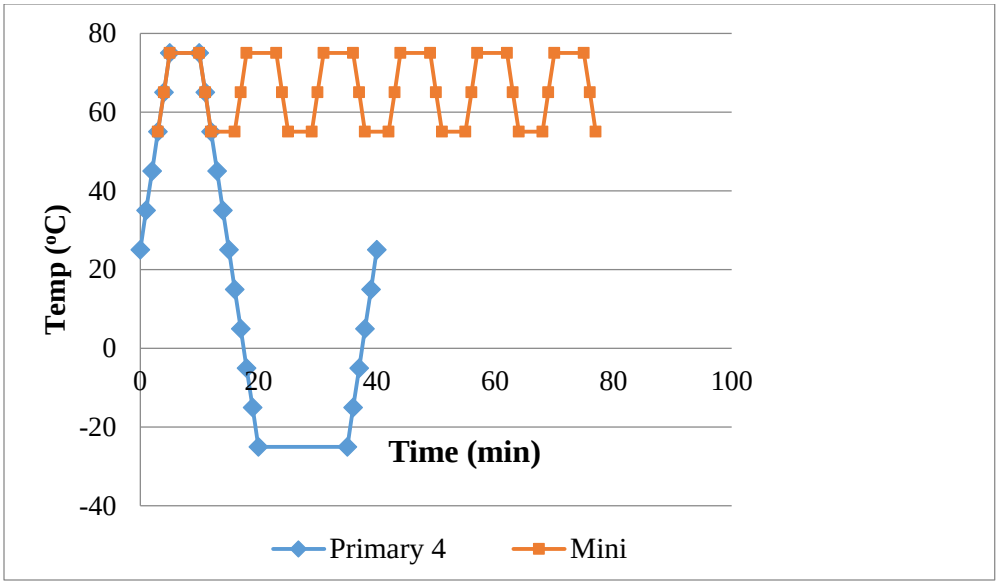

Figure 2.16: Segmenting method 4.

2.3.4 **Segmented Cycle Assessment**

Primary and mini cycles presented in Figure 2.13-Figure 2.16 were assessed by both Engelmaier model and Morrows model in this section.

2.3.4.1 **Engelmaier model based assessment**

The cycles to failure of the primary cycles under each segmenting method are plotted in Figure 2.17 and Figure 2.18 for 68 I/O and 84 I/O CLCCs, respectively. For comparison, the mean cycles to failure from the complex temperature cycling test is included in the Figure 2.17. The 84 I/O parts were predicted to have fewer cycles to failure than the 68 I/O parts because they have a larger package size. For the 68 I/O parts, it was found that the primary cycle by itself (before the damage from the mini-cycles was superposed) in segmenting method 3 predicted fewer cycles to failure than the complex test, suggesting that segmenting method 3 is a conservative approach. For 84 I/O parts, primary cycles 2 and 3 are predicted to have fewer cycles to failure than the complex test,

out of which primary cycle 2 has a better approximation to the complex test, making segmenting method 3 still the most conservative approach. The fact that the prediction for 84 I/O parts has, in general, a more conservative trend than that of 68 I/O parts reveals that the linear approximation of the strain range in Eqn. 2.3 is not accurate. Specifically, the package size should have a less significant effect on strain range than what the current linear estimation can describe. However, this study accepts, rather than addresses, this limitation of the Engelmaier model.

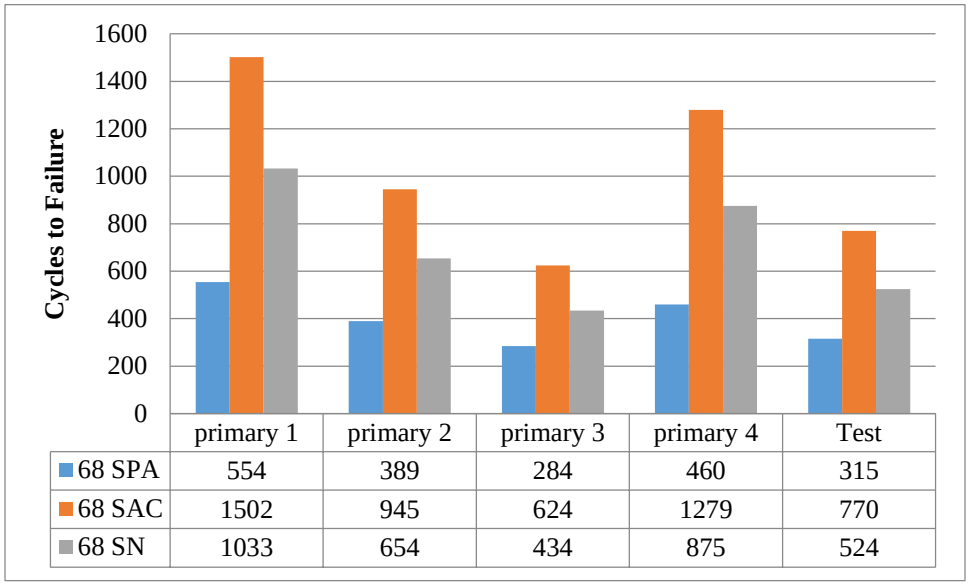

	primary 1	primary 2	primary 3	primary 4	Test
68 SPA	554	389	284	460	315
68 SAC	1502	945	624	1279	770
68 SN	1033	654	434	875	524

Figure 2.17: Life prediction of segmented primary cycles of 68 I/O CLCCs.

The cycles to failure of the 6 mini-cycles are presented in Figure 2.18. It was found that SAC305 solder is the most reliable and SnPbAg is the least reliable under the mini-cycles. This trend is consistent with the primary cycles. However, SnPbAg is relatively more vulnerable under the mini-cycles than SAC305 and SN100C solders, since the predicted life ratios between the 6 mini-cycles and the primary cycles are much smaller for SnPbAg solder than for the other solder materials, as

shown in Table 2.9. This suggests that SnPbAg solder is either more vulnerable under an elevated mean (the mean temperature of the mini-cycle is higher than the primary cycle), or that it manifested a faster creep rate (the cycle frequency of the mini-cycle is greater than that of the primary cycle) than SAC305 and SN100C solders.

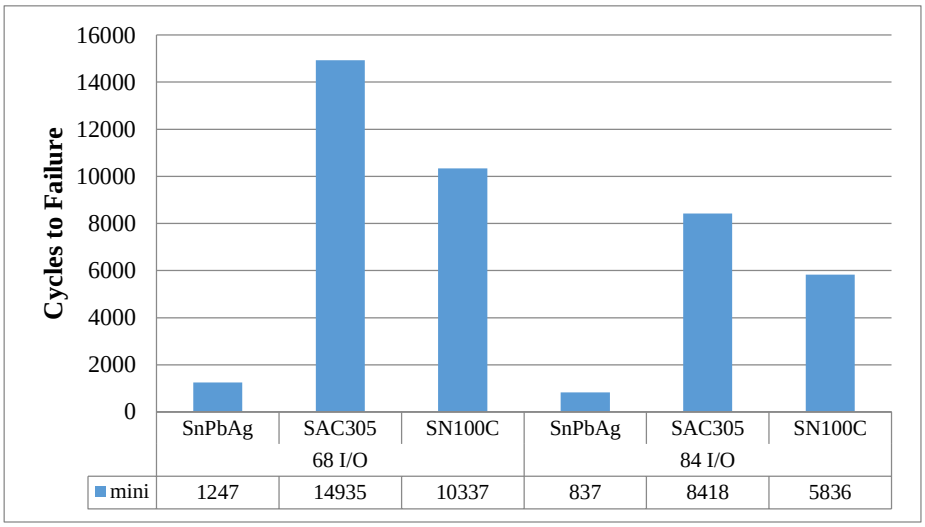

Figure 2.18: Life prediction of 6 segmented mini-cycles.

Table 2.9: Modeled Life Ratios between 6 Mini-Cycles and Primary Cycles

		primary 1	primary 2	primary 3	primary 4
68	**SPA**	2.25	3.21	4.39	2.71
	SAC	9.94	15.80	23.93	11.68
	SN	10.01	15.81	23.82	11.81
84	**SPA**	2.29	3.23	4.43	2.80
	SAC	9.99	15.73	23.58	12.20
	SN	10.03	15.73	23.44	12.34

2.3.4.2 **Morrow's model based assessment**

The von-Mises stress of the complex cycle was higher than the primary in segmentation method 2 and 3, as shown in Figure 2.19. When the von-Mises stress of the mini cycle got stabilized in Figure 2.20, it was not equivalent to the upper excursion of the complex cycle in Figure 2.19. The first mini cycle in the complex cycling had higher stress than the following mini cycles since the first mini cycle started at the end of the temperature rise period when the maximum expansion mismatch occurred. In another word, the stabilized strain energy from Figure 2.20 would be optimistic for estimating the mini cycles. The life predictions of the primary cycles under the four segmenting methods are tabulated in Table 2.10. The life predictions of the mini cycles were quoted from the upper excursion of the complex cycles.

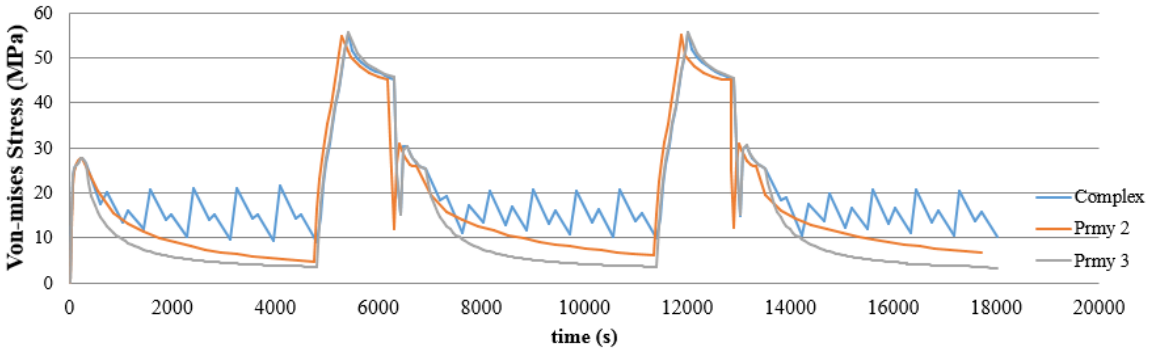

Figure 2.19: Von-Mises stress of complex cycle and primary cycle

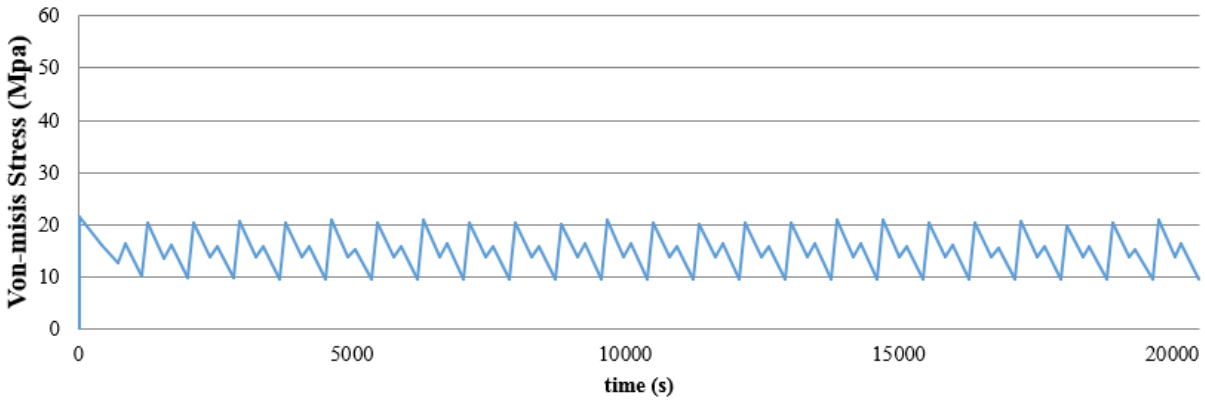

Figure 2.20: Von-Mises stress of mini cycles

Table 2.10: Segmented cycle assessment by Morrow's model

	SnPb (cycles)		SAC (cycles)	
	68 I/O	**84 I/O**	**68 I/O**	**84 I/O**
primary 1	637	370	1829	966
primary 2	404	251	1092	616
primary 3	277	128	516	393
primary 4	377	231	949	537
cplx-test	321	266	789	660
mini	3385	2406	11228	8159

2.3.5 **Modeling of the Complex Temperature Cycle by Damage Superposition**

Palmgren [Palmgren 1924] created the linear superposition model, and Miner [Miner 1945] further developed it. The linear superposition model, referred to as Miner's rule, states that "damage (defined as the inverse of life) can be superposed linearly and that failure occurs when the cumulative damage fraction (defined as fraction of life used up by an event or a series of events) equals unity." Even though Miner's rule does not consider the effect of the stress state of each loading, it is common practice to superpose damage from different loading sources for the sake of simplicity.

Miner's rule, as in Eqn. 2.6 is used to linearly superimpose the damage of the primary cycle and mini-cycles, thereby modeling the solder fatigue life under complex temperature cycling conditions. For segmenting methods 1 through 3, n is 6, and for segmenting method 4, n is 5.

$$\frac{1}{N_{cplx}} = \frac{1}{N_{pr}} + \frac{n}{N_{mini}} \qquad \textbf{Eqn. 2.7}$$

2.3.5.1 **Engelmaier model based superposition**

The cycles to failure from Miner's rule and from the mean of the complex test results are presented in Figure 2.21 through Figure 2.23, from which the error bar of the test is defined by the standard deviation of the test results. The relatively large variance in tested 84 I/O assemblies makes the predictions under segmenting methods 1, 2, and 4 fall within the test error bar. Method 3, which is a conservative approach defining the peak of the primary cycle at the maxima of the complex cycle, does not fall within the test error bar. A less scattered 68 I/O test result with a smaller error bar makes segmenting method 2 a better option than the others.

The Engelmaier model provides a more conservative prediction for 84 I/O parts than for 68 I/O parts, suggesting the inherent limitation of the Engelmaier model that estimates the linear relationship between package size and strain range. During the regression process, to generate the model parameters, 9 data points from both the 68 I/O and 84 I/O samples constituted the 18 data points for each solder material; so the model parameters were derived from a compromise between the 68 I/O and 84 I/O parts. Discrepancies between the 68 I/O and 84 I/O samples were found, even when the Engelmaier model is used to model the segmented primary cycles before Miner's rule is applied, as plotted in Figure 2.17 and Figure 2.18.

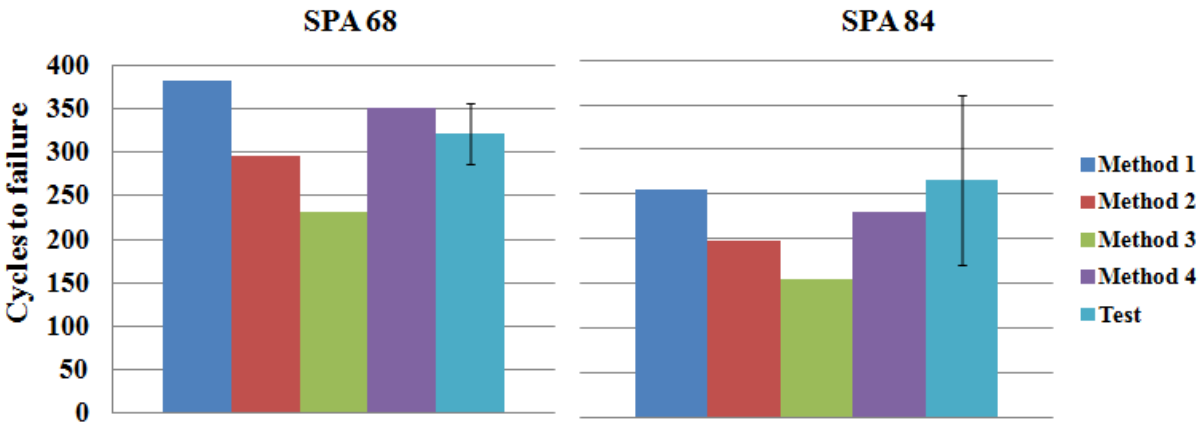

Figure 2.21: Engelmaier model based superposition and the complex test results of SnPbAg solder

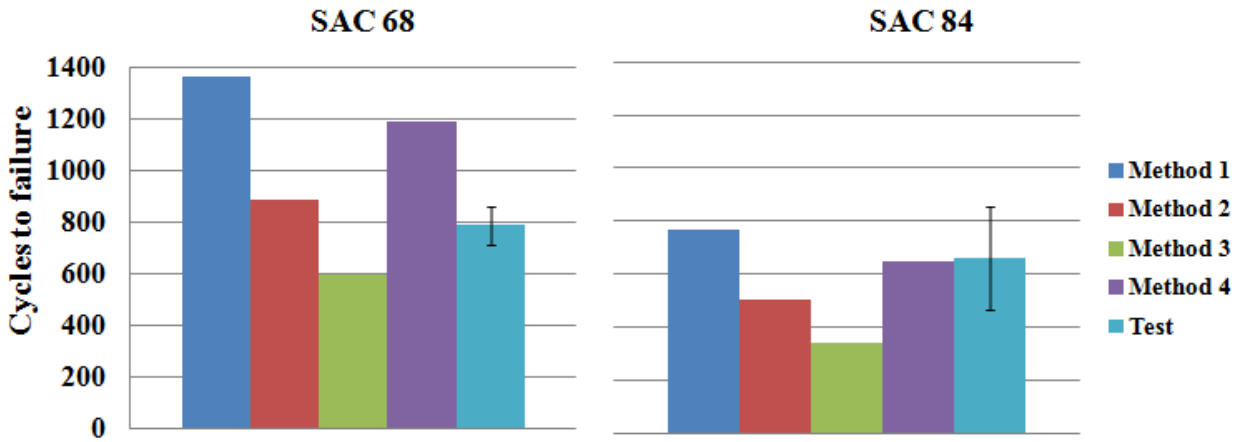

Figure 2.22: Engelmaier model based superposition and the complex test results of SAC305 solder

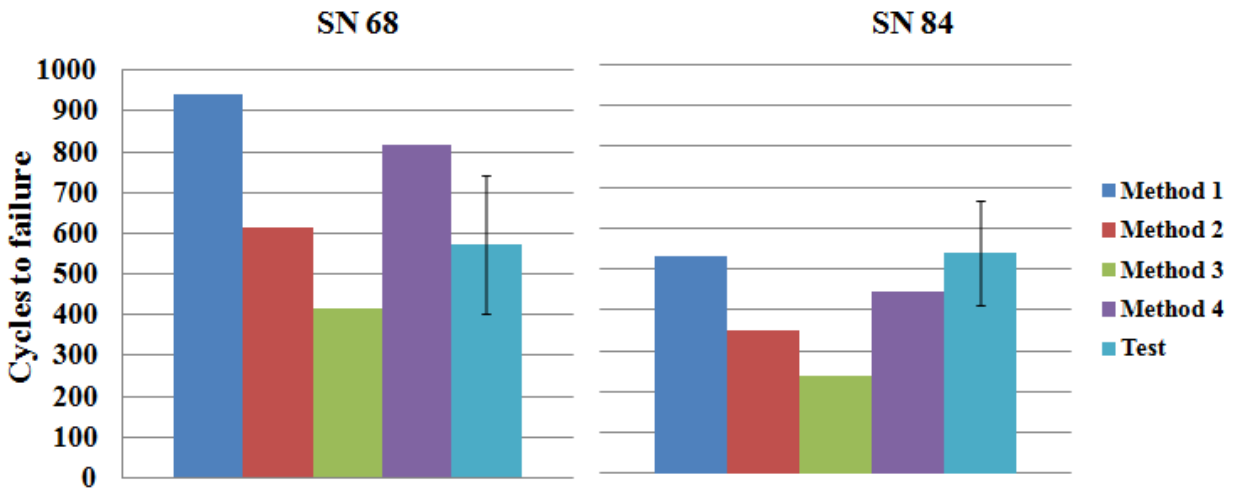

Figure 2.23: Engelmaier model based superposition and the complex test results of SN100C solder.

The root mean squares of the modeling errors of 68 I/O and 84 I/O assemblies under the complex cycle are calculated by Eqn. 2.8, and the results are plotted in Figure 2.24. The linear superposition introduces another modeling error on top of the errors from modeling the simple temperature cycles. The modeling accuracies of the Engelmaier model on a standard temperature cycling condition with a fixed ΔT (as in Table 2.1) are 21%, 22%, and 26% for Sn62Pb36Ag2, Sn96.5Ag3Cu0.5, and SN100C solder, respectively, while the modeling accuracies of the complex cycling using Miner's rule range from 27% to 76% for different solder materials under different segmenting methods.

Despite the limitations of the Engelmaier model and Miner's rule, modeling errors from all the segmenting methods are less than 100%; in other words, the modeling accuracy is within a factor of 0.5 to 2 of the complex test results. From the data, segmenting method 2 provides the best correlation with the complex temperature cycling test by defining the maximum temperature of

the primary cycle at the mean of the upper excursion of the complex cycle and keeping the mini cycle as the upper excursion of the complex cycle. In this study, method 3 generates around a 40% error as the second best approach; however, in a future application where the range of the mini cycle is large enough, defining the maxima of the primary cycle as the maxima of the complex cycle might incur a larger error than what is presented in this study. Segmenting the complex cycle according to the sequence of occurrence, as presented in method 4, provided 30%, 59%, and 40% errors for SnPbAg, SAC305, and SN100C solder, respectively, with only the prediction of SAC305 and SN100C soldered 68 I/O parts outside the error bar of the test, as shown in Figure 2.22 and Figure 2.23.

$$EMS\ of\ Errors\ \% = \sqrt{\frac{(Error\ of\ 68\ I/O)^2 + (Error\ of\ 84\ I/O)^2}{2}} \qquad \textbf{Eqn. 2.8}$$

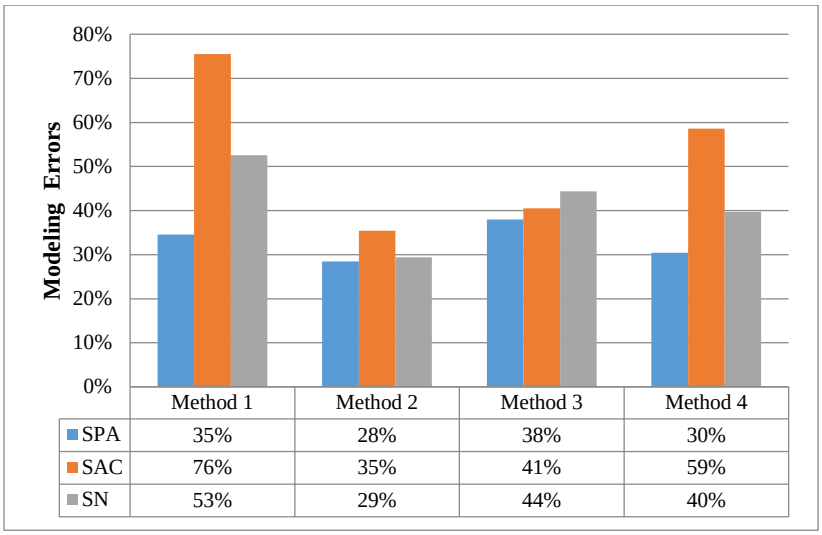

Figure 2.24: Root mean squares of 68 I/O and 84 I/O modeling errors.

2.3.5.2 **Morrow's model based superposition**

Prediction errors of Morrow's model based superposition for 68 I/O and 84 I/O CLCCs are presented in Figure 2.25 and Figure 2.26. Root mean square of the errors of the two size is presented in Figure 2.27. Based on Figure 2.27, segmenting method 2 (defining the maxima of primary at the mean of mini cycle) was recommended, for its best correlation with test. Also, segmenting method 4 (segmenting by time sequence) was recommended as well, for its broader application in the field condition with more complicated profile than the patterned complex cycle in this study. This conclusion was the same with the Engelmaier model based modeling approach. At the meantime, finite element analysis modeled the strain energy of the complex cycle directly without profile segmentation (refered to as "direct modeling") and use the cyclic energy under a complete complex temperature cycle as the input of Morrow's model. However, the direct modeling generated bigger modeling errors than superposition method 2 and method 4.

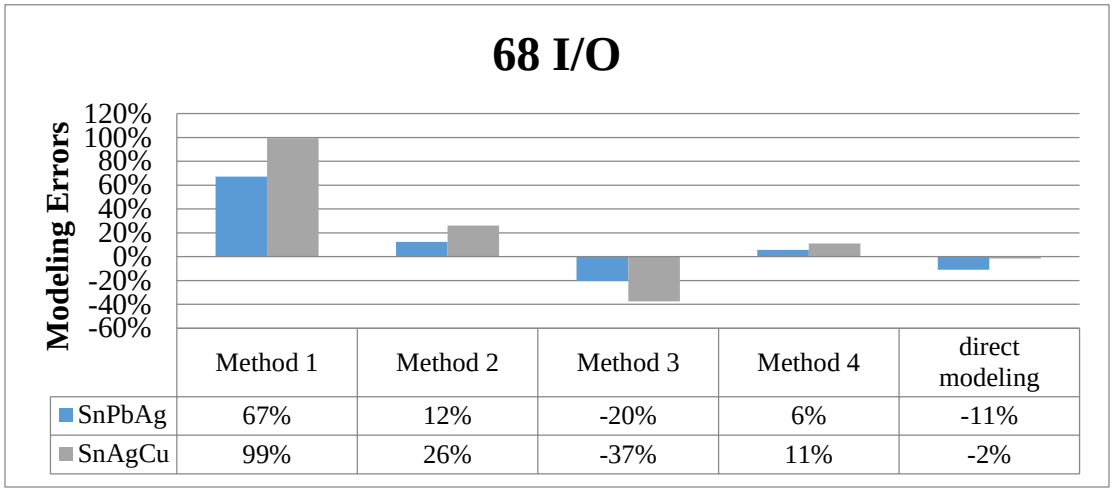

	Method 1	Method 2	Method 3	Method 4	direct modeling
SnPbAg	67%	12%	-20%	6%	-11%
SnAgCu	99%	26%	-37%	11%	-2%

Figure 2.25: Errors of Morrow's model for predicting 68 I/O CLCC part under complex temperature cycling.

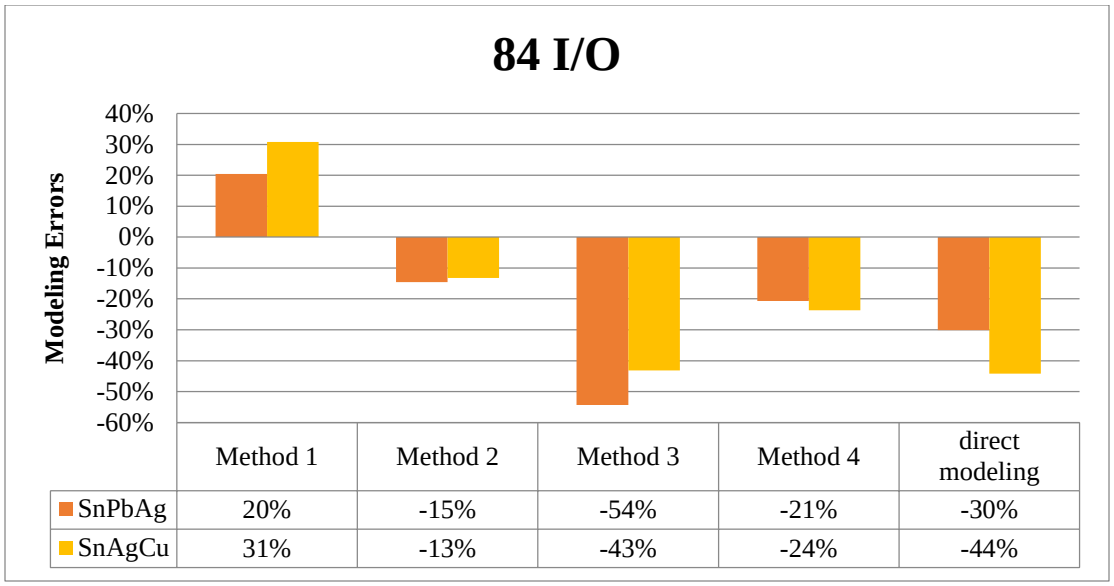

Figure 2.26: Errors of Morrow's model for predicting 84 I/O CLCC part under complex temperature cycling.

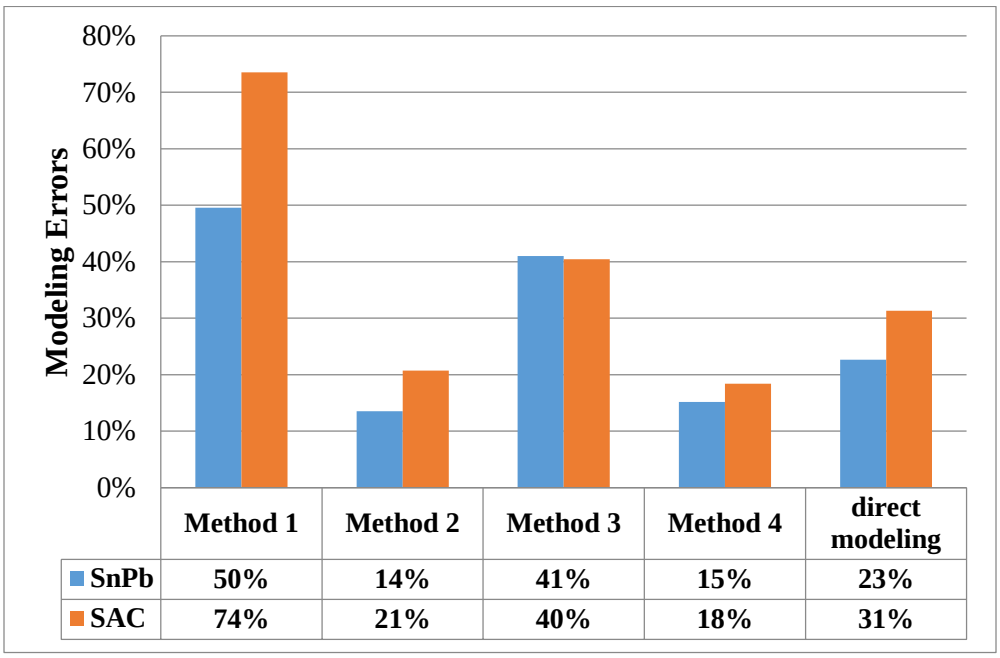

Figure 2.27: RMS of modeling errors for complex temperature cycling

2.3.6 **Approximation of the complex cycle by standard temperature cycle**

To investigate if the solder interconnect life under the complex temperature cycling test can be approximated by a standard temperature cycling (with single ΔT) and ignoring the temperature fluctuation during the upper excursion, the Engelmaier model and Morrow's model predictions for the primary cycles in segmenting method 1-4 were compared with the complex temperature cycling test in Figure 2.28-Figure 2.31. It was found that primary cycle in method 3 (defining the upper dwell of standard temperature cycling at the peak of the upper excursion of the complex cycle) should be adopted since it is the only conservative interpretation of the complex profile.

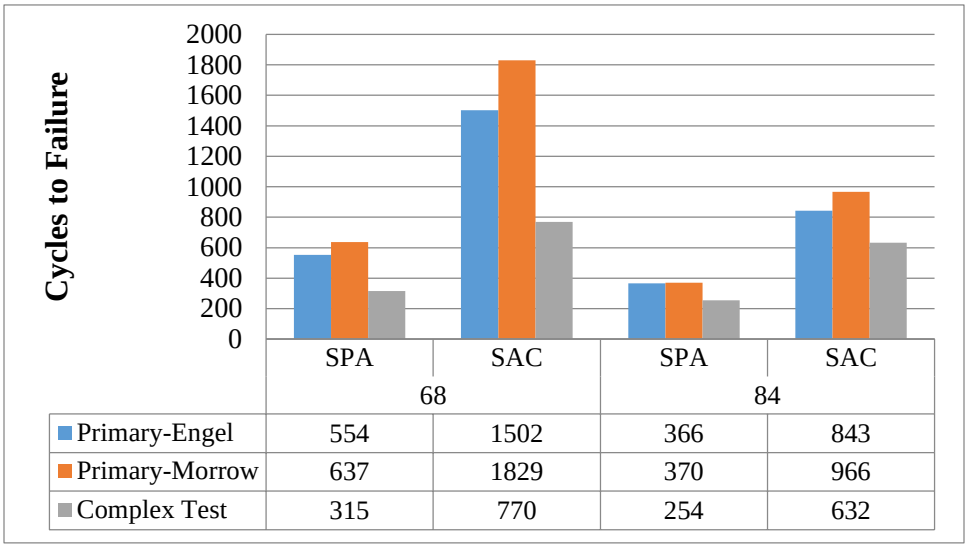

	SPA	SAC	SPA	SAC
	68		84	
Primary-Engel	554	1502	366	843
Primary-Morrow	637	1829	370	966
Complex Test	315	770	254	632

Figure 2.28: Comparison between complex test and prediction of primary cycle in segmenting method 1.

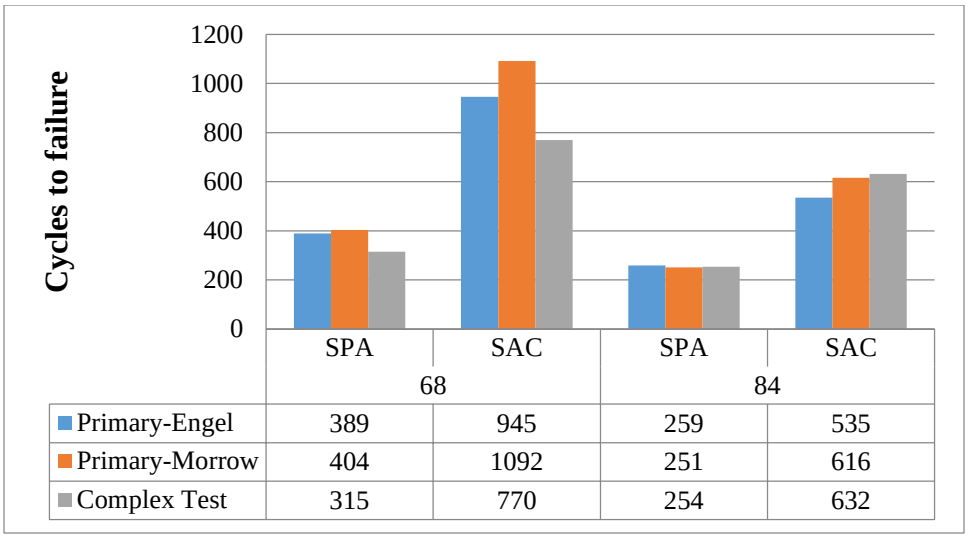

Figure 2.29: Comparison between complex test and prediction of primary cycle in segmenting method 2.

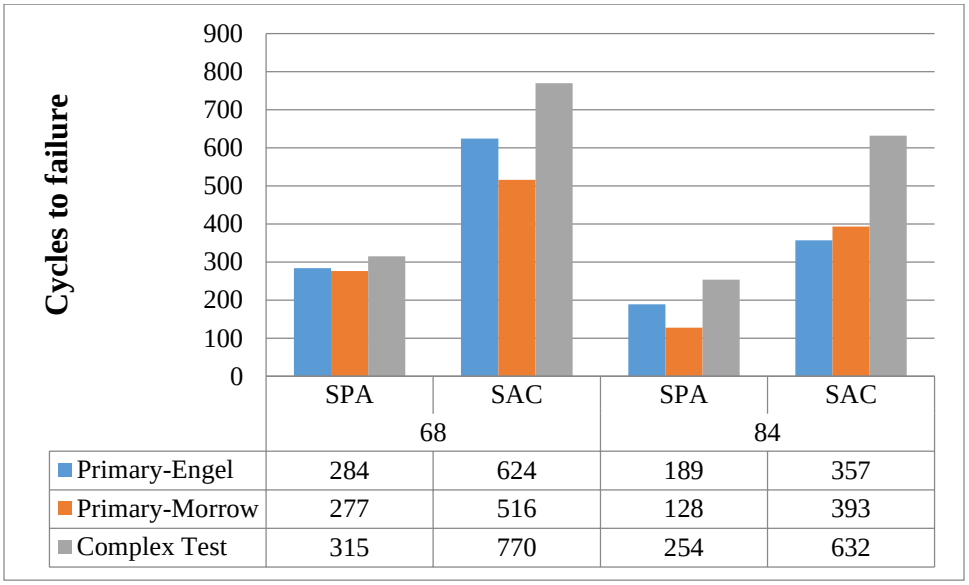

Figure 2.30: Comparison between complex test and prediction of primary cycle in segmenting method 3.

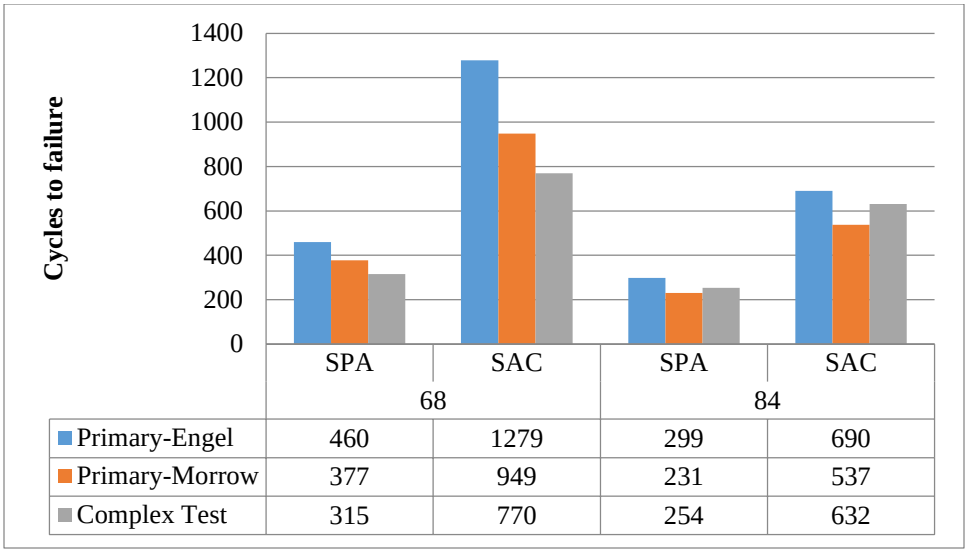

Figure 2.31: Comparison between complex test and prediction of primary cycle in segmenting method 4.

2.4 Summary

Strategies for assessing solder fatigue interconnect reliability under a chamber controlled complex temperature cycle with mini-cycles occurring at the upper excursion were investigated. Segmenting the complex cycle (with varying ΔT) is a prerequisite for applying the Engelmaier model. Several segmentation approaches were proposed based on analysis of the cycle pattern. One approach (method 2) targeted equating the solder damage under a complex cycle with the superposition of two pieces of damage: damage due to the averaged ΔT of the complex cycle and damage from the ΔT of the upper excursion (mini-cycles). In order to compensate for the possible inaccuracies of the Engelmaier model and Miner's rule, a conservative (method 3) and an optimistic (method 1) shift in defining the average ΔT of the complex cycle were also included. Another segmenting approach (method 4) partitioned the complex cycle into a set of half or complete cycles following the sequence of occurrence. This method (method 4) was expected to

have a broader application since any field thermal profiles can be partitioned in this fashion, as long as Miner's rule is proved to be capable of modeling the complex temperature cycling in this study. The optimal complex cycle segmenting method out of all the proposed candidates was determined by comparing with the result of the complex temperature cycling test.

Model parameters of Engelmaier model and Morrow's model for assessing standard temperature cycles (with single ΔT) were generated in this study first. Both the model were subsequently used to assess the damage of the segmented cycles. Based on the linear damage superposition (Miner's rule) of the predicted lives of the segmented cycles, modeling errors from all the proposed segmenting approaches were within 100%.

The authors recommend that analysts select a cycle segmentation method according to real conditions. For a temperature cycle with only three dwell points, such as in the case study presented in this paper, the average segmenting method (method 2) with the primary cycle maxima defined at the mean of the mini cycle is recommended; however, in a more complex situation with more than three dwell points, the complex cycle should be segmented according to the sequence of occurrence (method 4). Also, when a standard temperature cycling (with a single ΔT) was used to represent the damage of the field complex condition with multiple peak and valley during the usage, defining the upper dwell temperature at the peak temperature of the usage was the only conservative representation among all the other methods discussed in this study.

Chapter 3 Combined Temperature and Power Cycling

This chapter developed modeling approaches and quantified accuracies for predicting solder interconnect life under combined temperature and power cycling. The temperature history resultant from the combined temperature and power cycling was a complex temperature cycling with varying temperature mean and amplitude, as well as spatial thermal gradients. The modeling approaches included: 1) modeling the strain energy under the resultant complex temperature cycling and employing the energy based fatigue life models; 2) segmenting the resultant complex temperature cycle into multiple simple temperature cycles with a single temperature range for each , then assessing the life expectancy of the solder interconnect under the segmented simple temperature cycles and at last applying Miner's rule to superpose the damage; 3) estimating solder damage under the resultant complex temperature cycling by a standard temperature cycling with a single temperature range without damage superposition. Physical test of the combined cycle was also conducted to validate and quantify all the modeling approaches. Test specimens included plastic ball grid array (PBGA) packages mounted on PCB boards, assembled with either Sn37Pb or Sn96.5Ag3.0Cu0.5 (SAC305) solder.

3.1 Combined temperature and power cycling test

Combined power and temperature cycling tests were conducted with test vehicles composed of one 192 I/O peripheral ball grid array (BGA) surface mounted on printed circuit board (PCB) with either eutectic SnPb or SAC305 solder. The molding compound dimensions of each BGA were 14mm × 14mm × 1mm. A non-functional silicon die at the size of 12mm × 12mm × 0.25mm was attached to a 0.2 mm thick organic board inside each BGA. Each test board was 50mm × 55mm × 1.4 mm, constructed of 370HR laminate, and the copper lands were coated with OSP (Organic Solderability Preservative) finish. Once mounted on the test board, all the 192 solder interconnects

of the BGA created a resistance network that could be electrically monitored during an applied test condition. Solder ball layout of the BGA package is presented in Figure 3.1

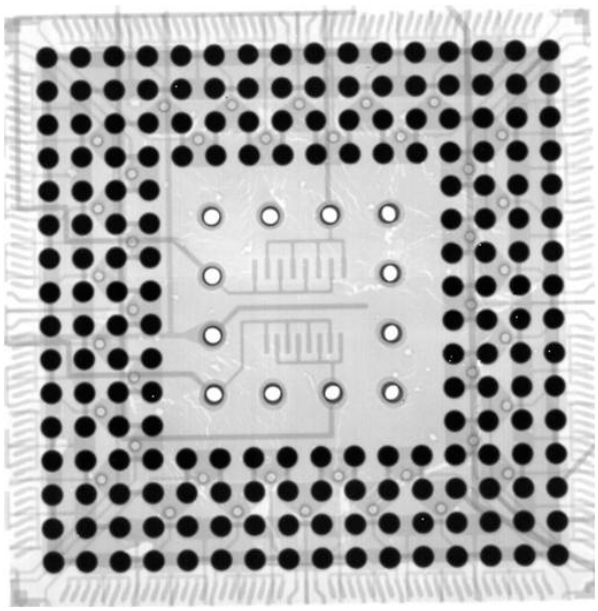

Figure 3.1: Solder ball layout of the BGA package under X-ray.

There are totally three sets of tests. The first is the combined temperature and power cycling test (named combined test) as in Figure 3.2. The temperature cycling portion of the combined test is from -40 ^{o}C to 100 ^{o}C, dwelling for 15 minutes and 60 minutes at the lower and higher extremes, respectively. The power cycling portion is achieved by foil heaters attached to top of the BGAs. The heater is 12 mm in diameter and has a resistance of 25 ohm. The heaters, which are attached on the BGA by thermal epoxy, are activated by 5 volt voltage stimuli with 5 minutes on followed by 5 minutes off duty cycle. The power cycling is applied only during the high temperature dwell portion of the concurrent temperature cycle. Six power cycles are applied during each high temperature dwell of the chamber. A thermocouple mounted on the back side of the PCB board

under the location of the BGA is used to monitor the resultant board temperature during the combined condition. Test vehicle with the heater attachment is shown in Figure 3.3. The second test is the stand-alone temperature cycling, the profile is as the temperature cycling portion in Figure 3.2. The third test is a power cycling activated by a 5 volt voltage stimuli with 5 minutes on followed by 5 minutes off duty cycle, under isothermal 100 ^{o}C constant temperature environment (named iso-thermal power cycling), as shown in Figure 3.4.

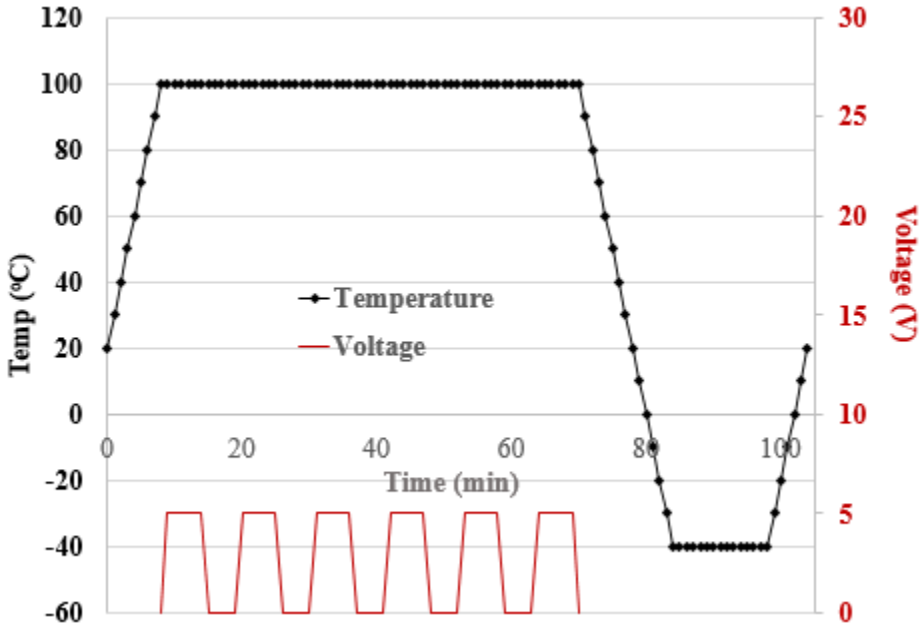

Figure 3.2: Combined Temperature and Power Cycling Profile.

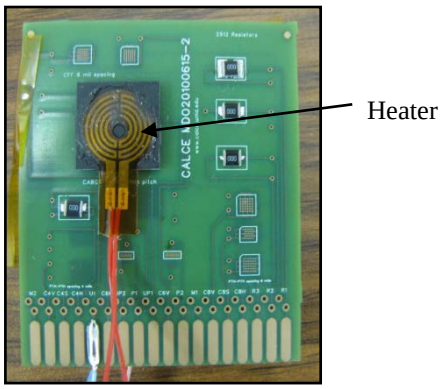

Figure 3.3: Test vehicle with heater.

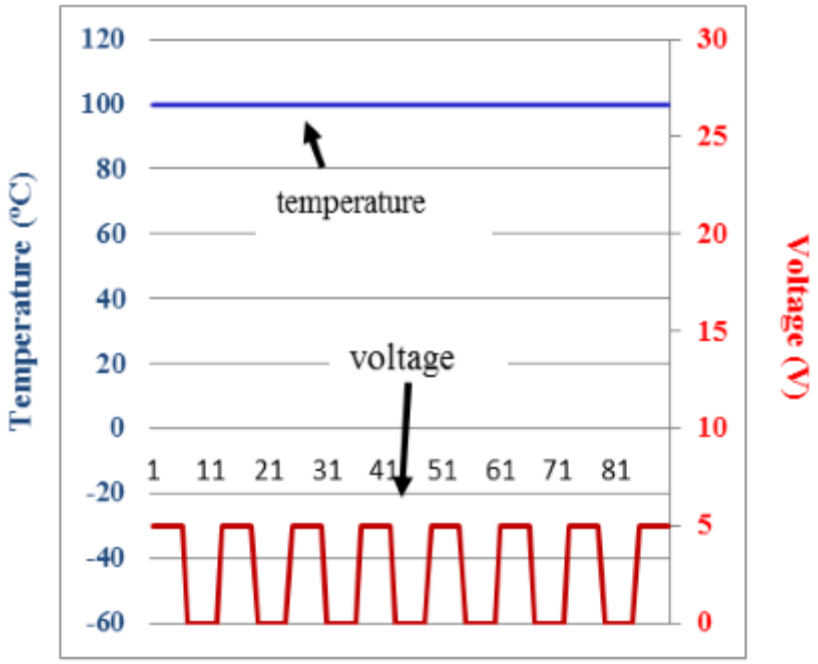

Figure 3.4: Iso-thermal power cycling profile.

Before the test was initiated, the resultant temperature profile under the combined temperature and power cycling were characterized with three test specimens created specifically for temperature characterization. Each temperature characterization specimen was instrumented with four thermocouples as in Figure 3.5. The placement of the thermocouples included: one at the top center of BGA and covered by the heater (T1), two at the corner of BGA top surface without the coverage of the heater (T2 and T3), and the other one at the back side of the PCB board but under the BGA location (T4). The power cycling generated an extra cyclic temperature rise (ΔT) sitting on top of the temperature cycling. The measurement in Figure 3.6 showed that the power cycling generated about 35 ^{o}C ΔT at the center of BGA surface and 20 ^{o}C ΔT at the corner of BGA surface and the bottom of PCB board. Thus, there was about 15 ^{o}C thermal gradient from the center to the corner of BGA top surface, and from the top surface of BGA to the bottom of the board.

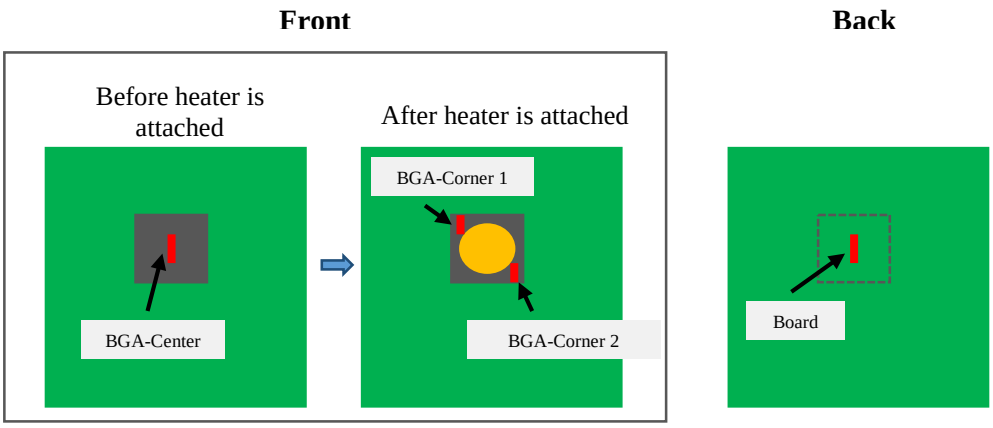

Figure 3.5: Thermocouple locations for thermal characterization

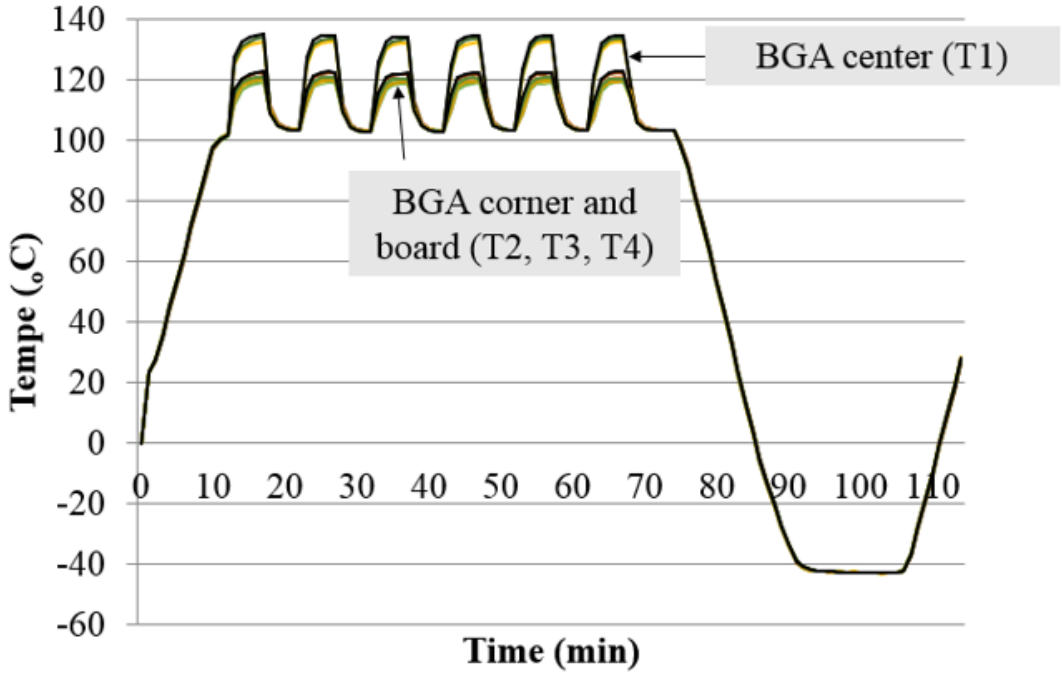

Figure 3.6: Resultant Temperature under the Combined Temperature and Power Cycling.

Table 3.1: Test Matrix

	Combined temperature and power cycle	Stand alone temperature cycle	Iso-thermal power cycle
SnPb	12	12	12
SAC305	12	12	12

Test matrix and sample size a listed in Table 3.1. Failure was defined as 20% increase in nominal resistance in 5 consecutive reading scans [IPC-9701A]. The test was terminated at 7800 cycles after the majority of test specimens had failed. After the parts were taken out from the chamber, micro-sectional analysis was conducted to investigate the failure site. From the micro-sectional analysis, solder joint cracks under both the combined test and the stand-alone temperature cycling test were initiated from the corner of the "solder neck" region at the component side, as shown in Figure 3.7. A Weibull plot of the failure data is presented in Figure 3.8. After 7800 cycles, all the parts under the combined test failed. For the stand-alone temperature cycling test, 11 out of 12 SnPb parts failed and 10 out of 12 SAC305 parts failed. One early failure of a SnPb specimen under the stand-alone temperature cycling occurred at 249 cycle, and it has not been included in the Weilbull plot. However, failure analysis of this part did not discover observable reasons for this early failure. By comparing the characteristic lives (η) of combined test and the stand-alone temperature cycling test, it was found that the involvement of power cycling degraded the thermal-cycled fatigue life of solder interconnect by 2/3 and 3/5 for SnPb and SAC305 solder, respectively.

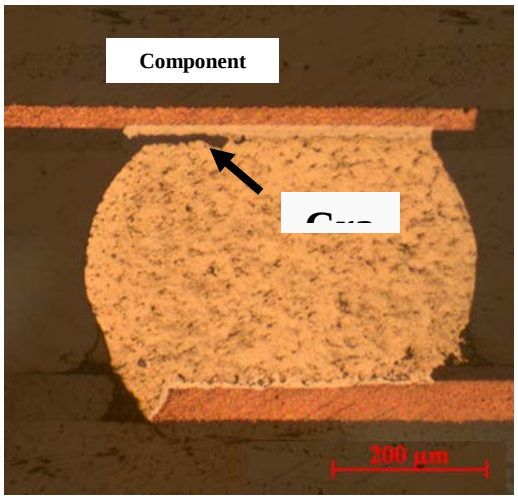

Figure 3.7: Crack in Solder Interconnect under Optical Microscope

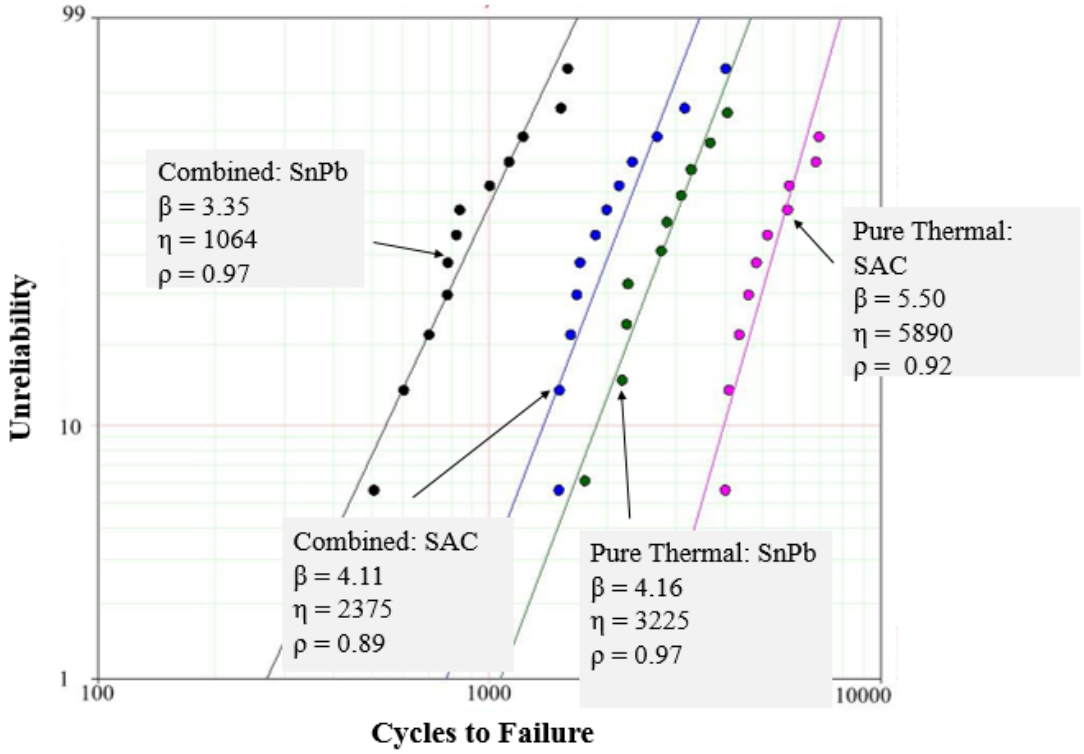

Figure 3.8: Reliability of combined cycling and stand-alone temperature cycling

3.2 Profile segmentation of the resultant complex temperature cycling

The temperature history resultant from the combined temperature and power cycling was a complex temperature cycling with varying temperature mean and amplitude, as well as spatial thermal gradient. Modeling of this complex temperature cycling could be based on analyzing the complete complex cycle, or segmenting the complex cycling into a couple of standard temperature cycle (with single ΔT in each) and applying damage superposition. In this section, four approaches to cycle segmentation were used. In methods 1 through 3, the complex cycle was segmented into a primary temperature cycle to represent the general ΔT of the complex profile and 6 consecutive mini temperature cycles to represent the minor temperature fluctuations at the upper excursion of the complex profile, as depicted in Figure 3.9-Figure 3.12. The upper dwells of the primary cycles were at the minima, mean, and maxima of the upper excursions of the complex profile for methods 1, 2, and 3, respectively, and the lower dwells of the primary cycles were the same as that of the complex temperature profile for all three methods. In method 4, the complex cycle was segmented according to the sequence of occurrence, with the primary cycle starting at the end of the mini cycles. In all the segmenting method, the mini cycles were defined as the upper excursion of the resultant complex temperature profile, except that there were only 5 mini cycles in method 4 whereas 6 mini cycles in method 1-3.

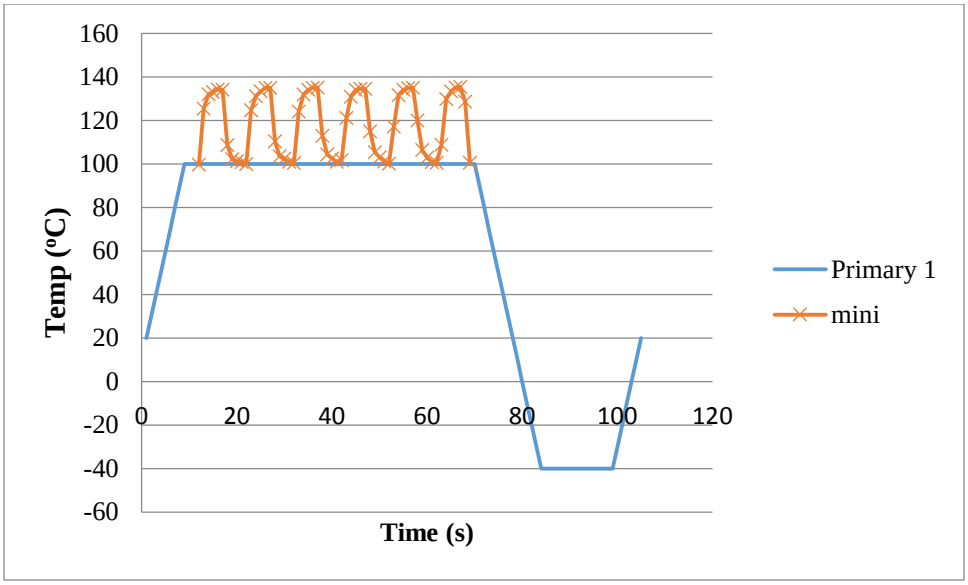

Figure 3.9: Segmenting method 1

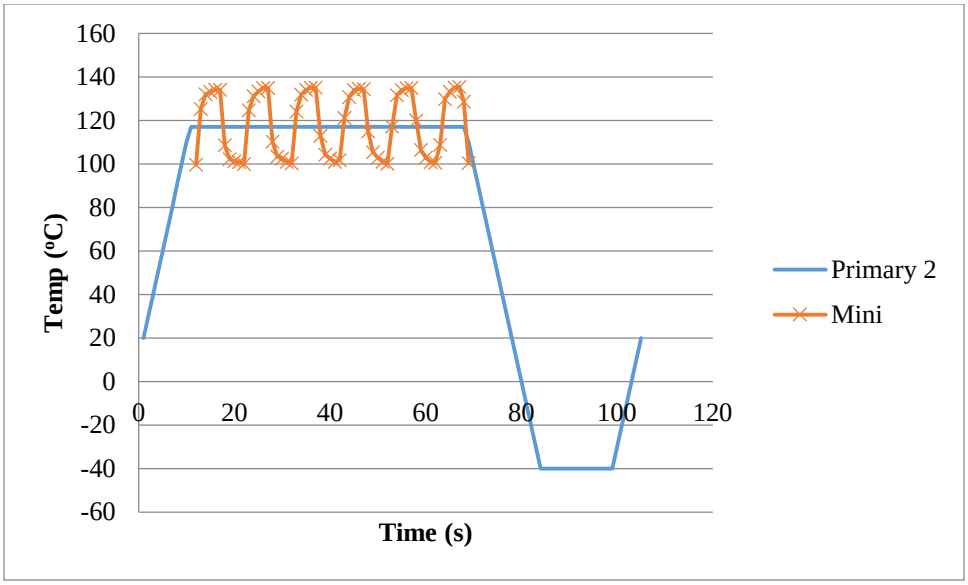

Figure 3.10: Segmenting method 2

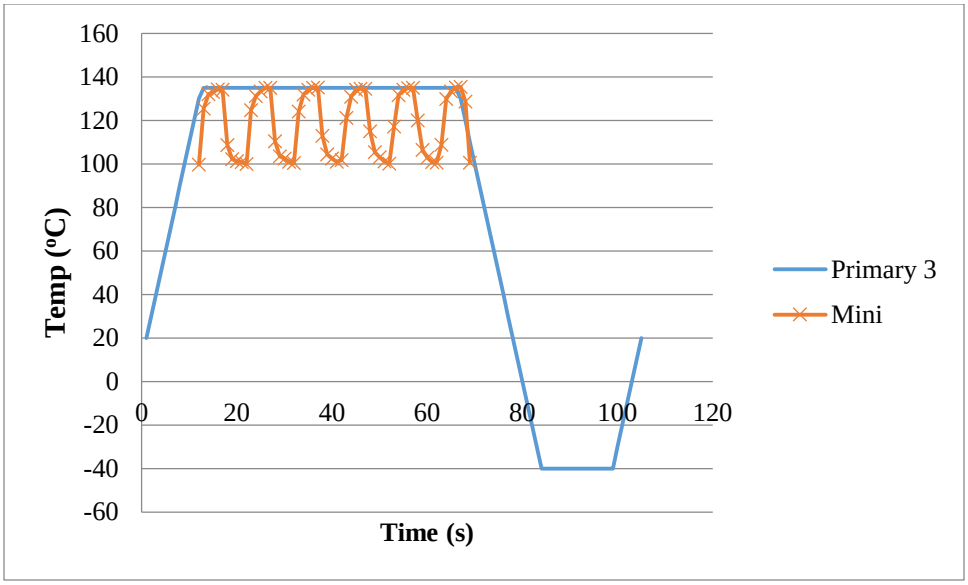

Figure 3.11: Segmenting method 3

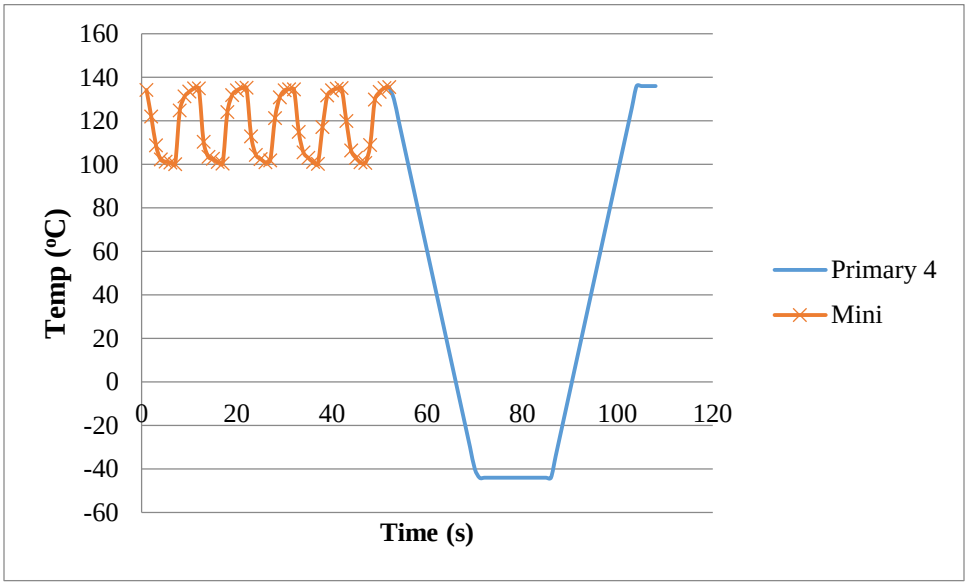

Figure 3.12: Segmenting method 4.

3.3 Finite element analysis

In order to model the solder stress/strain hysteresis under the combined temperature and power cycling, the resultant temperature distribution across the assembly under this combined condition needed to be characterized first. This section included the finite element modeling of resultant temperature history (with spatial thermal gradient) well as the subsequent thermo-mechanical modeling used to determine the cyclic strain energy in the solder interconnects.

3.3.1 **Power cycle induced spatial thermal gradient**

A 3D finite element transient thermal analysis using Ansys 14.2 was conducted to estimate the temperature distribution across the whole BGA assembly, and the monitored temperature in Figure 3.6 was compared with the temperature solution from FEA analysis. A quarter of the BGA assembly, consisting of epoxy molding compound (EMC), silicon die, substrate, copper metallization, solder interconnect and PCB, was modeled and shown in Figure 3.13. Thermal material properties were listed in Table 3.2. The BGA substrate was built with the BT epoxy, which has very similar thermal property to PCB board made of 370HR. The die attach and solder mask were not included in the model. A symmetric boundary condition was imposed on the cut surfaces, and the node at the bottom center of the PCB board was set to be fixed. To provide more accuracy in the high stress/strain region of the solder interconnect, the solder neck region at both component side and board side were modeled with four layers of solder elements. Eight node 3D elements with temperature as the only degree of freedom were used to mesh the model.

The resistance of the heater was 25 Ohm and the output of the heater was 1W. Since the heater is exposed to the surrounding air above the BGA, only part of heat contributes to the temperature rise of the assembly. To determine the thermal efficiency of the heater in this assembly, the applied heat flux in the simulation was varied in an effort to match the temperatures measurement in Figure 3.6. Through iterations, it was found that at 40% of the power (0.4W for the whole assembly or 0.1W for this quarter model) the model matched best with the monitored temperature results. Comparison between monitored temperature from the characterization test and the computed results from FEA analysis after 5-minute power on is presented in Table 3.3. The temperature distribution from FEA after 5-minute power on is presented in Figure 3.14. The temperature difference between the hottest and coolest location was about 30K through the whole assembly, and the spatial thermal gradients through all the solder balls was about 5K, as shown in Figure 3.15. The average ΔT of the whole assembly due to the power cycling of heater was about 25K.

Table 3.2: Thermal material properties [Dan 2001]

Material	k (W/(m·K))	c (J/(kg·°C))	ρ (kg/m^3)
PCB	0.25	878.6	1938
Copper	401	386	8940
Molding Compound	1	800	2200
Silicon Die	83	712	2329
Substrate	0.25	878.6	1938
Solder	43.6	180	8420

Table 3.3: Temperature comparison between monitoring and modeling after 5 minutes power on

Location	Monitoring (K)	Modeling (K)
BGA Center	405	406
BGA Corner	394	397
Board	393	393

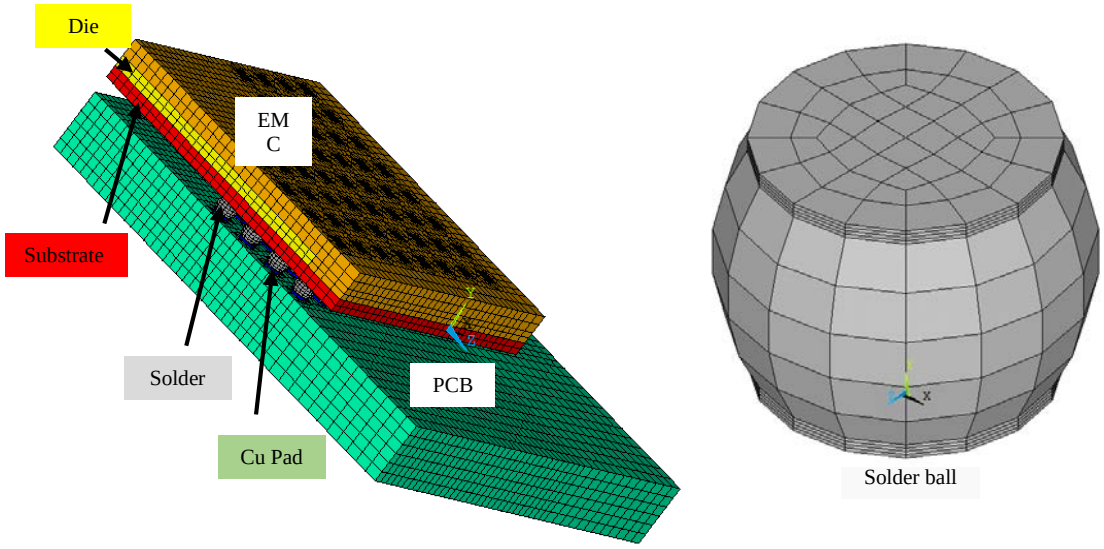

Figure 3.13: FEA model.

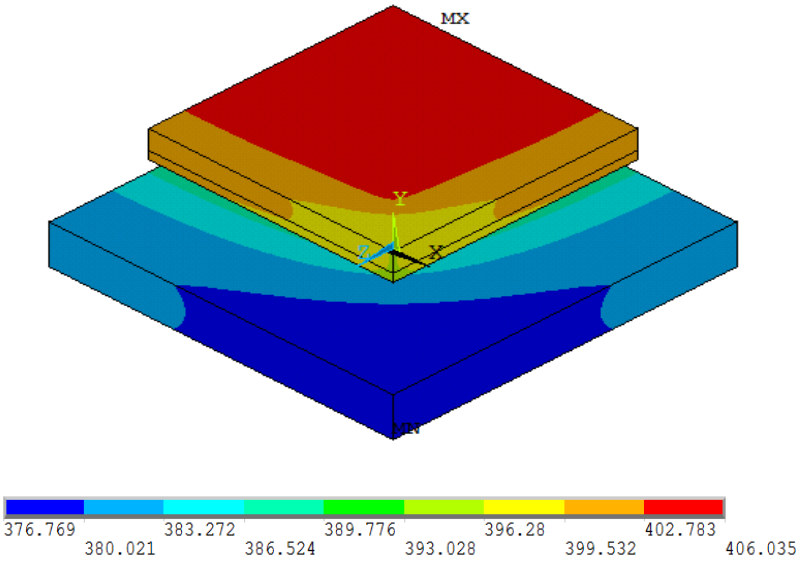

Figure 3.14: Temperature (K) distribution after power on for 5 minutes.

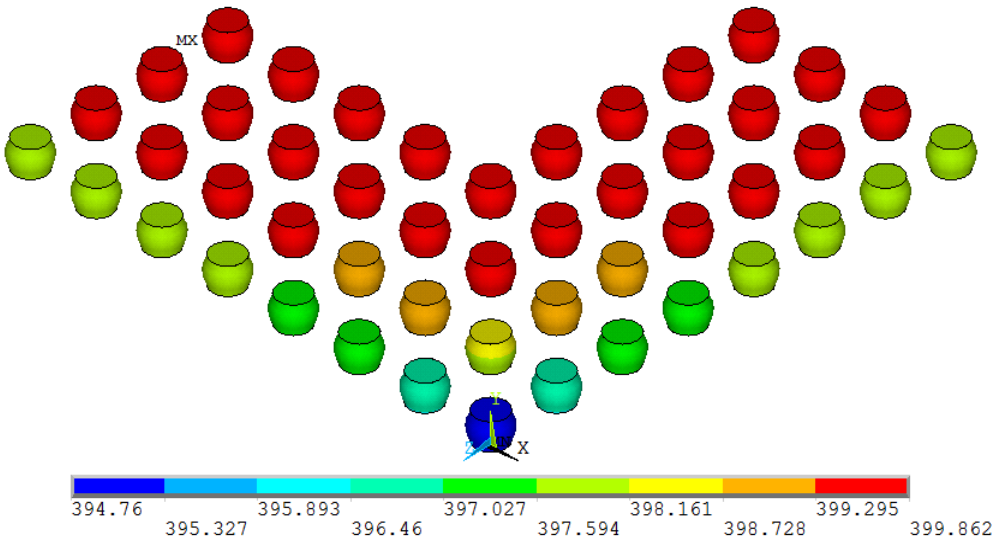

Figure 3.15: Thermal gradients (K) through solder balls.

3.3.2 **Thermo-mechanical modeling**

The finite element model depicted in Figure 3.13 was also used for the thermo-mechanical analysis, with the result from the thermal simulation used as temperature input. Solder was modeled with temperature dependent elastic and inelastic properties; other materials were modeled with a linear elasticity (see Table 3.4). Elastic-plastic deformation of solder was modeled by Ramberg-Osgood strain hardening rule defined in Eqn. 3.1:

$$\sigma = C_{pl}\varepsilon_{pl}^{\ n} \qquad \textbf{Eqn. 3.1}$$

where C_{pl} and n are temperature-dependent constants, which are summarized in Table 3.5. Since the elastic-plastic constants for SAC305 was not available in literature, so the constants of SnAg3.8Cu0.7 (SAC387) were substituted for SAC305 in this study.

The creep response of the solder was modeled by the generalized Garofalo's equation defined in Eqn. 3.2, and model constants are summarized in Table 3.6:

$$\frac{\partial \varepsilon}{\partial t} = C_1[\sinh(C_2\sigma)]^{C_3}\exp(\frac{-C_4}{T}) \qquad \textbf{Eqn. 3.2}$$

Table 3.4: Elastic material properties [Dan 2001]

Material	E (MPa)	CTE (ppm/ºC)	Poisson's Ratio
EMC	18600	12	0.4
Copper	121000	17	0.34
PWB	17200	X/Y: 16.4 Z: 64	0.28
Silicon Die	130000	2.6	0.278
Substrate	17200	X/Y: 16.4 Z: 64	0.28
Sn37Pb [Zhang 2004]	2.92E4-44.2T(K)	23.9	0.4
SAC387 [Zhang 2004] (SAC305)	4.37E4-22.3T(K)	20.9	0.4

Table 3.5: Plastic model constants for Sn37Pb and SAC305 solders [Zhang 2004]

Solder Alloy	C_{pl} (MPa)	*n*
Sn37Pb	152.5-0.6*T(ºC)	0.25-0.00028*T(ºC)
SAC387 (SAC305)	121.6-0.4*T(ºC)	0.29-0.00046*T(ºC)

Table 3.6: Solder Creep Model Constants

Solder Alloy	C1(1/s)	C2 (1/Pa)	C3	C4
Sn37Pb [Zhang 2004]	6640	1.15E-07	2.2	7130
SAC305 [Cuddalorepatta 2010]	6.07	1.8E-07	2.3	6714

The analysis got stabilized within three cycles and the incremental energy accumulated per cycle remained unchanged. Typical distribution of strain energy of the corner solder interconnect at the end of the third max excursion is presented in Figure 3.16, and the time history of strain energy at the max-stressed node is presented in Figure 3.17, with the cyclic strain energy (ΔW) identified.

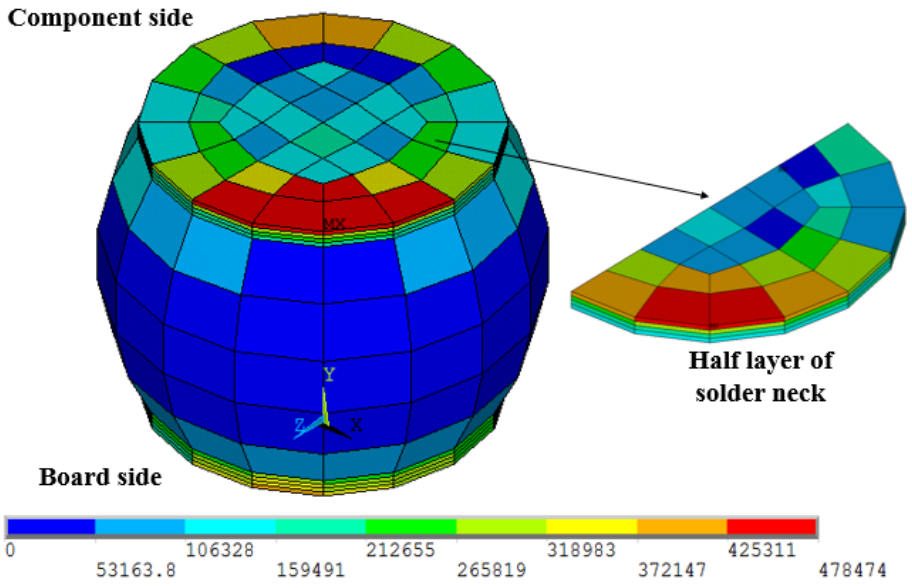

Figure 3.16: Creep energy density (J/m^3)

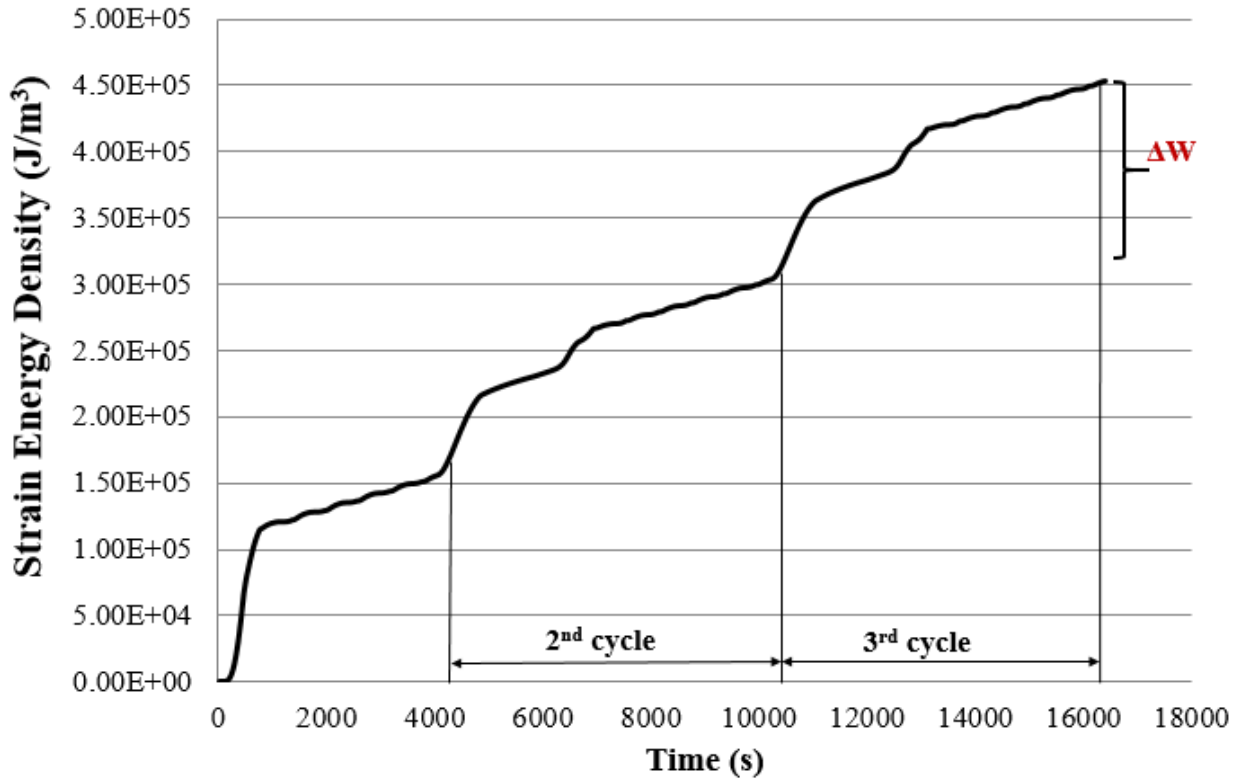

Figure 3.17: Time history of strain energy density

Six thermal profiles were loaded in the thermo-mechanical analysis. The first one was the direct output of the transient thermal analysis, referred to as "combine", and second one took the average across all the nodes in the FEA model, referred to as "uniform ΔT". Both of profiles were complex temperature cycling with temperature fluctuation during the upper excursion, but the "combine" included spatial thermal gradient whereas the "uniform ΔT" ignored that. The primary cycles in the four segmentation methods were also loaded, referred to as "primary 1" to "primary 4".

The cyclic plastic energy density (ΔW_{pl}) and creep energy density (ΔW_{cr}) averaged from the solder neck region at component side (referred as total 4L) and from the right half of the solder neck

region at the component side (referred as half layer) for eutectic SnPb and SAC305 solder are presented in Table 3.7 and Table 3.8. The ΔW_{pl} is more than one magnitude lower than the ΔW_{cr} for Sn37Pb solder, while these two part of energy are comparable for SAC305 solder, since SAC305 is a more stiff material than Sn37Pb. Also, it was found that both ΔW_{pl} and ΔW_{cr} under "uniform ΔT" were higher than under the "combine", indicating that the analysis would be conservative if the spatial thermal gradient was ignored. By comparing the strain energy among the four primary cycles, the energy increases from "primary 1" to "primary 3" due to the increase of maximum temperature. The energy from "primary 4" lies between "primary 2" and "primary 3" for Sn37Pb solder, while the energy from "primary 4" is smaller than "primary 2" for SAC305 solder, manifesting a quicker creep rate and more vulnerability to higher temperature of Sn37Pb solder compared to SAC305 solder. The energy of the "mini" cycle is quoted from the upper excursion of the "complex", instead of analyzing the resultant temperature under iso-thermal power cycling profile (as in Figure 3.4), since the latter method would generate an optimistic energy. It has to be noted there is ignorable amount of ΔW_{pl} in mini cycle, due to the small temperature amplitude in mini cycle profile. The energy results averaged from the total solder neck (total 4L) and half of the solder neck (half neck) are very close, indicating the robustness of element selections. In the following section, the energy partitioning (EP) model prediction using the strain energy averaged from the half layer elements will be presented. This element selection scheme was recommended by Zhang's study [Zhang 2005], in which the EP model constants were generated.

Table 3.7: Strain energy density for Sn37Pb solder

	ΔW_{pl} (N▪mm/mm^3)		ΔW_{cr} (N▪mm/mm^3)	
	total 4L	**half neck**	**total 4L**	**half neck**
combine	0.00314	0.00327	0.08120	0.08430
uniform ΔT	0.00318	0.00323	0.09690	0.10200
primary 1	0.00300	0.00309	0.05930	0.06210
primary 2	0.00316	0.00329	0.07960	0.08370
primary 3	0.00420	0.00450	0.10200	0.10700
primary 4	0.00319	0.00332	0.09300	0.09730
mini	0	0	0.01720	0.01890

Table 3.8: Strain energy density for SAC305 solder

	ΔW_{pl} (N▪mm/mm^3)		ΔW_{cr} (N▪mm/mm^3)	
	total 4L	**half neck**	**total 4L**	**half neck**
combine	0.05220	0.04930	0.06770	0.06700
uniform ΔT	0.05640	0.05380	0.08020	0.07920
primary 1	0.04490	0.04260	0.05180	0.05170
primary 2	0.05900	0.05600	0.07560	0.07490
primary 3	0.07560	0.07270	0.10600	0.10400
primary 4	0.05550	0.05300	0.08900	0.08820
mini	0.00001	0.00001	0.03010	0.03100

3.4 Life prediction of combined temperature and power cycling

Finite element analysis (FEA) assisted energy partitioning model can assess the complex temperature cycling resultant from the combined temperature and power cycling condition directly, by calculating the strain energy under a complete complex temperature cycle without profile segmentation and damage superposition. However, the resultant complex temperature cycle can also be segmented into multiple standard temperature cycles (with single ΔT in each), then assessing segmented standard temperature cycles using physical tests, Engelmaier model or energy partitioning model, and at last applying Miner's rule to superpose the damage. Different modeling

approaches targeting to predict solder interconnect fatigue life under the combined temperature cycling were discussed in this section.

3.4.1 **Experiments based superposition**

According to Miner's rule, the damage of the combined temperature and power cycling test could be calculated as the summation of damage from the temperature cycling test and from the iso-thermal power cycling test, with the damage linearly interpreted as the inverse of the mean cycles to failure (N_{50}), as described in Eqn. 3.3:

$$\frac{1}{N_{combine}} = \frac{1}{N_{ther}} + \frac{1}{N_{pw}} \qquad \textbf{Eqn. 3.3}$$

The cycles to failure of the combined test and the stand-alone temperature cycling test were presented in Figure 3.8. At the meantime, the iso-thermal power cycling test has been conducted for 20000 cycles and no parts has been failed. If 20000 cycles were used as the fatigue life of the power cycling test, which is a conservative approximation, the linear superposition applied directly from the test results of the stand-alone temperature cycling and iso-thermal power cycling overestimates the fatigue life, as shown in Figure 3.18. Thus, there were solder damage due to the interaction between the temperature cycling and power cycling portion that cannot be capture by the direct application of Miner's rule. In another word, it is experimentally demonstrated that segmenting method 1 (as in Figure 3.9) with Miner's rule over estimated the combined test.

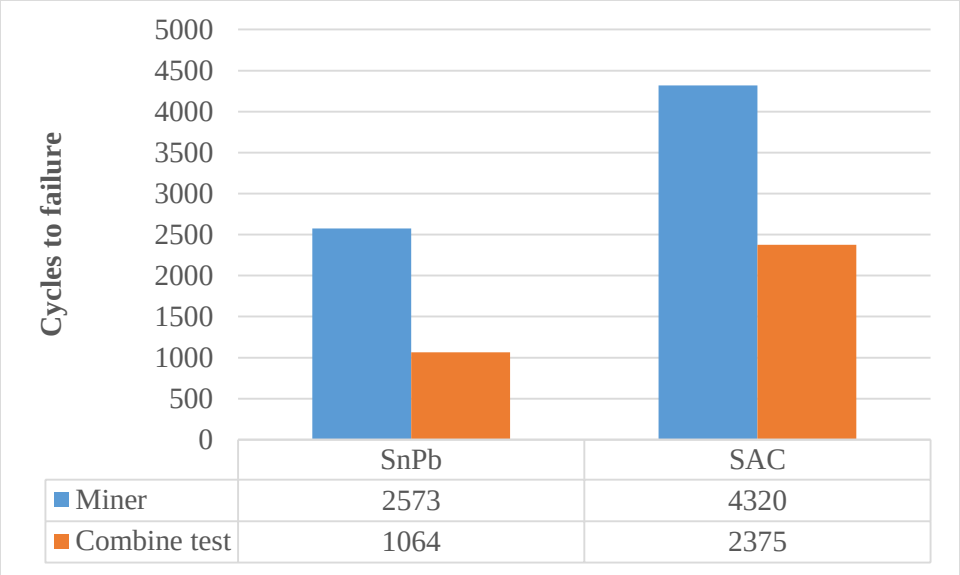

Figure 3.18: Superposition based on test results.

3.4.2 Engelmaier model and energy partitioning model based damage superposition

Another way to predict the solder interconnect life under the combined cycling was modeling the complex temperature cycling resultant from the combined loading, using the segmenting methods proposed in Figure 3.9-Figure 3.12. Linear superposition in Eqn. 3.4 was used to superpose the damage from primary cycles and mini cycles; for segmenting methods 1 through 3, n is 6; and n is 5 for segmenting method 4.

$$\frac{1}{N_{combine}} = \frac{1}{N_{pr}} + \frac{n}{N_{mini}} \qquad \textbf{Eqn. 3.4}$$

Engelmaier model and EP model were used to predict the solder interconnect life under all the segmented primary cycles and mini cycles. Only the primary cycle in segmenting method 1 and the mini cycles (iso-thermal power cycling) were physically tested, and a comparison between test data and life prediction under these two conditions are presented in Table 3.9.

Table 3.9: Comparison between test and prediction for segmented cycle

	Engelmaier (cycles)		EP (cycles)	
	SnPb	**SAC**	**SnPb**	**SAC**
primary 1 (TC-test)	2953	5510	2953	5510
	1921	5383	1514	5865
mini (iso-power)	40928	15131	4971	9976
	20000+	20000+	20000+	20000+

Engelmaier model and EP model based damage superposition for modeling the combine test is presented in Figure 3.19 and Figure 3.20. After damage superposition by Miner's rule, EP model provided more conservative predictions for SnPb than SAC solder interconnect, whereas Engelmaier model had more conservative estimations for SAC solder. When Engelmaier model was used, segmenting method 2 and method 3 were preferable than the others since method 2 and method 3 provided the best prediction for SAC and SnPb solder respectively, and less than 40% error for the other solder. When EP model was used as in Figure 3.20, Miner's rule generated acceptable errors (less than $\pm$22%) under all the segmenting methods for SnPb solder interconnect, while method 3 (in Figure 3.11) defining the maxima of the primary cycle at the peak of mini cycle and dwelling for one hour generated the least modeling errors for SAC solder. Modeling of the complete "combined" thermal profile by FEA, using the strain energy under a complete complex temperature cycling (as in Figure 3.6) as the input of EP model, overestimated the combined test by 17% and 127% for SnPb and SAC solder interconnect. In general, method 3 was recommended for segmenting the resultant complex temperature cycling profile, since it can provide a closer correlation to the combined test results than all the other methods when both energy partitioning model and Engelmaier model were used for predicting solder interconnect fatigue life for Sn37Pb and SAC solder.

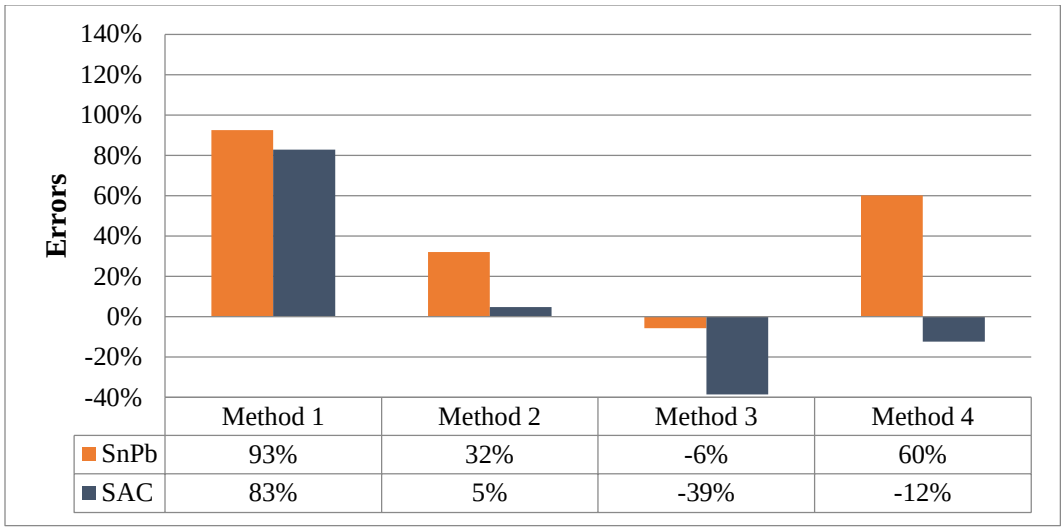

Figure 3.19: Engelmaier model based errors of superposition for modeling the combined temperature and power cycling.

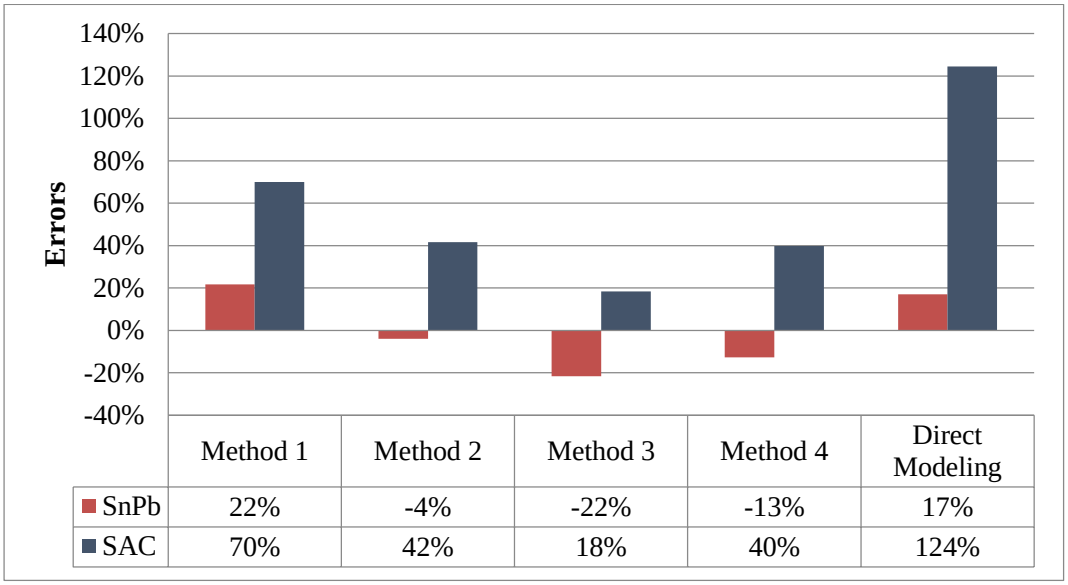

Figure 3.20: EP model based errors of superposition for modeling the combined temperature and power cycling.

3.4.3 **Approximation of combine test by standard temperature cycling**

To investigate if the solder interconnect life under the combined temperature and power cycling test can be approximated by a standard temperature cycling (with single ΔT) and ignoring the temperature fluctuation during the upper excursion, the primary cycles assessed by EP model and Engelmaier model predictions were compared with the combined temperature and power cycling test. As shown in Figure 3.21, the primary cycle in method 3 provided the best approximation of the combined test for Sn37Pb solder. From Figure 3.22, it was found for the SAC305 solder, primary cycles from segmenting method 2, method 3 and method 4 assessed by Engelmaier model can be used to present the combined test, among which method 4 provided the closest approximation; while all the primary cycles was optimistic for representing the combined test if the primary cycles were assessed by EP model.

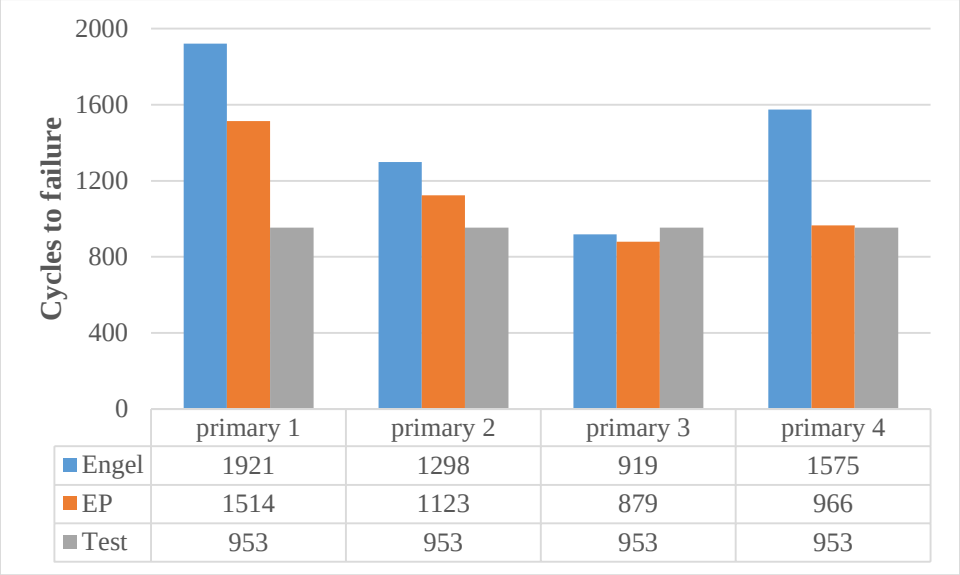

	primary 1	primary 2	primary 3	primary 4
Engel	1921	1298	919	1575
EP	1514	1123	879	966
Test	953	953	953	953

Figure 3.21: Approximation of the combined test by primary cycle for SnPb solder.

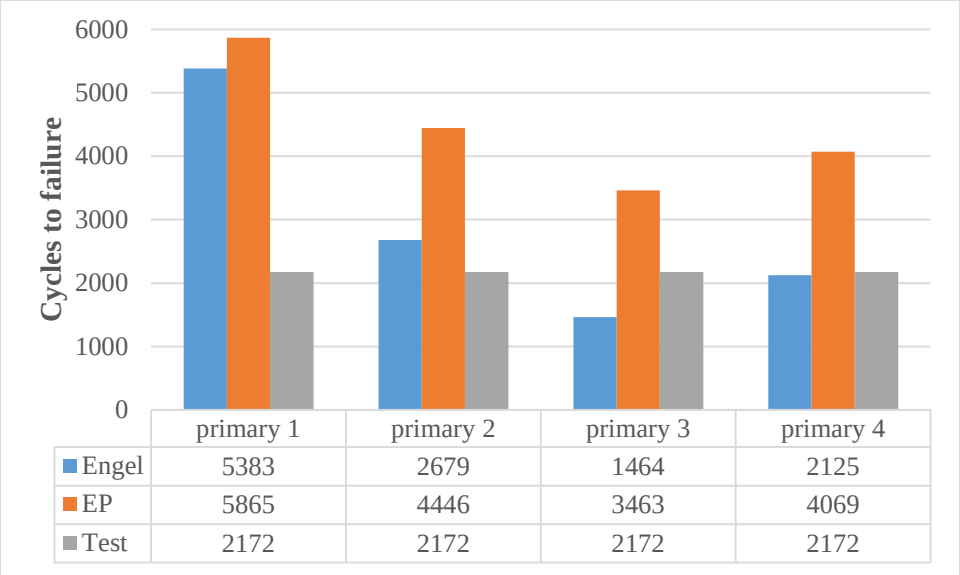

Figure 3.22: Approximation of the combined test by primary cycle for SAC305 solder.

3.4.4 **Effect of spatial thermal gradient**

In order to predict solder interconnect life by damage superposition approach, the complex temperature cycling profile (with multiple ΔT) needs to be segmented into multiple standard temperature cycling profile first. By comparing the optimal methods of segmentation between the chamber controlled complex cycling in chapter 2 (without spatial thermal gradient) and the combined temperature cycling and power cycling in this chapter (with spatial thermal gradient), it was found the segmenting method 2 (defining the max of primary cycle at the mean of the upper excursion of the complex cycle) is optimal for the condition without spatial thermal gradient, whereas the segmenting method 3 (defining the max of primary cycle at the peak of the upper excursion of the complex cycle) is optimal for the condition with spatial thermal gradient.

After the solidification process in the reflow, assembly tends to have convex warpage (edge of the part curved down) if the devise has a smaller coefficient of thermal expansion than the PCB board

[Au 2011]. Under a power cycling condition, involvement of spatial thermal gradient ($\Delta T_{device} > \Delta T_{pcb}$) will increase warpage. Thus, when spatial thermal gradient existed, a more conservative segmentation method is required in order to compensate the aggregated out-of-plane deformation.

3.5 Summary

This section developed the modeling approaches and quantified prediction accuracies for estimating solder interconnect life under combined temperature and power cycling. The resultant temperature history under the combined cycling was a complex temperature cycling with varying temperature mean, amplitude and spatial thermal gradient

Modeling of solder interconnect life under the combined condition can be achieved by modeling the strain energy under the resultant complex temperature cycling and employing the energy partition models. This method was at least optimistic for SAC305 soldered BGA parts, since it overestimated the combined test by 17% and 127% for SnPb and SAC solder interconnect.

Damage superposition can also be used to predict the solder interconnect life under the combined test. Profile segmentation for decomposing the resultant complex temperature cycling (with multiple ΔT) into primary cycle and mini cycle (with single ΔT) was the prerequisite for damage superposition. It was found the method 3 (defining the max of primary cycle at the peak of the upper excursion of the complex cycle) was optimal for segmenting the complex temperature cycling resultant from the combined loading. It has to be noted that after the profile segmentation,

the primary cycle and mini cycle were assessed by Engelmaier model and EP model instead of physical test, and the superposition was conducted by linear damage superposition (Miner's rule).

The solder interconnect damage under the combined test was also approximated by just the primary cycles (with single ΔT) by ignoring the temperature fluctuation at the upper excursion and without superimposing the damage from mini cycle. It was found the primary cycle in method 3 (defining the max of primary cycle at the peak of the upper excursion of the complex cycle) provided the best approximation to the combined test for the Sn37Pb soldered BGA parts. For SAC305 parts, the primary cycle in method 3 was also recommend but it had to be assessed by Engelmaier model; primary cycles under all the segmentation methods would be optimistic for representing the combined test if they are assessed by EP model.

Chapter 4 Contributions and Suggestions for Future Work

Electronic devices are under concurrent loading of the power cycling of the devices and the temperature cycling from the surrounding environment. Temperature histories under these concurrent loading would be a complex condition with varying cyclic temperature mean and amplitude, as well as spatial thermal gradient. Conventional test methods to assess the thermo-mechanical fatigue reliability of solder interconnect are the temperature cycling tests, such as those specified in IPC standards. These temperature cycling tests apply only two temperature extremes, constant ramp rates, and hold times at both ends of the cycle. Thus, there are at least two features of the field that the temperature cycling test cannot capture: the multiple temperature ranges (ΔT) in the cyclic excursion and the spatial thermal gradient from the die to the printed circuit board.

Very limited past studies has been on modeling of the complex temperature cycling with varying mean and amplitude (multiple ΔT), and the damage superposition based modeling approach for predicting solder interconnect life under complex temperature cycling was not available in literature. Thus, a systematical study on the solder interconnect fatigue life prediction under the complex temperature cycling condition with varying temperature mean and amplitude and spatial thermal gradient is needed.

This study developed modeling approaches and quantified accuracies for predicting solder interconnect life under complex temperature cycling. The modeling approaches includes: 1) modeling the strain energy under the complete resultant complex temperature cycling and employing the energy based fatigue life models; 2) segmenting the resultant complex temperature cycle into multiple simple temperature cycles with a single temperature range for each first, then

assessing segmented simple temperature cycles and at last applying Miner's rule to superpose the damage; 3) approximating solder damage under the resultant complex temperature cycling by a standard temperature cycling with a single temperature range. Case studies of ceramic leadless chip carriers assembled by Sn36Pb62Ag2 and SnAg3.0Cu0.5 solder under chamber controlled complex temperature cycling (without spatial thermal gradient), and plastic ball grid array packages assembled by Sn63Pb37 and SnAg3.0Cu0.5 solder under combined temperature and power cycling condition were covered in this dissertation. Section 4.1 summarized the primary contributions of the dissertation while section 4.2 presents the limitation of this study.

4.1 Contributions of the study

1) This study determined the applicability and quantified the prediction errors of Miner's rule on modeling a complex temperature cycling condition, with and without spatial thermal gradients.
2) This study determined an approach to segment the complex temperature cycling into standard temperature cycling, as a prerequisite to apply damage superposition.
3) This study provided the model parameters of Engelmaier model and Morrow's model for predicting the solder life under standard temperature cycling. The new parameters have robust prediction especially on leadless chip carriers.
4) This study developed a superposition based modeling method to consider the stress interaction between segmented cycles.
5) This study provided guidelines for designing the standard temperature cycling profile to represent the solder damage under actual use condition with multiple temperature range.

6) This study provided fatigue life data of solder interconnect under combined temperature and power cycling condition that can be used for the validation of modeling approaches.

4.2 Limitation of this study

1) Most the segmented temperature cycles (with a single ΔT) were assessed by fatigue life models instead of physical tests.
2) The developed approaches for model the complex temperature cycling were only validated by one set of complex temperature cycling test, for the condition with and without spatial thermal gradient each.
3) The effect of the loading interaction between the power and temperature cycling on the solder micro-structure was not discussed in this study.

Appendices

Appendix A: Ansys input file for material property of Sn37Pb solder

```
MPTEMP,1,218
MPTEMP,2,233
MPTEMP,3,273
MPTEMP,4,298
MPTEMP,5,323
MPTEMP,6,363
MPTEMP,7,398

MPDATA,EX,5,,19564
MPDATA,EX,5,,18901
MPDATA,EX,5,,17133
MPDATA,EX,5,,16028
MPDATA,EX,5,,14923
MPDATA,EX,5,,13155
MPDATA,EX,5,,11608

MPDATA,EY,5,,19564
MPDATA,EY,5,,18901
MPDATA,EY,5,,17133
MPDATA,EY,5,,16028
MPDATA,EY,5,,14923
MPDATA,EY,5,,13155
MPDATA,EY,5,,11608

MPDATA,EZ,5,,19564
MPDATA,EZ,5,,18901
MPDATA,EZ,5,,17133
MPDATA,EZ,5,,16028
MPDATA,EZ,5,,14923
MPDATA,EZ,5,,13155
MPDATA,EZ,5,,11608


MPDATA,NUXY,5,,0.4
MPDATA,NUXY,5,,0.4
MPDATA,NUXY,5,,0.4
MPDATA,NUXY,5,,0.4
MPDATA,NUXY,5,,0.4
MPDATA,NUXY,5,,0.4
MPDATA,NUXY,5,,0.4

MPDATA,NUYZ,5,,0.4
MPDATA,NUYZ,5,,0.4
MPDATA,NUYZ,5,,0.4
MPDATA,NUYZ,5,,0.4
MPDATA,NUYZ,5,,0.4
MPDATA,NUYZ,5,,0.4
MPDATA,NUYZ,5,,0.4
```

```
MPDATA,NUXZ,5,,0.4
MPDATA,NUXZ,5,,0.4
MPDATA,NUXZ,5,,0.4
MPDATA,NUXZ,5,,0.4
MPDATA,NUXZ,5,,0.4
MPDATA,NUXZ,5,,0.4
MPDATA,NUXZ,5,,0.4


MPDATA,ALPX,5,,23.9e-6
MPDATA,ALPX,5,,23.9e-6
MPDATA,ALPX,5,,23.9e-6
MPDATA,ALPX,5,,23.9e-6
MPDATA,ALPX,5,,23.9e-6
MPDATA,ALPX,5,,23.9e-6
MPDATA,ALPX,5,,23.9e-6

MPDATA,ALPY,5,,23.9e-6
MPDATA,ALPY,5,,23.9e-6
MPDATA,ALPY,5,,23.9e-6
MPDATA,ALPY,5,,23.9e-6
MPDATA,ALPY,5,,23.9e-6
MPDATA,ALPY,5,,23.9e-6
MPDATA,ALPY,5,,23.9e-6

MPDATA,ALPZ,5,,23.9e-6
MPDATA,ALPZ,5,,23.9e-6
MPDATA,ALPZ,5,,23.9e-6
MPDATA,ALPZ,5,,23.9e-6
MPDATA,ALPZ,5,,23.9e-6
MPDATA,ALPZ,5,,23.9e-6
MPDATA,ALPZ,5,,23.9e-6



!SOLDER CREEP PROPERTY
TB,CREE,5,1,4,8
TBDATA,,6640,0.115,2.2,7130,,


!DEFINE SOLDER PLASTIC PROPERTY
TB,MISO,5,7 , , ,
!*
TBTEMP,218,1
!*
TBMODIF,1,1,0.001762
TBMODIF,1,2,34.46941247
TBMODIF,2,1,0.0019
TBMODIF,2,2,35.16617392
TBMODIF,3,1,0.002
TBMODIF,3,2,35.64817284
TBMODIF,4,1,0.003
TBMODIF,4,2,39.69829868
TBMODIF,5,1,0.005
TBMODIF,5,2,45.46221098
```

```
TBMODIF,6,1,0.007
TBMODIF,6,2,49.70876047
TBMODIF,7,1,0.01
TBMODIF,7,2,54.64418009
TBMODIF,8,1,0.03
TBMODIF,8,2,73.14285276
TBMODIF,9,1,0.04
TBMODIF,9,2,78.94609187
TBMODIF,10,1,0.06
TBMODIF,10,2,87.91546061
TBMODIF,11,1,0.08
TBMODIF,11,2,94.89077562
TBMODIF,12,1,0.1
TBMODIF,12,2,100.6801639
TBMODIF,13,1,0.2
TBMODIF,13,2,121.0144621
TBMODIF,14,1,0.3
TBMODIF,14,2,134.76338
TBMODIF,15,1,0.4
TBMODIF,15,2,145.4556635
TBMODIF,16,1,0.5
TBMODIF,16,2,154.33007
TBMODIF,17,1,0.6
TBMODIF,17,2,161.9814401
TBMODIF,18,1,0.7
TBMODIF,18,2,168.745785
TBMODIF,19,1,0.8
TBMODIF,19,2,174.8332362
TBMODIF,20,1,0.9
TBMODIF,20,2,180.3847737



!*
TBTEMP,233,2
!*
TBMODIF,1,1,0.00179
TBMODIF,1,2,33.82127077
TBMODIF,2,1,0.0019
TBMODIF,2,2,34.35224704
TBMODIF,3,1,0.002
TBMODIF,3,2,34.81558882
TBMODIF,4,1,0.003
TBMODIF,4,2,38.70515237
TBMODIF,5,1,0.005
TBMODIF,5,2,44.22987122
TBMODIF,6,1,0.007
TBMODIF,6,2,48.29301477
TBMODIF,7,1,0.01
TBMODIF,7,2,53.00840171
TBMODIF,8,1,0.03
TBMODIF,8,2,70.62667836
TBMODIF,9,1,0.04
TBMODIF,9,2,76.13823052
TBMODIF,10,1,0.06
```

```
TBMODIF,10,2,84.64431921
TBMODIF,11,1,0.08
TBMODIF,11,2,91.24977753
TBMODIF,12,1,0.1
TBMODIF,12,2,96.72632993
TBMODIF,13,1,0.2
TBMODIF,13,2,115.9241031
TBMODIF,14,1,0.3
TBMODIF,14,2,128.8750306
TBMODIF,15,1,0.4
TBMODIF,15,2,138.9321573
TBMODIF,16,1,0.5
TBMODIF,16,2,147.2704707
TBMODIF,17,1,0.6
TBMODIF,17,2,154.4535221
TBMODIF,18,1,0.7
TBMODIF,18,2,160.7993607
TBMODIF,19,1,0.8
TBMODIF,19,2,166.5067386
TBMODIF,20,1,0.9
TBMODIF,20,2,171.7089186
```

```
!*
TBTEMP,273,3
!*
TBMODIF,1,1,0.001845
TBMODIF,1,2,31.60595637
TBMODIF,2,1,0.0019
TBMODIF,2,2,31.83891386
TBMODIF,3,1,0.002
TBMODIF,3,2,32.24982353
TBMODIF,4,1,0.003
TBMODIF,4,2,35.69029662
TBMODIF,5,1,0.005
TBMODIF,5,2,40.55200621
TBMODIF,6,1,0.007
TBMODIF,6,2,44.11074103
TBMODIF,7,1,0.01
TBMODIF,7,2,48.22473432
TBMODIF,8,1,0.03
TBMODIF,8,2,63.46731962
TBMODIF,9,1,0.04
TBMODIF,9,2,68.20007331
TBMODIF,10,1,0.06
TBMODIF,10,2,75.47578806
TBMODIF,11,1,0.08
TBMODIF,11,2,81.10401243
TBMODIF,12,1,0.1
TBMODIF,12,2,85.75705209
TBMODIF,13,1,0.2
TBMODIF,13,2,101.9828965
```

```
TBMODIF,14,1,0.3
TBMODIF,14,2,112.8626277
TBMODIF,15,1,0.4
TBMODIF,15,2,121.2787861
TBMODIF,16,1,0.5
TBMODIF,16,2,128.2367033
TBMODIF,17,1,0.6
TBMODIF,17,2,134.2170399
TBMODIF,18,1,0.7
TBMODIF,18,2,139.4904109
TBMODIF,19,1,0.8
TBMODIF,19,2,144.2255954
TBMODIF,20,1,0.9
TBMODIF,20,2,148.5355713


!*
TBTEMP,298,4
!*
TBMODIF,1,1,0.001863
TBMODIF,1,2,29.85138062
TBMODIF,2,1,0.0019
TBMODIF,2,2,29.99437544
TBMODIF,3,1,0.002
TBMODIF,3,2,30.37057309
TBMODIF,4,1,0.003
TBMODIF,4,2,33.515304
TBMODIF,5,1,0.005
TBMODIF,5,2,37.94481233
TBMODIF,6,1,0.007
TBMODIF,6,2,41.17764659
TBMODIF,7,1,0.01
TBMODIF,7,2,44.90582692
TBMODIF,8,1,0.03
TBMODIF,8,2,58.64664373
TBMODIF,9,1,0.04
TBMODIF,9,2,62.89313974
TBMODIF,10,1,0.06
TBMODIF,10,2,69.40543044
TBMODIF,11,1,0.08
TBMODIF,11,2,74.43095049
TBMODIF,12,1,0.1
TBMODIF,12,2,78.57831254
TBMODIF,13,1,0.2
TBMODIF,13,2,92.99358427
TBMODIF,14,1,0.3
TBMODIF,14,2,102.6226353
TBMODIF,15,1,0.4
TBMODIF,15,2,110.0533523
TBMODIF,16,1,0.5
TBMODIF,16,2,116.1856279
TBMODIF,17,1,0.6
TBMODIF,17,2,121.4488626
TBMODIF,18,1,0.7
TBMODIF,18,2,126.0844481
```

```
TBMODIF,19,1,0.8
TBMODIF,19,2,130.2427522
TBMODIF,20,1,0.9
TBMODIF,20,2,134.0243248


!*
TBTEMP,323,5
!*
TBMODIF,1,1,0.001863
TBMODIF,1,2,27.79113747
TBMODIF,2,1,0.0019
TBMODIF,2,2,27.92041946
TBMODIF,3,1,0.002
TBMODIF,3,2,28.26045616
TBMODIF,4,1,0.003
TBMODIF,4,2,31.09830401
TBMODIF,5,1,0.005
TBMODIF,5,2,35.0827
TBMODIF,6,1,0.007
TBMODIF,6,2,37.98212215
TBMODIF,7,1,0.01
TBMODIF,7,2,41.31769531
TBMODIF,8,1,0.03
TBMODIF,8,2,53.54719241
TBMODIF,9,1,0.04
TBMODIF,9,2,57.30892297
TBMODIF,10,1,0.06
TBMODIF,10,2,63.06374882
TBMODIF,11,1,0.08
TBMODIF,11,2,67.49402463
TBMODIF,12,1,0.1
TBMODIF,12,2,71.14364115
TBMODIF,13,1,0.2
TBMODIF,13,2,83.78748751
TBMODIF,14,1,0.3
TBMODIF,14,2,92.20122789
TBMODIF,15,1,0.4
TBMODIF,15,2,98.67843353
TBMODIF,16,1,0.5
TBMODIF,16,2,104.0142902
TBMODIF,17,1,0.6
TBMODIF,17,2,108.5874873
TBMODIF,18,1,0.7
TBMODIF,18,2,112.610588
TBMODIF,19,1,0.8
TBMODIF,19,2,116.21584
TBMODIF,20,1,0.9
TBMODIF,20,2,119.4915847


!*
TBTEMP,363,6
!*
TBMODIF,1,1,0.00181
```

TBMODIF,1,2,23.82113082
TBMODIF,2,1,0.0019
TBMODIF,2,2,24.08241522
TBMODIF,3,1,0.002
TBMODIF,3,2,24.36171025
TBMODIF,4,1,0.003
TBMODIF,4,2,26.68659032
TBMODIF,5,1,0.005
TBMODIF,5,2,29.93399539
TBMODIF,6,1,0.007
TBMODIF,6,2,32.28600204
TBMODIF,7,1,0.01
TBMODIF,7,2,34.981323
TBMODIF,8,1,0.03
TBMODIF,8,2,44.78092793
TBMODIF,9,1,0.04
TBMODIF,9,2,47.77264822
TBMODIF,10,1,0.06
TBMODIF,10,2,52.33167452
TBMODIF,11,1,0.08
TBMODIF,11,2,55.82784442
TBMODIF,12,1,0.1
TBMODIF,12,2,58.69974715
TBMODIF,13,1,0.2
TBMODIF,13,2,68.59741868
TBMODIF,14,1,0.3
TBMODIF,14,2,75.14378878
TBMODIF,15,1,0.4
TBMODIF,15,2,80.16398841
TBMODIF,16,1,0.5
TBMODIF,16,2,84.28779399
TBMODIF,17,1,0.6
TBMODIF,17,2,87.81417622
TBMODIF,18,1,0.7
TBMODIF,18,2,90.91054679
TBMODIF,19,1,0.8
TBMODIF,19,2,93.68085798
TBMODIF,20,1,0.9
TBMODIF,20,2,96.19443466

!*
TBTEMP,398,7
!*
TBMODIF,1,1,0.001695
TBMODIF,1,2,19.65953261
TBMODIF,2,1,0.0017
TBMODIF,2,2,19.67198663
TBMODIF,3,1,0.002
TBMODIF,3,2,20.37150672
TBMODIF,4,1,0.003
TBMODIF,4,2,22.22709841
TBMODIF,5,1,0.005
TBMODIF,5,2,24.80734311

```
TBMODIF,6,1,0.007
TBMODIF,6,2,26.66845039
TBMODIF,7,1,0.01
TBMODIF,7,2,28.79398026
TBMODIF,8,1,0.03
TBMODIF,8,2,36.46555033
TBMODIF,9,1,0.04
TBMODIF,9,2,38.79221701
TBMODIF,10,1,0.06
TBMODIF,10,2,42.32570701
TBMODIF,11,1,0.08
TBMODIF,11,2,45.02627813
TBMODIF,12,1,0.1
TBMODIF,12,2,47.23910954
TBMODIF,13,1,0.2
TBMODIF,13,2,54.83061935
TBMODIF,14,1,0.3
TBMODIF,14,2,59.82500895
TBMODIF,15,1,0.4
TBMODIF,15,2,63.64211451
TBMODIF,16,1,0.5
TBMODIF,16,2,66.76982738
TBMODIF,17,1,0.6
TBMODIF,17,2,69.43912207
TBMODIF,18,1,0.7
TBMODIF,18,2,71.77906239
TBMODIF,19,1,0.8
TBMODIF,19,2,73.86965143
TBMODIF,20,1,0.9
TBMODIF,20,2,75.76416514
```

Appendix B: Ansys input file for material property of SAC305 solder

```
MPTEMP,1,218
MPTEMP,2,233
MPTEMP,3,273
MPTEMP,4,298
MPTEMP,5,323
MPTEMP,6,363
MPTEMP,7,398

MPDATA,EX,5,,38838
MPDATA,EX,5,,38504
MPDATA,EX,5,,37612
MPDATA,EX,5,,37054
MPDATA,EX,5,,36497
MPDATA,EX,5,,35605
MPDATA,EX,5,,34824


MPDATA,EY,5,,38838
MPDATA,EY,5,,38504
MPDATA,EY,5,,37612
MPDATA,EY,5,,37054
MPDATA,EY,5,,36497
MPDATA,EY,5,,35605
MPDATA,EY,5,,34824


MPDATA,EZ,5,,38838
MPDATA,EZ,5,,38504
MPDATA,EZ,5,,37612
MPDATA,EZ,5,,37054
MPDATA,EZ,5,,36497
MPDATA,EZ,5,,35605
MPDATA,EZ,5,,34824


MPDATA,NUXY,5,,0.4
MPDATA,NUXY,5,,0.4
MPDATA,NUXY,5,,0.4
MPDATA,NUXY,5,,0.4
MPDATA,NUXY,5,,0.4
MPDATA,NUXY,5,,0.4
MPDATA,NUXY,5,,0.4

MPDATA,NUYZ,5,,0.4
MPDATA,NUYZ,5,,0.4
MPDATA,NUYZ,5,,0.4
MPDATA,NUYZ,5,,0.4
MPDATA,NUYZ,5,,0.4
MPDATA,NUYZ,5,,0.4
MPDATA,NUYZ,5,,0.4

MPDATA,NUXZ,5,,0.4
MPDATA,NUXZ,5,,0.4
```

```
MPDATA,NUXZ,5,,0.4
MPDATA,NUXZ,5,,0.4
MPDATA,NUXZ,5,,0.4
MPDATA,NUXZ,5,,0.4
MPDATA,NUXZ,5,,0.4


MPDATA,ALPX,5,,20.9e-6
MPDATA,ALPX,5,,20.9e-6
MPDATA,ALPX,5,,20.9e-6
MPDATA,ALPX,5,,20.9e-6
MPDATA,ALPX,5,,20.9e-6
MPDATA,ALPX,5,,20.9e-6
MPDATA,ALPX,5,,20.9e-6

MPDATA,ALPY,5,,20.9e-6
MPDATA,ALPY,5,,20.9e-6
MPDATA,ALPY,5,,20.9e-6
MPDATA,ALPY,5,,20.9e-6
MPDATA,ALPY,5,,20.9e-6
MPDATA,ALPY,5,,20.9e-6
MPDATA,ALPY,5,,20.9e-6

MPDATA,ALPZ,5,,20.9e-6
MPDATA,ALPZ,5,,20.9e-6
MPDATA,ALPZ,5,,20.9e-6
MPDATA,ALPZ,5,,20.9e-6
MPDATA,ALPZ,5,,20.9e-6
MPDATA,ALPZ,5,,20.9e-6
MPDATA,ALPZ,5,,20.9e-6



!SOLDER CREEP PROPERTY
TB,CREE,5,1,4,8
TBDATA,,866,0.11,4,8575,,


!DEFINE SOLDER PLASTIC PROPERTY
TB,MISO,5,7 , , ,
!*
TBTEMP,218,1
!*
TBMODIF,1,1,0.0002805
TBMODIF,1,2,10.89400756
TBMODIF,2,1,0.001
TBMODIF,2,2,16.26501394
TBMODIF,3,1,0.002
TBMODIF,3,2,20.23807484
TBMODIF,4,1,0.003
TBMODIF,4,2,22.99803717
TBMODIF,5,1,0.005
TBMODIF,5,2,27.01715922
TBMODIF,6,1,0.007
TBMODIF,6,2,30.04096311
TBMODIF,7,1,0.01
```

TBMODIF,7,2,33.61665057
TBMODIF,8,1,0.03
TBMODIF,8,2,47.53251255
TBMODIF,9,1,0.04
TBMODIF,9,2,52.04559228
TBMODIF,10,1,0.06
TBMODIF,10,2,59.14329674
TBMODIF,11,1,0.08
TBMODIF,11,2,64.75878811
TBMODIF,12,1,0.1
TBMODIF,12,2,69.47914091
TBMODIF,13,1,0.2
TBMODIF,13,2,86.45083604
TBMODIF,14,1,0.3
TBMODIF,14,2,98.2405469
TBMODIF,15,1,0.4
TBMODIF,15,2,107.5682133
TBMODIF,16,1,0.5
TBMODIF,16,2,115.4090011
TBMODIF,17,1,0.6
TBMODIF,17,2,122.2378012
TBMODIF,18,1,0.7
TBMODIF,18,2,128.325762
TBMODIF,19,1,0.8
TBMODIF,19,2,133.8439401
TBMODIF,20,1,0.9
TBMODIF,20,2,138.9079503

!*
TBTEMP,233,2
!*
TBMODIF,1,1,0.00028972
TBMODIF,1,2,11.15559133
TBMODIF,2,1,0.001
TBMODIF,2,2,16.34626118
TBMODIF,3,1,0.002
TBMODIF,3,2,20.24212417
TBMODIF,4,1,0.003
TBMODIF,4,2,22.93837397
TBMODIF,5,1,0.005
TBMODIF,5,2,26.85225627
TBMODIF,6,1,0.007
TBMODIF,6,2,29.78836519
TBMODIF,7,1,0.01
TBMODIF,7,2,33.25205069
TBMODIF,8,1,0.03
TBMODIF,8,2,46.66192259
TBMODIF,9,1,0.04
TBMODIF,9,2,50.9910242
TBMODIF,10,1,0.06
TBMODIF,10,2,57.78302575
TBMODIF,11,1,0.08
TBMODIF,11,2,63.14389766
TBMODIF,12,1,0.1
TBMODIF,12,2,67.64231054

TBMODIF,13,1,0.2
TBMODIF,13,2,83.76374472
TBMODIF,14,1,0.3
TBMODIF,14,2,94.92107081
TBMODIF,15,1,0.4
TBMODIF,15,2,103.7274581
TBMODIF,16,1,0.5
TBMODIF,16,2,111.1170705
TBMODIF,17,1,0.6
TBMODIF,17,2,117.5439496
TBMODIF,18,1,0.7
TBMODIF,18,2,123.2669554
TBMODIF,19,1,0.8
TBMODIF,19,2,128.4491947
TBMODIF,20,1,0.9
TBMODIF,20,2,133.2007971

!*
TBTEMP,273,3
!*
TBMODIF,1,1,0.00031075
TBMODIF,1,2,11.6878009
TBMODIF,2,1,0.001
TBMODIF,2,2,16.40338865
TBMODIF,3,1,0.002
TBMODIF,3,2,20.05544366
TBMODIF,4,1,0.003
TBMODIF,4,2,22.55790373
TBMODIF,5,1,0.005
TBMODIF,5,2,26.15982752
TBMODIF,6,1,0.007
TBMODIF,6,2,28.84111236
TBMODIF,7,1,0.01
TBMODIF,7,2,31.98405878
TBMODIF,8,1,0.03
TBMODIF,8,2,43.98440676
TBMODIF,9,1,0.04
TBMODIF,9,2,47.81134624
TBMODIF,10,1,0.06
TBMODIF,10,2,53.7771073
TBMODIF,11,1,0.08
TBMODIF,11,2,58.45607764
TBMODIF,12,1,0.1
TBMODIF,12,2,62.36394429
TBMODIF,13,1,0.2
TBMODIF,13,2,76.24867017
TBMODIF,14,1,0.3
TBMODIF,14,2,85.762758
TBMODIF,15,1,0.4
TBMODIF,15,2,93.22469527
TBMODIF,16,1,0.5
TBMODIF,16,2,99.45689032
TBMODIF,17,1,0.6
TBMODIF,17,2,104.8570023

TBMODIF,18,1,0.7
TBMODIF,18,2,109.650851
TBMODIF,19,1,0.8
TBMODIF,19,2,113.9802673
TBMODIF,20,1,0.9
TBMODIF,20,2,117.9407547

!*
TBTEMP,298,4
!*
TBMODIF,1,1,0.00032036
TBMODIF,1,2,11.87092215
TBMODIF,2,1,0.001
TBMODIF,2,2,16.2991214
TBMODIF,3,1,0.002
TBMODIF,3,2,19.76974413
TBMODIF,4,1,0.003
TBMODIF,4,2,22.1331111
TBMODIF,5,1,0.005
TBMODIF,5,2,25.51686646
TBMODIF,6,1,0.007
TBMODIF,6,2,28.02360473
TBMODIF,7,1,0.01
TBMODIF,7,2,30.95025237
TBMODIF,8,1,0.03
TBMODIF,8,2,42.02836198
TBMODIF,9,1,0.04
TBMODIF,9,2,45.53422007
TBMODIF,10,1,0.06
TBMODIF,10,2,50.97759209
TBMODIF,11,1,0.08
TBMODIF,11,2,55.22996347
TBMODIF,12,1,0.1
TBMODIF,12,2,58.77115078
TBMODIF,13,1,0.2
TBMODIF,13,2,71.2854751
TBMODIF,14,1,0.3
TBMODIF,14,2,79.80727167
TBMODIF,15,1,0.4
TBMODIF,15,2,86.46451349
TBMODIF,16,1,0.5
TBMODIF,16,2,92.00837083
TBMODIF,17,1,0.6
TBMODIF,17,2,96.80088277
TBMODIF,18,1,0.7
TBMODIF,18,2,101.0471337
TBMODIF,19,1,0.8
TBMODIF,19,2,104.8756718
TBMODIF,20,1,0.9
TBMODIF,20,2,108.3729096

```
!*
TBTEMP,323,5
!*
TBMODIF,1,1,0.00032645
TBMODIF,1,2,11.91469034
TBMODIF,2,1,0.001
TBMODIF,2,2,16.06548008
TBMODIF,3,1,0.002
TBMODIF,3,2,19.33164079
TBMODIF,4,1,0.003
TBMODIF,4,2,21.54195344
TBMODIF,5,1,0.005
TBMODIF,5,2,24.68986408
TBMODIF,6,1,0.007
TBMODIF,6,2,27.01064062
TBMODIF,7,1,0.01
TBMODIF,7,2,29.70938816
TBMODIF,8,1,0.03
TBMODIF,8,2,39.83685849
TBMODIF,9,1,0.04
TBMODIF,9,2,43.01735719
TBMODIF,10,1,0.06
TBMODIF,10,2,47.93581237
TBMODIF,11,1,0.08
TBMODIF,11,2,51.76291608
TBMODIF,12,1,0.1
TBMODIF,12,2,54.94063921
TBMODIF,13,1,0.2
TBMODIF,13,2,66.11023741
TBMODIF,14,1,0.3
TBMODIF,14,2,73.66905229
TBMODIF,15,1,0.4
TBMODIF,15,2,79.55064873
TBMODIF,16,1,0.5
TBMODIF,16,2,84.43425954
TBMODIF,17,1,0.6
TBMODIF,17,2,88.64619355
TBMODIF,18,1,0.7
TBMODIF,18,2,92.37083822
TBMODIF,19,1,0.8
TBMODIF,19,2,95.72353634
TBMODIF,20,1,0.9
TBMODIF,20,2,98.78169136


!*
TBTEMP,363,6
!*
TBMODIF,1,1,0.0003269
TBMODIF,1,2,11.64029319
TBMODIF,2,1,0.001
TBMODIF,2,2,15.36999636
TBMODIF,3,1,0.002
TBMODIF,3,2,18.26038045
```

```
TBMODIF,4,1,0.003
TBMODIF,4,2,20.1969648
TBMODIF,5,1,0.005
TBMODIF,5,2,22.93177689
TBMODIF,6,1,0.007
TBMODIF,6,2,24.93246037
TBMODIF,7,1,0.01
TBMODIF,7,2,27.24418149
TBMODIF,8,1,0.03
TBMODIF,8,2,35.80025405
TBMODIF,9,1,0.04
TBMODIF,9,2,38.45438575
TBMODIF,10,1,0.06
TBMODIF,10,2,42.53262289
TBMODIF,11,1,0.08
TBMODIF,11,2,45.68587377
TBMODIF,12,1,0.1
TBMODIF,12,2,48.29184129
TBMODIF,13,1,0.2
TBMODIF,13,2,57.37329884
TBMODIF,14,1,0.3
TBMODIF,14,2,63.45796029
TBMODIF,15,1,0.4
TBMODIF,15,2,68.16255773
TBMODIF,16,1,0.5
TBMODIF,16,2,72.05061759
TBMODIF,17,1,0.6
TBMODIF,17,2,75.39146204
TBMODIF,18,1,0.7
TBMODIF,18,2,78.33667562
TBMODIF,19,1,0.8
TBMODIF,19,2,80.98077625
TBMODIF,20,1,0.9
TBMODIF,20,2,83.38701977



!*
TBTEMP,398,7
!*
TBMODIF,1,1,0.00031555
TBMODIF,1,2,10.98870147
TBMODIF,2,1,0.001
TBMODIF,2,2,14.3685526
TBMODIF,3,1,0.002
TBMODIF,3,2,16.88116817
TBMODIF,4,1,0.003
TBMODIF,4,2,18.54999146
TBMODIF,5,1,0.005
TBMODIF,5,2,20.88928371
TBMODIF,6,1,0.007
TBMODIF,6,2,22.5890682
TBMODIF,7,1,0.01
TBMODIF,7,2,24.54217352
TBMODIF,8,1,0.03
TBMODIF,8,2,31.68427062
```

```
TBMODIF,9,1,0.04
TBMODIF,9,2,33.875988
TBMODIF,10,1,0.06
TBMODIF,10,2,37.22486985
TBMODIF,11,1,0.08
TBMODIF,11,2,39.79985082
TBMODIF,12,1,0.1
TBMODIF,12,2,41.91920352
TBMODIF,13,1,0.2
TBMODIF,13,2,49.24957604
TBMODIF,14,1,0.3
TBMODIF,14,2,54.1182462
TBMODIF,15,1,0.4
TBMODIF,15,2,57.86180406
TBMODIF,16,1,0.5
TBMODIF,16,2,60.94296059
TBMODIF,17,1,0.6
TBMODIF,17,2,63.58185408
TBMODIF,18,1,0.7
TBMODIF,18,2,65.90195779
TBMODIF,19,1,0.8
TBMODIF,19,2,67.98004446
TBMODIF,20,1,0.9
TBMODIF,20,2,69.86737165
```

Appendix C: Ansys input file for the solution of temperature cycling loading

```
MAX_chamber              = 100 +273
MINTEMP                  = -40+273

T_DWELL_max_SEC      = 60*60
T_DWELL_CHAMBER_SEC      = 15*60
T_RAMP_UP_SEC        = 14*60
T_RAMP_DOWN_SEC   = 14*60

TREF=298

!define only the corner solder to be recorded


allsel
/SOLU
antype,transient,new      !specifies new transient analysis
TRNOPT,FULL
tref,298
CRPLIM,50,0



!step 1: set to ambient
allsel
bfunif,temp,298
solcon,on              !turn on the optimized nonlinear solver
nlgeom,on               !turn on the large drformation effect
autots,on
ptime0=10
ptime=ptime0
time,ptime    !time at the end of load step
deltim,10,10,10
KBC,0
RATE,1
NEQIT,1000
cnvtol,f,0.05
crplim,10,on          !creep criterion
CUTCONTROL,PLSLIMIT,0.15,
outres,all,none
outres,strs,last,SOLDER
outres,epel,last,SOLDER
outres,epth,last,SOLDER
outres,eppl,last,SOLDER
outres,epcr,last,SOLDER
SOLVE


!step 2: set to max chamber
allsel
bfunif,temp,373
solcon,on              !turn on the optimized nonlinear solver
nlgeom,on               !turn on the large drformation effect
```

```
autots,on
ptime0=460
ptime=ptime0
time,ptime    !time at the end of load step
deltim,10,10,10
KBC,0
RATE,1
NEQIT,1000
cnvtol,f,0.05
crplim,50,on          !creep criterion
CUTCONTROL,PLSLIMIT,0.15,
outres,all,none
outres,strs,all,SOLDER
outres,epel,all,SOLDER
outres,epth,all,SOLDER
outres,eppl,all,SOLDER
outres,epcr,all,SOLDER
SOLVE


!step 3: first max dwell
allsel
bfunif,temp,373
solcon,on             !turn on the optimized nonlinear solver
nlgeom,on              !turn on the large drformation effect
autots,on
ptime3=T_DWELL_max_SEC
ptime=ptime+ptime3
time,ptime    !time at the end of load step
deltim,30,30,30
KBC,0
RATE,1
NEQIT,1000
cnvtol,f,0.05
crplim,50,on          !creep criterion
CUTCONTROL,PLSLIMIT,0.15,
outres,all,none
outres,strs,all,SOLDER
outres,epel,all,SOLDER
outres,epth,all,SOLDER
outres,eppl,all,SOLDER
outres,epcr,all,SOLDER
SOLVE


!step 4: first ramp down
allsel
bfunif,temp,MINTEMP
solcon,on             !turn on the optimized nonlinear solver
nlgeom,on              !turn on the large drformation effect
autots,on
ptime4=T_RAMP_DOWN_SEC
ptime=ptime+ptime4
time,ptime    !time at the end of load step
deltim,30,30,30
KBC,0
```

```
RATE,1
NEQIT,1000
cnvtol,f,0.05
crplim,50,on          !creep criterion
CUTCONTROL,PLSLIMIT,0.15,
outres,all,none
outres,strs,all,SOLDER
outres,epel,all,SOLDER
outres,epth,all,SOLDER
outres,eppl,all,SOLDER
outres,epcr,all,SOLDER
SOLVE


!step 5: first low dwell
allsel
bfunif,temp,MINTEMP
solcon,on             !turn on the optimized nonlinear solver
nlgeom,on              !turn on the large drformation effect
autots,on
ptime5=T_DWELL_CHAMBER_SEC
ptime=ptime+ptime5
time,ptime    !time at the end of load step
deltim,30,30,30
KBC,0
RATE,1
NEQIT,1000
cnvtol,f,0.05
crplim,50,on          !creep criterion
CUTCONTROL,PLSLIMIT,0.15,
outres,all,none
outres,strs,all,SOLDER
outres,epel,all,SOLDER
outres,epth,all,SOLDER
outres,eppl,all,SOLDER
outres,epcr,all,SOLDER
SOLVE


!step 6: second ramp up
allsel
bfunif,temp,MAX_chamber
solcon,on             !turn on the optimized nonlinear solver
nlgeom,on              !turn on the large drformation effect
autots,on
ptime6=T_RAMP_UP_SEC
ptime=ptime+ptime6
time,ptime    !time at the end of load step
deltim,10,10,10
KBC,0
RATE,1
NEQIT,1000
cnvtol,f,0.05
crplim,50,on          !creep criterion
CUTCONTROL,PLSLIMIT,0.15,
outres,all,none
```

```
outres,strs,all,SOLDER
outres,epel,all,SOLDER
outres,epth,all,SOLDER
outres,eppl,all,SOLDER
outres,epcr,all,SOLDER
SOLVE


!step 7: second max
allsel
bfunif,temp,MAX_chamber
solcon,on               !turn on the optimized nonlinear solver
nlgeom,on               !turn on the large drformation effect
autots,on
ptime7=T_DWELL_max_SEC
ptime=ptime+ptime7
time,ptime    !time at the end of load step
deltim,30,30,30
KBC,0
RATE,1
NEQIT,1000
cnvtol,f,0.05
crplim,50,on          !creep criterion
CUTCONTROL,PLSLIMIT,0.15,
outres,all,none
outres,strs,all,SOLDER
outres,epel,all,SOLDER
outres,epth,all,SOLDER
outres,eppl,all,SOLDER
outres,epcr,all,SOLDER
SOLVE


!step 8: second ramp down
allsel
bfunif,temp,MINTEMP
solcon,on               !turn on the optimized nonlinear solver
nlgeom,on               !turn on the large drformation effect
autots,on
ptime8=T_RAMP_DOWN_SEC
ptime=ptime+ptime8
time,ptime    !time at the end of load step
deltim,30,30,30
KBC,0
RATE,1
NEQIT,1000
cnvtol,f,0.05
crplim,50,on          !creep criterion
CUTCONTROL,PLSLIMIT,0.15,
outres,all,none
outres,strs,all,SOLDER
outres,epel,all,SOLDER
outres,epth,all,SOLDER
outres,eppl,all,SOLDER
outres,epcr,all,SOLDER
```

```
SOLVE


!step 9: second low dwell
allsel
bfunif,temp,MINTEMP
solcon,on               !turn on the optimized nonlinear solver
nlgeom,on                !turn on the large drformation effect
autots,on
ptime9=T_DWELL_CHAMBER_SEC
ptime=ptime+ptime9
time,ptime    !time at the end of load step
deltim,30,30,30
KBC,0
RATE,1
NEQIT,1000
cnvtol,f,0.05
crplim,50,on           !creep criterion
CUTCONTROL,PLSLIMIT,0.15,
outres,all,none
outres,strs,all,SOLDER
outres,epel,all,SOLDER
outres,epth,all,SOLDER
outres,eppl,all,SOLDER
outres,epcr,all,SOLDER
SOLVE


!step 10: third ramp up
allsel
bfunif,temp,MAX_chamber
solcon,on               !turn on the optimized nonlinear solver
nlgeom,on                !turn on the large drformation effect
autots,on
ptime10=T_RAMP_UP_SEC
ptime=ptime+ptime10
time,ptime    !time at the end of load step
deltim,10,10,10
KBC,0
RATE,1
NEQIT,1000
cnvtol,f,0.05
crplim,50,on           !creep criterion
CUTCONTROL,PLSLIMIT,0.15,
outres,all,none
outres,strs,all,SOLDER
outres,epel,all,SOLDER
outres,epth,all,SOLDER
outres,eppl,all,SOLDER
outres,epcr,all,SOLDER
SOLVE



!step 11: third max dwell
allsel
```

```
bfunif,temp,MAX_chamber
solcon,on               !turn on the optimized nonlinear solver
nlgeom,on               !turn on the large drformation effect
autots,on
ptime11=T_DWELL_max_SEC
ptime=ptime+ptime11
time,ptime    !time at the end of load step
deltim,30,30,30
KBC,0
RATE,1
NEQIT,1000
cnvtol,f,0.05
crplim,50,on            !creep criterion
CUTCONTROL,PLSLIMIT,0.15,
outres,all,none
outres,strs,all,SOLDER
outres,epel,all,SOLDER
outres,epth,all,SOLDER
outres,eppl,all,SOLDER
outres,epcr,all,SOLDER
SOLVE
```

Appendix D: Ansys input file for the solution of temperature cycling loading by global-local model

```
RESUME,'68-local model','db','C:\Ansys\CLCC\submodeling\Superposition\SnPb\68 IO\',0,0

/prep7
!select all node at the cut boundary at local model
FLST,5,3,5,ORDE,3
FITEM,5,37
FITEM,5,80
FITEM,5,84
ASEL,S, , ,P51X
nsla,s
nSEL,a,LOC,Z,9.709
nsel,a,loc,z,10.7
nsel,a,loc,x,-0.134
nsel,a,loc,x,1.434
nplot
nwrite,local,nd   !record node of interest


!select the solder element that the results will be stored, and name it as “solder”
vsel,s,,,27,28,1
eslv,s
eplot
cm,SOLDER,elem
finish

allsel
eplot

save



!step 1 10s
/filname,global-model
RESUME,'global-model','db',     !resume the global model
/post1
set,1
cbdof,local,nd,,local,cb   !at set 1, store the displacement of the nodes at the cut boundary into the file “local. cb”
save
finish


/filname, local-model
RESUME,'local-model','db',     !resume the local model

/solu
antype,static,new         !start new analysis in local model since it is the start of the local solution
outres,all,all
!load step 1: set to ambient
/input,local,cb   !input the displacement which is stored at the “local.cb”
```

```
tref,298
BF,all,TEMP,298  !set the environmental temperature which is the thermal loading at the current time step
time,10
deltim,10,10,10
solcon,on                !turn on the optimized nonlinear solver
nlgeom,on
KBC,0
RATE,1
NEQIT,1000
cnvtol,f,0.05
crplim,5,on           !creep criterion
CUTCONTROL,PLSLIMIT,0.15,
outres,all,none
outres,strs,LAST,SOLDER    !store the results for only “solder” element
outres,epel,LAST,SOLDER
outres,epth,LAST,SOLDER
outres,eppl,LAST,SOLDER
outres,epcr,LAST,SOLDER
solve
save
finish



!!!!!!!!!!!!!!!!!!!!!!!!!!!!!!!!!!!!!!!!!!!!!!!!!!!!
!first climb
!step 2: 40s



/filname,global-model
RESUME,'global-model','db',   ,     !resume the global model
/POST1
SET,2,
cbdof,local,nd,,local,cb    !at set 2, store the displacement and update the “local.cb” file
save
finish


/filname, local-model
RESUME,'local-model','db',


/solu
antype,static,REST     ! define it is restart of analysis so the analysis follows the previous step
outres,all,all
/input,local,cb   !use the displacement in the current “local.cb” as the boundary condition
tref,298
BF,all,TEMP,303
time,40
deltim,10,10,10
solcon,on                !turn on the optimized nonlinear solver
nlgeom,on
KBC,0
RATE,1
```

```
NEQIT,1000
cnvtol,f,0.05
crplim,50,on            !creep criterion
CUTCONTROL,PLSLIMIT,0.15,
outres,all,none
outres,strs,LAST,SOLDER
outres,epel,LAST,SOLDER
outres,epth,LAST,SOLDER
outres,eppl,LAST,SOLDER
outres,epcr,LAST,SOLDER
solve
save
finish
```

!continue the analysis of the local model following the process in step 2

Appendix E: Ansys input file for post processing

```
!select the elements under interest
vsel,s,,,4
vsel,a,,,513
vsel,a,,,504
vsel,a,,,1368
ESLV,S


eplot

/post1   !in the general post processor
set,7,last,1  !decide by loadstep, not by set
etable,vtable1,volu   !store the volume in the table “vtable”
etable,psd1table,send,plastic    !PLASTIC WORK DENSITY
etable,csd1table,send,creep    ! CREEP WORK DENSITY
etable,esd1table,send,elastic    ! ELASTIC STRAIN ENERGY DENSITY
smult,pw1table,vtable1,psd1table     !PLASTIC WORK
smult,cw1table,vtable1,csd1table    !CREEP WORK
smult,ew1table,vtable1,esd1table     ! ELASTIC STRAIN ENERGY
ssum


set,11,last,1
etable,vtable2,volu
etable,psd2table,send,plastic
etable,csd2table,send,creep
etable,esd2table,send,elastic
smult,pw2table,vtable2, psd2table
smult,cw2table,vtable2, csd2table
smult,ew2table,vtable2, esd2table
ssum
```

Appendix F: Ansys input file for geometry and meshing of BGA

```
!model in SI unit
/PREP7
/tit, CABGA-112-2D
!GEOMETRY
BALL_R=0.25e-3
SOLDER_NECK_H=0.018e-3
HALF_SOLDER_NECK_W=0.182e-3
SOLDER_H=0.276e-3
PAD_H=0.041e-3 !width is as neck width
SOLDER_HEIGHT=SOLDER_H+PAD_H+SOLDER_NECK_H
HALF_SOLDER_HEIGHT=SOLDER_H/2+PAD_H+SOLDER_NECK_H
SOLDER_NECK_HEIGHT=SOLDER_HEIGHT+SOLDER_NECK_H
BOTTOM_NECK_HEIGHT=PAD_H+SOLDER_NECK_H
METAL_H=0.023e-3
METAL_HEIGHT=SOLDER_NECK_HEIGHT+METAL_H
PITCH=0.8e-3
PITCH_BE=PITCH/2-HALF_SOLDER_NECK_W
HALF_PITCH=PITCH/2
PCB_HEIGHT=-1.35e-3
SUB_H=0.28e-3
SUB_HEIGHT=METAL_HEIGHT+SUB_H
HALF_DIE_W=6e-3
DIE_H=0.26e-3
DIE_HEIGHT=SUB_HEIGHT+DIE_H
HALF_EPOXY_W=7e-3
EPXOY_H1=0.396e-3
EPXOY_HEIGHT=DIE_HEIGHT+EPXOY_H1



K,1,0,0,0
K,2,HALF_SOLDER_NECK_W,0,0
K,3,0,PAD_H,0
K,4,HALF_SOLDER_NECK_W,PAD_H,0
K,5,0,BOTTOM_NECK_HEIGHT,0
K,6,HALF_SOLDER_NECK_W,BOTTOM_NECK_HEIGHT,0
K,7,0,SOLDER_HEIGHT,0
K,8,HALF_SOLDER_NECK_W,SOLDER_HEIGHT,0
K,9,0,SOLDER_NECK_HEIGHT,0
K,10,HALF_SOLDER_NECK_W,SOLDER_NECK_HEIGHT,0
K,11,0,METAL_HEIGHT,0
K,12,HALF_SOLDER_NECK_W,METAL_HEIGHT,0
K,13,0,HALF_SOLDER_HEIGHT,0
A,1,2,4,3
A,3,4,6,5
L,5,6
L,5,7
L,7,8
LARC,6,8,13,BALL_R
AL,6,10,9,8
A,7,8,10,9
A,9,10,12,11


K,14,0,PCB_HEIGHT,0
K,15,0,SUB_HEIGHT,0
```

```
K,16,0,DIE_HEIGHT,0
K,17,0,EPXOY_HEIGHT,0
K,18,HALF_SOLDER_NECK_W,SUB_HEIGHT,0,0
K,19,HALF_SOLDER_NECK_W,DIE_HEIGHT,0
K,20,HALF_SOLDER_NECK_W,EPXOY_HEIGHT,0
K,21,HALF_SOLDER_NECK_W,PCB_HEIGHT,0
A,14,21,2,1
A,11,12,18,15
A,15,18,19,16
A,16,19,20,17


ALLSEL
APLOT

ASEL,S,LOC,X,0,BALL_R
VROTAT,ALL, , , , ,5, 7,90, ,


KGEN,2,12, , ,PITCH_BE, , , ,0
KGEN,2,27, , ,, ,-PITCH_BE , ,0
KGEN,2,33, , ,PITCH/2, , , ,0
A,12,32,34,33,27
METAL_TOTAL=METAL_HEIGHT-PCB_HEIGHT
AGEN,2,38, , , ,-METAL_TOTAL, , ,0
FLST,8,3,4
FITEM,8,20
FITEM,8,23
FITEM,8,26
VDRAG,      38, , , , , ,P51X
VDRAG,      39, , , , , ,      18
ALLSEL
VSYMM,X,ALL, , , ,0,0
ALLSEL
VSYMM,Z,ALL, , , ,0,0
ALLSEL
VGEN,4,ALL, , , , ,-PITCH, ,0
ALLSEL
VGEN,8,ALL, , , -PITCH, ,, ,0
VSEL,S,LOC,Z,-3.5*PITCH,0.5*PITCH,
VSEL,R,LOC,X,-3.5*PITCH,0.5*PITCH,
VGEN,2,ALL, , , , ,-4*PITCH, ,0
ALLSEL
VPLOT


ASEL,S,LOC,X,-3.5*PITCH,-3.5*PITCH
ASEL,R,LOC,Z,-3.5*PITCH,-7.5*PITCH
ASEL,R,LOC,Y,METAL_HEIGHT,EPXOY_HEIGHT
VDRAG,ALL, , , , , ,    8144

ASEL,S,LOC,X,-3.5*PITCH,-3.5*PITCH
ASEL,R,LOC,Z,-3.5*PITCH,-7.5*PITCH
ASEL,R,LOC,Y,PCB_HEIGHT,0
VDRAG,ALL, , , , , ,    8155
```

```
VSEL,S,LOC,X,-3.5*PITCH,-4*PITCH
VSEL,R,LOC,Z,-3.5*PITCH,-7.5*PITCH
VGEN,8,ALL, , ,-0.5*PITCH, , , ,0

MOLD_WIDTH=7E-3
MOLD_SHIFT=MOLD_WIDTH-8*PITCH
KGEN,2,163, , ,MOLD_SHIFT, , , ,0
L,163,12578
ASEL,S,LOC,X,0.5*PITCH,0.5*PITCH
VDRAG,ALL, , , , , ,    22801
KGEN,2,163, , ,, , MOLD_SHIFT, ,0
L,163,12771
ASEL,S,LOC,Z,0.5*PITCH,0.5*PITCH
VDRAG,ALL, , , , , ,    23218

BOARD_SHIFT=3E-3
MOLD_CORD=MOLD_WIDTH-7.5*PITCH
KGEN,2,12968, , ,, , BOARD_SHIFT, ,0
L,12968,12970
ASEL,S,LOC,Z,MOLD_CORD,MOLD_CORD
ASEL,R,LOC,Y,PCB_HEIGHT,0
VDRAG,ALL, , , , , ,    23651
KGEN,2,12970, , ,BOARD_SHIFT, , , ,0
L,   12970,   13037
ASEL,S,LOC,X,MOLD_CORD,MOLD_CORD
ASEL,R,LOC,Y,PCB_HEIGHT,0
VDRAG,ALL, , , , , ,    23785

ALLSEL
VGLUE,ALL
ALLSEL
NUMMRG,ALL, , , ,LOW
ALLSEL
NUMCMP,ALL

/prep7
!1-PWB
!2-CU
!3-OVERMOLD
!4-DIE
!5-SOLDER
!6-SUBSTRATE

!Add color to different materials
/NUMBER,1
/PNUM,MAT,1
/COLOR,NUM,GCYA,1
/COLOR,NUM,BLUE,2
/COLOR,NUM,ORAN,3
/COLOR,NUM,YELL,4
/COLOR,NUM,LGRA,5
/COLOR,NUM,RED,6

ET,1,SOLID70   !8 node brick thermal element
```

```
LSEL,S,LOC,Y,BOTTOM_NECK_HEIGHT,SOLDER_HEIGHT
LSEL,U,LOC,Y,SOLDER_HEIGHT,SOLDER_HEIGHT
LSEL,U,LOC,Y,BOTTOM_NECK_HEIGHT,BOTTOM_NECK_HEIGHT
LPLOT
LESIZE,all, , ,5, , , , ,1

LSEL,S,LOC,Y,PAD_H,BOTTOM_NECK_HEIGHT
LSEL,A,LOC,Y,SOLDER_HEIGHT,SOLDER_NECK_HEIGHT
LSEL,U,LOC,Y,PAD_H,PAD_H
LSEL,U,LOC,Y,BOTTOM_NECK_HEIGHT,BOTTOM_NECK_HEIGHT
LSEL,U,LOC,Y,SOLDER_HEIGHT,SOLDER_HEIGHT
LSEL,U,LOC,Y,SOLDER_NECK_HEIGHT,SOLDER_NECK_HEIGHT
LPLOT
LESIZE,all, , ,1, , , , ,1


LSEL,S,LOC,Y,PAD_H,PAD_H
LSEL,A,LOC,Y,BOTTOM_NECK_HEIGHT,BOTTOM_NECK_HEIGHT
LSEL,A,LOC,Y,SOLDER_HEIGHT,SOLDER_HEIGHT
LSEL,A,LOC,Y,SOLDER_NECK_HEIGHT,SOLDER_NECK_HEIGHT
LPLOT
LESIZE,all, , ,3, , , , ,1

VSEL,S,LOC,Y,PAD_H,SOLDER_NECK_HEIGHT
MAT,5
MSHAPE,0,2D
MSHKEY,1
VPLOT
VMESH, ALL



LSEL,S,LOC,Y,0,PAD_H
LSEL,A,LOC,Y,SOLDER_NECK_HEIGHT,METAL_HEIGHT
LSEL,U,LOC,Y,0,0
LSEL,U,LOC,Y,PAD_H,PAD_H
LSEL,U,LOC,Y,SOLDER_NECK_HEIGHT,SOLDER_NECK_HEIGHT
LSEL,U,LOC,Y,METAL_HEIGHT,METAL_HEIGHT
LPLOT
LESIZE,all, , ,1, , , , ,1

VSEL,S,LOC,Y,0,PAD_H
VSEL,A,LOC,Y,SOLDER_NECK_HEIGHT,METAL_HEIGHT
MAT,2
MSHAPE,0,3D
MSHKEY,1
VPLOT
VMESH, ALL


LSEL,S,LOC,Y,METAL_HEIGHT,EPXOY_HEIGHT
LSEL,U,LOC,Y,METAL_HEIGHT,METAL_HEIGHT
LSEL,U,LOC,Y,SUB_HEIGHT,SUB_HEIGHT
LSEL,U,LOC,Y,DIE_HEIGHT,DIE_HEIGHT
```

```
LSEL,U,LOC,Y,EPXOY_HEIGHT,EPXOY_HEIGHT
LPLOT
LESIZE,all, , ,2, , , , ,1



*DO,I,1,8
VSEL,S,LOC,Y,METAL_HEIGHT,SUB_HEIGHT
VSEL,R,LOC,X,-(I-1)*PITCH-HALF_SOLDER_NECK_W,-(I-1)*PITCH+HALF_SOLDER_NECK_W
MAT,6
MSHAPE,0,2D
MSHKEY,1
VPLOT
VMESH, ALL
*ENDDO



*DO,I,1,8
VSEL,S,LOC,Y,SUB_HEIGHT,DIE_HEIGHT
VSEL,R,LOC,X,-(I-1)*PITCH-HALF_SOLDER_NECK_W,-(I-1)*PITCH+HALF_SOLDER_NECK_W
MAT,4
MSHAPE,0,2D
MSHKEY,1
VPLOT
VMESH, ALL
*ENDDO


*DO,I,1,8
VSEL,S,LOC,Y,DIE_HEIGHT,EPXOY_HEIGHT
VSEL,R,LOC,X,-(I-1)*PITCH-HALF_SOLDER_NECK_W,-(I-1)*PITCH+HALF_SOLDER_NECK_W
MAT,3
MSHAPE,0,2D
MSHKEY,1
VPLOT
VMESH, ALL
*ENDDO



*DO,I,1,8
LSEL,S,LOC,Y,METAL_HEIGHT,METAL_HEIGHT
LSEL,A,LOC,Y,DIE_HEIGHT,DIE_HEIGHT
LSEL,A,LOC,Y,EPXOY_HEIGHT,EPXOY_HEIGHT
LSEL,R,LOC,X,-(I-1)*PITCH+0.5*PITCH,-(I-1)*PITCH+PITCH*0.5
LESIZE,all, , ,2, , , , ,1
*ENDDO

*DO,I,1,8
LSEL,S,LOC,Y,METAL_HEIGHT,METAL_HEIGHT
LSEL,A,LOC,Y,DIE_HEIGHT,DIE_HEIGHT
LSEL,A,LOC,Y,EPXOY_HEIGHT,EPXOY_HEIGHT
LSEL,R,LOC,Z,-(I-1)*PITCH+0.5*PITCH,-(I-1)*PITCH+PITCH*0.5
LESIZE,all, , ,2, , , , ,1
```

```
*ENDDO

*DO,I,1,8
LSEL,S,LOC,Y,METAL_HEIGHT,METAL_HEIGHT
LSEL,A,LOC,Y,DIE_HEIGHT,DIE_HEIGHT
LSEL,A,LOC,Y,EPXOY_HEIGHT,EPXOY_HEIGHT
LSEL,R,LOC,Z,-(I-1)*PITCH,-(I-1)*PITCH
LESIZE,all, , ,1, , , , ,1
*ENDDO

*DO,I,1,8
LSEL,S,LOC,Y,METAL_HEIGHT,METAL_HEIGHT
LSEL,A,LOC,Y,DIE_HEIGHT,DIE_HEIGHT
LSEL,A,LOC,Y,EPXOY_HEIGHT,EPXOY_HEIGHT
LSEL,R,LOC,X,-(I-1)*PITCH,-(I-1)*PITCH
LESIZE,all, , ,1, , , , ,1
*ENDDO

!manually
LSEL,S,LOC,Y,METAL_HEIGHT,METAL_HEIGHT
LSEL,A,LOC,Y,DIE_HEIGHT,DIE_HEIGHT
LSEL,A,LOC,Y,EPXOY_HEIGHT,EPXOY_HEIGHT
lsel,r,loc,z,0.5*pitch
lplot
LESIZE,all, , ,2, , , , ,1

LSEL,S,LOC,Y,METAL_HEIGHT,METAL_HEIGHT
LSEL,A,LOC,Y,DIE_HEIGHT,DIE_HEIGHT
LSEL,A,LOC,Y,EPXOY_HEIGHT,EPXOY_HEIGHT
lsel,r,loc,z,-7.5*pitch
lplot
LESIZE,all, , ,2, , , , ,1


!manually
LSEL,S,LOC,Y,METAL_HEIGHT,METAL_HEIGHT
LSEL,A,LOC,Y,DIE_HEIGHT,DIE_HEIGHT
LSEL,A,LOC,Y,EPXOY_HEIGHT,EPXOY_HEIGHT
lsel,r,loc,z,0.5*pitch
lplot
LESIZE,all, , ,2, , , , ,1


!manully
LSEL,S,LOC,Y,METAL_HEIGHT,METAL_HEIGHT
LSEL,A,LOC,Y,DIE_HEIGHT,DIE_HEIGHT
LSEL,A,LOC,Y,EPXOY_HEIGHT,EPXOY_HEIGHT
lsel,r,loc,x,-7.5*pitch
lplot
LESIZE,all, , ,2, , , , ,1


!manually
LSEL,S,LOC,Y,METAL_HEIGHT,METAL_HEIGHT
LSEL,A,LOC,Y,DIE_HEIGHT,DIE_HEIGHT
LSEL,A,LOC,Y,EPXOY_HEIGHT,EPXOY_HEIGHT
```

```
lsel,r,loc,x,0.5*pitch
lplot
LESIZE,all, , ,2, , , , ,1

LSEL,S,LOC,Y,METAL_HEIGHT,METAL_HEIGHT
LSEL,A,LOC,Y,DIE_HEIGHT,DIE_HEIGHT
LSEL,A,LOC,Y,EPXOY_HEIGHT,EPXOY_HEIGHT
lsel,r,loc,z,-7.5*pitch
lplot
LESIZE,all, , ,2, , , , ,1

*DO,I,1,4
allsel
VSEL,S,LOC,Y,METAL_HEIGHT,SUB_HEIGHT
VSEL,R,LOC,X,(-0.5-(i-1))*PITCH,(0.5-(i-1))*PITCH
VSEL,R,LOC,Z,0.5*PITCH,-7.5*PITCH
VPLOT
MAT,6
MSHAPE,0,2D
MSHKEY,1
VPLOT
Vsweep, ALL
*ENDDO


*DO,I,5,8
allsel
VSEL,S,LOC,Y,METAL_HEIGHT,SUB_HEIGHT
VSEL,R,LOC,X,(-0.5-(i-1))*PITCH,(0.5-(i-1))*PITCH
VSEL,R,LOC,Z,0.5*PITCH,-3.5*PITCH
VPLOT
MAT,6
MSHAPE,0,2D
MSHKEY,1
VPLOT
Vsweep, ALL
*ENDDO


VSEL,S,LOC,Y,METAL_HEIGHT,SUB_HEIGHT
vsel,r,loc,x,-3.5*pitch,-7.5*pitch
vsel,r,loc,z,-3.5*pitch,-7.5*pitch
MAT,6
MSHAPE,0,2D
MSHKEY,1
VPLOT
Vmesh, ALL


*DO,I,1,4
allsel
VSEL,S,LOC,Y,DIE_HEIGHT,SUB_HEIGHT
VSEL,R,LOC,X,(-0.5-(i-1))*PITCH,(0.5-(i-1))*PITCH
VSEL,R,LOC,Z,0.5*PITCH,-7.5*PITCH
VPLOT
MAT,4
```

```
MSHAPE,0,2D
MSHKEY,1
VPLOT
Vsweep, ALL
*ENDDO


*DO,I,5,8
allsel
VSEL,S,LOC,Y,DIE_HEIGHT,SUB_HEIGHT
VSEL,R,LOC,X,(-0.5-(i-1))*PITCH,(0.5-(i-1))*PITCH
VSEL,R,LOC,Z,0.5*PITCH,-3.5*PITCH
VPLOT
MAT,4
MSHAPE,0,2D
MSHKEY,1
VPLOT
Vsweep, ALL
*ENDDO


VSEL,S,LOC,Y,DIE_HEIGHT,SUB_HEIGHT
vsel,r,loc,x,-3.5*pitch,-7.5*pitch
vsel,r,loc,z,-3.5*pitch,-7.5*pitch
MAT,4
MSHAPE,0,2D
MSHKEY,1
VPLOT
Vmesh, ALL


VSEL,S,LOC,Y,DIE_HEIGHT,SUB_HEIGHT
vsel,r,loc,x,0,HALF_SOLDER_NECK_W
vplot
vclear,all
MAT,3
MSHAPE,0,2D
MSHKEY,1
VPLOT
Vmesh, ALL


VSEL,S,LOC,Y,DIE_HEIGHT,SUB_HEIGHT
vsel,r,loc,x,HALF_SOLDER_NECK_W,0.5*pitch
vplot
vclear,all
MAT,3
MSHAPE,0,2D
MSHKEY,1
VPLOT
Vsweep, ALL


VSEL,S,LOC,Y,DIE_HEIGHT,SUB_HEIGHT
vsel,r,loc,z,0,HALF_SOLDER_NECK_W
vplot
```

```
vclear,all
MAT,3
MSHAPE,0,2D
MSHKEY,1
VPLOT
Vmesh, ALL


VSEL,S,LOC,Y,DIE_HEIGHT,SUB_HEIGHT
vsel,r,loc,z,HALF_SOLDER_NECK_W,0.5*pitch
vplot
vclear,all
MAT,3
MSHAPE,0,2D
MSHKEY,1
VPLOT
Vsweep, ALL



*DO,I,1,4
allsel
VSEL,S,LOC,Y,DIE_HEIGHT,EPXOY_HEIGHT
VSEL,R,LOC,X,(-0.5-(i-1))*PITCH,(0.5-(i-1))*PITCH
VSEL,R,LOC,Z,0.5*PITCH,-7.5*PITCH
VPLOT
MAT,3
MSHAPE,0,2D
MSHKEY,1
VPLOT
Vsweep, ALL
*ENDDO


*DO,I,5,8
allsel
VSEL,S,LOC,Y,DIE_HEIGHT,EPXOY_HEIGHT
VSEL,R,LOC,X,(-0.5-(i-1))*PITCH,(0.5-(i-1))*PITCH
VSEL,R,LOC,Z,0.5*PITCH,-3.5*PITCH
VPLOT
MAT,3
MSHAPE,0,2D
MSHKEY,1
VPLOT
Vsweep, ALL
*ENDDO


VSEL,S,LOC,Y,DIE_HEIGHT,EPXOY_HEIGHT
vsel,r,loc,x,-3.5*pitch,-7.5*pitch
vsel,r,loc,z,-3.5*pitch,-7.5*pitch
MAT,3
MSHAPE,0,2D
MSHKEY,1
VPLOT
Vmesh, ALL
```

```
VSEL,S,LOC,Y,METAL_HEIGHT,SUB_HEIGHT
VSEL,R,LOC,X,0.5*PITCH,1E-3
VPLOT
MAT,6
MSHAPE,0,2D
MSHKEY,1
VMESH, ALL


VSEL,S,LOC,Y,METAL_HEIGHT,SUB_HEIGHT
VSEL,R,LOC,Z,0.5*PITCH,1E-3
VPLOT
MAT,6
MSHAPE,0,2D
MSHKEY,1
VMESH, ALL


VSEL,S,LOC,Y,EPXOY_HEIGHT,SUB_HEIGHT
VSEL,R,LOC,X,0.5*PITCH,1E-3
VPLOT
MAT,3
MSHAPE,0,2D
MSHKEY,1
VMESH, ALL


VSEL,S,LOC,Y,EPXOY_HEIGHT,SUB_HEIGHT
VSEL,R,LOC,Z,0.5*PITCH,1E-3
VPLOT
MAT,3
MSHAPE,0,2D
MSHKEY,1
VMESH, ALL



*DO,I,1,8
VSEL,S,LOC,Y,0,PCB_HEIGHT
VSEL,R,LOC,X,-(I-1)*PITCH-HALF_SOLDER_NECK_W,-(I-1)*PITCH+HALF_SOLDER_NECK_W
MAT,1
MSHAPE,0,2D
MSHKEY,1
VPLOT
VMESH, ALL
*ENDDO


!!!!!!!!!!!!!!!!!!!!!!!!!!!!!!
!DEFINE PWB LINES INTO 2 MANYALLY

LSEL,S,LOC,Y,0,PCB_HEIGHT
LSEL,U,LOC,Y,0
LSEL,U,LOC,Y,PCB_HEIGHT
```

```
LPLOT
LESIZE,all, , ,6, , , , ,1


*DO,I,1,8
VSEL,S,LOC,Y,0,PCB_HEIGHT
VSEL,R,LOC,X,-(I-1)*PITCH-HALF_SOLDER_NECK_W,-(I-1)*PITCH+HALF_SOLDER_NECK_W
MAT,1
MSHAPE,0,2D
MSHKEY,1
VPLOT
VMESH, ALL
*ENDDO


lsel,s,loc,y,0,
lsel,a,loc,y,PCB_HEIGHT
lplot
LESIZE,all, , ,2, , , , ,1



*DO,I,1,8
LSEL,S,LOC,Y,0
LSEL,A,LOC,Y,PCB_HEIGHT
LSEL,R,LOC,X,-(I-1)*PITCH+0.5*PITCH,-(I-1)*PITCH+PITCH*0.5
LESIZE,all, , ,2, , , , ,1
*ENDDO


*DO,I,1,8
LSEL,S,LOC,Y,0
LSEL,A,LOC,Y,PCB_HEIGHT
LSEL,R,LOC,Z,-(I-1)*PITCH+0.5*PITCH,-(I-1)*PITCH+PITCH*0.5
LESIZE,all, , ,2, , , , ,1
*ENDDO



*DO,I,1,4
allsel
VSEL,S,LOC,Y,0,PCB_HEIGHT
VSEL,R,LOC,X,(-0.5-(i-1))*PITCH,(0.5-(i-1))*PITCH
VSEL,R,LOC,Z,0.5*PITCH,-7.5*PITCH
VPLOT
MAT,1
MSHAPE,0,3D
MSHKEY,1
VPLOT
Vsweep, ALL
*ENDDO


*DO,I,5,8
allsel
VSEL,S,LOC,Y,0,PCB_HEIGHT
```

```
VSEL,R,LOC,X,(-0.5-(i-1))*PITCH,(0.5-(i-1))*PITCH
VSEL,R,LOC,Z,0.5*PITCH,-3.5*PITCH
VPLOT
MAT,1
MSHAPE,0,3D
MSHKEY,1
VPLOT
Vsweep, ALL
*ENDDO


VSEL,S,LOC,Y,0,PCB_HEIGHT
vsel,r,loc,x,-3.5*pitch,-7.5*pitch
vsel,r,loc,z,-3.5*pitch,-7.5*pitch
MAT,1
MSHAPE,0,3D
MSHKEY,1
VPLOT
Vmesh, ALL


!manually
LSEL,S,LOC,Y,0,
lsel,a,loc,y,PCB_HEIGHT
LSEL,R,LOC,X,1E-3,4e-3
lsel,u,loc,x,1e-3
lsel,u,loc,x,4e-3
LPLOT
LESIZE,all, , ,10, , , , ,1


LSEL,S,LOC,Y,0,
lsel,a,loc,y,PCB_HEIGHT
LSEL,R,LOC,z,1E-3,4e-3
lsel,u,loc,z,1e-3
lsel,u,loc,z,4e-3
LPLOT
LESIZE,all, , ,10, , , , ,1


vsel,s,loc,y,0,PCB_HEIGHT
vplot
MAT,1
MSHAPE,0,3D
MSHKEY,1
VPLOT
Vmesh, ALL
```

Bibliography

1. IPC-SM-785, “Guidelines for Accelerated Reliability Testing for Surface Mount Solder Attachment”, Northbrook, IL, Nov. 1992.
2. IPC-9701A, “Performance Test Methods and Qualification Requirements for Surface Mount Solder Attachments”, Northbrook, IL, Jan. 2002.
3. L.F, Coffin, “A Study of the Effect of Cyclic Thermal Stress on a Ductile Metal”, Transactions of ASME, vol. 76, pp 931-950, 1954.
4. S. S. Manson, “Fatigue: A Complex Subject-Some Simple Approximations”, Experimental Mechanics, vol 5, pp 193-226, 1965.
5. W. Engelmaier, “Fatigue life of Leadless Chip Carrier Solder Joint During Power Cycling”, IEEE Transactions on Component, Hybrids and Manufacturing Technology, Vol, 6, No.3, Sep. 1983.
6. J.D. Morrow, “Cyclic Plastic Strain Energy and Fatigue of Metals”, Proceeding of Symposium in Internal Friction, Damping, and Cyclic Plasticity, ASTM, STP-378, p 45-87, 1965
7. R. Darveaux, and, K. Banerji, "Constitutive Relations for Tin-Based Solder Joints", IEEE Transactions on CHMT, Vol. 15, No. 6, pp. 1013-1024, Dec.1992.
8. R. Darveaux,, “Effect of Simulation Methodology on Solder Joint Crack Growth Correlations,” Proceedings of 50th Electronic Components &Technology Conference, pp. 1048-1058. May 2000.
9. R. Darveaux, K. Banerji, A. Mawer, G. Dody, “Reliability of Plastic Ball Grid Array Assembly”, Ball Grid Array Technology, J. Lau, Ed., McGraw Hill, Inc., New York, 1995.
10. X. Zhang, S.W. Lee, K. Choi, Y. Kim, “Computational parametric analyzes on the solder joint reliability of bottom leaded plastic (BLP) package”, IEEE Transactions on Advanced Packaging,v 25, n4,p514-521, Nov. 2002
11. M. Spraul, W. Nüchter, A. Möller, B. Wunderle, B. Michel, “Reliability of SnPb and SnPb-free flip-chips under different test conditions”. Proceedings of the EuroSimE, p437–442, 2004
12. Schubert, R. Dudek, E. Auerswald, A. Gollhardt, B. Michel, B. Reichl, “Fatigue life models for SnAgCu and SnPb solder joints evaluated by experiments and simulation”, Proceedings of Electronic Components & Technology Conference, p603-610, 2003.
13. H.R. Ghorbani, J.K. Spelt, “An analytical elasto-creep model of solder joints in leadless chip resistors: part 2-applications in fatigue reliability predictions for SnPb and lead-free solders”, IEEE Transactions on Advanced Packaging, p695-704, 2007.
14. Perkins, S.K. Sitaraman, “Universal fatigue life prediction equation for ceramic ball grid array (CBGA) packages”, Microelectronics Reliability, p2260-2274, 2007.
15. Andersson, Z. Lai, J. Liu, H. Jiang, Y. Yu, “Comparison of isothermal mechanical fatigue properties of lead-free solder joints and bulk solders”, Materials Science and Engineering A, p20-27, 2005.
16. R. Dudek, H. Walter, R. Doering, B. Michel, “Thermal fatigue modelling for SnAgCu and SnPb solder joints”, 5th International Conference on Thermal and Mechanical Simulation and Experiments in Micro-electronics and Micro-Systems, p557-564, 2004.

17. Y. Lai T. Wang, H. Tsai, J. Wu, “A study of cyclic bending reliability of bare-dietype chip-scale packages”, EuroSimE, p313-316, 2004.
18. T. Hannach, H. Worrack, W. Müller, T. Hauck, “Creep in microelectronic solder joints: finite element simulations versus semi-analytical methods”, Archive of Applied Mechanics, v 79, n 6-7,p 605-617, July 2009
19. M. Pei, “Field Condition Reliability Assessment for SnPb and SnAgCu Solder Joints in Power Cycling Including Mini Cycles”, 2006 Electronic Components and Technology Conference.
20. Y. Lai, T. Wang, C. Lee, “Thermal-Mechanical Coupling Analysis for Coupled Power and Thermal Cycling Reliability of Board-Level Electronic Packages”, IEEE Transactions on Device and Material Reliability, Vol. 8, No. 1, Mar. 2008.
21. M. Sham, J. Kim, J. Park, “Thermal Performance of Flip Chip Packages: Numerical Study of Thermo-mechanical Interactions”, Computational Material Science, Vol 43, , p 469-480, 2008
22. P. Hegde, D. Whalley and V. Silberschmidt, “3D Study of Thermal Stresses in Lead-free Surface Mount Devices”, Journal of Thermal Stresses, Vol. 31, p1039-1055, 2008
23. P. Hall, T.D. Dudderar and J. Argyle, “Thermal Deformations Observed n Leadless Ceramic Chip Carriers Surface Mounted to Printed Wiring Boards”, IEEE Transaction in Components, Hybrids, and Manufacturing Technology, Vol. 6, No.4, Dec. 1983
24. Palmgren, A., “Die Lebensdauer von Kugellagern,” VDI Zeitschrift, No. 14, p 339-441, 1924
25. M. A. Miner, “Cumulative Damage in Fatigue”, Journal of Applied Mechanics, Vol.12,1945
26. K. Upadhyayula and A. Dasgupta, “An incremental damage superposition approach for reliability of electronic interconnects under combined accelerated stresses,” presented at the ASME Int. Mech. Eng. Congr. Expo., Dallas, TX, Nov. 16–21, 1997
27. H. Qi, “Plastic Ball Grid Array Solder joint Reliability Assessment under Combined thermal cycling and Vibration,” Ph.D Thesis, University of Maryland, 2006.
28. E. George, M. Osterman, M. Pecht, “Thermal Cycling Reliability of Lead-Free Solders (SAC305 and Sn3.5Ag) for High-Temperature Applications”, IEEE Transactions on Device and Material Reliability, Vol. 11, No. 2, Jun. 2011.
29. F.X. Che, H.L. Pang, “Vibration reliability test and finite element analysis for flip chip solder joints”, Microelectronics Reliability, v 49, n 7, p 754-760, July 2009
30. M. Osterman and P. Chauhan, Effect of temperature cycling parameters on the durability of Pb-free solders, IMAPS 2009 42nd International Symposium on Microelectronics, San Jose Convention Center - San Jose, California, USA, Nov. 2009.
31. M. Osterman, Modeling Temperature Cycle Fatigue Life of SN100C Solder, 2011 SMTA International Conference on Soldering and Reliability, May 2011.
32. Y. Kojima and M. Kikuchi, K. Maisunaga and N. Yamazaki, “The Reliability of Reflow Solder by Hot Air Reflow”, IEEE Component, Hybrids and Manufacturing Technology Symposium, 1989.
33. M. Osterman, A. Dasgupta, B. Han, “A strain range based model for life assessment of Pb-free SAC solder interconnects”, 2006 Electronic Components and Technology Conference
34. Dan B. Marghitu, Mechanical Engineer's Handbook, Academic Press, Aug 20, 2001

35. Q. Zhang, “Isothermal Mechanical and Thermomechanical Durability Characterization of Selected Pb-free Solders,” Ph.D Thesis, University of Maryland, 2004.
36. G. Cuddalorepatta, M. Williams, and A. Dasgupta, “Viscoplastic Creep Response and Microstructure of As- fabricated Microscale Sn3.0Ag0.5Cu Solder Interconnects”, Journal of Electronic Materials, Vol. 39, No. 10, p2292-2309, 2010
37. K. Au, J. Beleran, Y. Yang, Y. Zhang, S. Kriangsak, P. Wilson, Y. Drake, S. Nathapong, “Multi Chip Stacking and Reliability Challenges using TSV-micro C4 Solder Interconnection for FCCSP TSV package”, 13th Electronics Packaging Technology Conference, 2011